
Doctoral Dissertations

Student Theses and Dissertations

Spring 2016

Evaluating of scale-up methodologies of gas-solid spouted beds for coating triso nuclear fuel particles using advanced measurement techniques

Neven Y. Ali

Follow this and additional works at: https://scholarsmine.mst.edu/doctoral_dissertations

 Part of the [Nuclear Engineering Commons](#)

Department: Mining and Nuclear Engineering

Recommended Citation

Ali, Neven Y., "Evaluating of scale-up methodologies of gas-solid spouted beds for coating triso nuclear fuel particles using advanced measurement techniques" (2016). *Doctoral Dissertations*. 2466.
https://scholarsmine.mst.edu/doctoral_dissertations/2466

This thesis is brought to you by Scholars' Mine, a service of the Missouri S&T Library and Learning Resources. This work is protected by U. S. Copyright Law. Unauthorized use including reproduction for redistribution requires the permission of the copyright holder. For more information, please contact scholarsmine@mst.edu.

**EVALUATING OF SCALE-UP METHODOLOGIES OF GAS-SOLID SPOUTED
BEDS FOR COATING TRISO NUCLEAR FUEL PARTICLES USING
ADVANCED MEASUREMENT TECHNIQUES**

by

NEVEN Y. ALI

A DISSERTATION

**Presented to the Faculty of the Graduate School of the
MISSOURI UNIVERSITY OF SCIENCE AND TECHNOLOGY**

In Partial Fulfillment of the Requirements for the Degree

DOCTOR OF PHILOSOPHY

in

NUCLEAR ENGINEERING

2016

Approved by:

**Muthanna Al-Dahhan, Advisor
Hyoungh K. Lee
Carlos H. Castano
Ayodeji B. Alajo
Xinhua Liang**

© 2016

NEVEN Y. ALI

All Rights Reserved

PUBLICATION DISSERTATION OPTION

The Introduction section of this dissertation provides brief information about generations of nuclear reactors, TRISO fuel production process, and gas-solid spouted beds, along with the motivation and the objectives of this study. The literature review section presents a critical review of the literature in the scale-up of gas-solid spouted beds. The body of this dissertation consists of four manuscripts that have been prepared in the style of the relevant journals. The four manuscripts are in the following order:

- I. Pages 57 -107, the first paper “Demonstrating the non-similarity in local holdups of gas-solid spouted beds obtained by CT with scale-up methodology based on dimensionless groups” has been accepted with minor revisions in the Journal of Chemical Engineering Research and Design.
- II. Pages 108-158, the second paper “An advanced evaluation of spouted beds scale-up for coating TRISO nuclear fuel particles using radioactive particle tracking (RPT)” has been submitted to the Journal of Experimental Thermal and Fluid Science.
- III. Pages 159-200, the third paper “Evaluating the new mechanistic scale-up methodology of gas-solid spouted beds using gamma ray computed tomography (CT)” ready to be submitted to the journal of Powder Technology after the publication of Paper 1.
- IV. Pages 201-244, the fourth paper “An advanced evaluation the new mechanistic scale-up methodology of gas-solid spouted using radioactive particle tracking (RPT)” has been prepared to be submitted to the Journal of Particuology.

Finally, concluding remarks and recommendations for future work in the study of spouted beads are given in the last section.

ABSTRACT

The work focuses on implementing for the first time advanced non-invasive measurement techniques to evaluate the scale-up methodology of gas-solid spouted beds for hydrodynamics similarity that has been reported in the literature based on matching dimensionless groups and the new mechanistic scale up methodology that has been developed in our laboratory based on matching the radial profile of gas holdup since the gas dynamics dictate the hydrodynamics of the gas-solid spouted beds. These techniques are gamma-ray computed tomography (CT) to measure the cross-sectional distribution of the phases' holdups and their radial profiles along the bed height and radioactive particle tracking (RPT) to measure in three-dimension (3D) solids velocity and their turbulent parameters. The measured local parameters and the analysis of the results obtained in this work validate our new methodology of scale up of gas-solid spouted beds by comparing for the similarity the phases' holdups and the dimensionless solids velocities and their turbulent parameters that are non-dimensionalized using the minimum spouting superficial gas velocity. However, the scale-up methodology of gas-solid spouted beds that is based on matching dimensionless groups has not been validated for hydrodynamics similarity with respect to the local parameters such as phases' holdups and dimensionless solids velocities and their turbulent parameters. Unfortunately, this method was validated in the literature by only measuring the global parameters. Thus, this work confirms that validation of the scale-up methods of gas-solid spouted beds for hydrodynamics similarity should reside on measuring and analyzing the local hydrodynamics parameters.

ACKNOWLEDGMENTS

First and foremost, my praises and thanks are to God for giving me everything to accomplish this tough and long journey. I wish there is a way to express really my gratefulness and gratitude to my advisor Dr. Muthanna Al-Dahhan. It has been an honor to be his Ph.D. student. I would like to thank him for accepting me as his Ph.D. student and giving me the opportunity to work in his unique laboratory. I am also very thankful for his contributions of time, funding, great efforts to explain topics clearly and simply, encouragement and his patience. I would have lost without his valuable guidance. I hope that I could be as lively, smart and energetic as Dr. Al-Dahhan. Furthermore, I appreciatively would like to thank my committee members, Dr. Hyoungh K. Lee, Dr. Carlos H. Castano, Dr. Ayodeji B. Alajo, and Dr. Xinhua Liang for their support, patience, taking the interest in my work and examining my dissertation. I would like to give special thank to an inspiring and magnificent mother who has led me here. I have never had someone who believes in me more than her. Thank you for sitting next to me and listening to me kindly, when grief and fear took their toll in my soul. Thank you for making me who I am today. I would like to acknowledge with profound gratitude our research group member and collaborator Thaar Al-Juwaya for his valuable assistant and insightful discussions and suggestions. I wholeheartedly thank my family and friends who have supported me through my academic path. My sincere thanks are to Sheila Johnson for her help, support and the friendship. My special thanks go to Julie Otto for the being my family in U.S. My appreciation to Marlene Albrecht, Krista Welschmeyer and Dean Lenz for providing all the help that the students need.

TABLE OF CONTENTS

	Page
PUBLICATION DISSERTATION OPTION	iii
ABSTRACT.....	iv
ACKNOWLEDGMENTS	v
LIST OF ILLUSTRATIONS.....	x
LIST OF TABLES.....	xvi
 SECTION	
1. INTRODUCTION	1
1.1 THE NEED FOR NUCLEAR ENERGY.....	1
1.2 NUCLEAR REACTOR TYPES.....	4
1.3 GENERATIONS OF NUCLEAR REACTORS.....	8
1.3.1 First Generation.....	9
1.3.2 Second Generation.....	9
1.3.3 Third Generation.....	10
1.3.4 Fourth Generation.....	11
1.4 TRISO NUCLEAR FUEL PARTICLES.....	16
1.5 TRISO NUCLEAR FUEL PARTICLES COATING PROCESS.....	17
1.6 GAS-SOLID SPOUTED BED FOR COATING TRISO NUCLEAR FUEL PARTICLES.....	19
1.7 MOTIVATION	20
1.8 OBJECTIVES	22
2. LITERATURE REVIEW.....	25
2.1 REVIEW OF THE NEW SCALE-UP METHODOLOGY.....	26

2.2 LITERATURE REVIEW OF THE REPORTED SCALE-UP METHODOLOGY BASED ON MATCHING DIMENSIONLESS GROUPS.	32
PAPER	
I. Demonstrating the non-similarity in local holdups of gas-solid spouted beds obtained by CT with scale-up methodology based on dimensionless groups. (CT)....	44
1. Introduction.....	45
2. Experimental Work.....	49
2.1 Experimental Set-up of Spouted Beds.....	49
2.2 Experimental conditions.....	50
2.3 Dual Source Gamma Ray Computed Tomography (DSCT).....	51
3. Results and Discussion	56
3.1 The accuracy and reproducibility of the results	56
3.2 Solids and gas holdups of Case A	57
3.2.1 Solids holdups profiles for the Reference case (Case A).....	57
3.2.2 Cross sectional distribution of solids holdup for the Reference case (Case A).	58
3.2.3 Gas holdup profiles for the reference case (case A)	59
3.3 Demonstrating the non-similarity in local holdups with matching dimensionless groups.	60
3.4 The non-similarity in local holdups with mismatching dimensionless groups. 63	
4. Conclusion	66
II. An advanced evaluation of spouted beds scale-up for coating TRISO nuclear fuel particles using radioactive particle tracking (RPT).....	93
1. Introduction.....	94
2. Experimental work.....	98
2.1 Spouted beds setup	98

2.2	Experimental conditions.....	99
2.3	The Radioactive Particle Tracking (RPT) Technique.....	100
3.	Results and discussion	105
3.1	Radial Profiles of the Averaged Particles Velocity.....	105
3.1.1	Radial Profiles of the Averaged Axial Particles Velocity	105
3.1.2	Radial Profiles of the Averaged Radial Particles Velocity.....	109
3.2	Radial Profiles of the Averaged Particle Normal Stresses.....	111
3.2.1	Radial profiles of the Averaged Axial Particle Normal stresses.....	111
3.2.2	Radial Profiles of the Averaged Radial particle Normal stresses	113
3.2.3	Radial Profiles of the Averaged Azimuthal Particle Normal stresses .	114
3.3	Radial Profiles of the Averaged Particle Shear stresses.....	115
3.4	Radial Profiles of the Averaged particles turbulent kinetic energy.....	116
4.	Conclusion	117
III.	Evaluating the new mechanistic scale-up methodology of gas-solid spouted beds using gamma ray computed tomography (CT).	143
1.	Introduction.....	144
2.	Experimental Work.....	147
2.1	Experimental Set-up of the Spouted Beds.....	147
2.2	Experimental conditions.....	148
2.3	Dual Source Gamma Ray Computed Tomography (DSCT).....	148
3.	Results and Discussion	149
3.1	Assessing [13] sets of conditions for matching and mismatching radial profiles of gas holdups using CT.....	149
3.2	Assessing the new mechanistic scale-up methodology using CT technique..	150
3.3	Solids and gas holdups along the bed height using CT technique at the conditions when the radial profiles of the gas holdup are not similar.....	154

3.4 Comparison between the measurements of CT technique of this work and the optical fiber probe technique of [13]	157
4. Conclusion	158
IV. An advanced evaluation the new mechanistic scale-up methodology of gas-solid spouted using radioactive particle tracking (RPT).....	185
1. Introduction.....	186
2. Experimental work.....	190
2.1 Spouted beds setup	190
2.2 Experimental conditions.....	191
2.3 The Radioactive Particle Tracking (RPT) Technique.....	192
3. Results and Discussion	192
3.1 Solids Velocity Field	193
3.1.1 Azimuthally and axially averaged radial profiles of axial particles velocity.....	193
3.1.2 Azimuthally and axially averaged radial profiles of radial particles velocity.....	197
3.2 Azimuthally and axially averaged radial profiles of the particles normal stresses.....	199
3.3 Azimuthally and axially averaged radial profiles of particles shear stresses .	201
3.4 Azimuthally and axially averaged radial profiles of the particles turbulent kinetic energy	203
4. Concluding Remarks.....	204
SECTION	
3. CONCLUDING REMARKS AND RECOMMENDATIONS	228
REFERENCES	233
VITA	238

LIST OF ILLUSTRATIONS

		Page
PAPER I		
Figure 1.	Schematic diagram of spouted beds.....	79
Figure 2.	Schematic diagram of 0.076 m and 0.152 m spouted beds.....	80
Figure 3.	Photograph of the DSCT technique, and 0.152 m spouted bed inside the setup for scan.	81
Figure 4.	The computational domain is discretized into cells of size x	82
Figure 5.	Reproducibility of CT measurements for (a) cross-sectional solids holdup distributions and (b) their radial profiles with the associated error bars for three CT scans at $z/D=1.8$ (Conditions; Case A in Table 1).....	83
Figure 6.	Radial profiles of solids holdup along the bed height of the 0.152 m spouted bed using conditions in Case A (reference case) listed in Table 1.	84
Figure 7.	Cross sectional distribution and corresponding frequency distribution of solids holdup for Case A along the bed height of the 0.152 m spouted bed.....	85
Figure 8.	Radial profiles of gas holdup along the bed height of the 0.152 m spouted bed using conditions in Case A (reference case) listed in Table 1.	86
Figure 9.	Comparison of radial profiles of solids holdup at z/D levels of 0.8, 1.1, 1.8, and 2.4 for Case A (0.152 m) and Case B (0.076 m) spouted beds.....	87
Figure 10.	Cross sectional image and corresponding frequency distribution of solids holdup for Case B along the bed height of the 0.076 m spouted bed.	88
Figure 11.	Comparison of radial profiles of gas holdup at z/D levels of 0.8, 1.1, 1.8, and 2.4 for Case A (0.152 m) and Case B (0.076 m) spouted beds.....	89
Figure 12.	Comparison of radial profiles of solids holdup at z/D levels of 0.8, 1.1, 1.8, and 2.4 for Case A (0.152 m) and Case C (0.076 m) spouted beds.....	90
Figure 13.	Cross sectional image and corresponding frequency distribution of solids holdup for Case C along the bed height of the 0.076 m spouted bed.	91
Figure 14.	Comparison of radial profiles of gas holdup at z/D levels of 0.8, 1.1, 1.8, and 2.4 for Case A (0.152 m) and Case C (0.076 m) spouted beds.....	92

PAPER II

Fig. 1.	Schematic diagram of spouted beds.....	130
Fig. 2.	Schematic diagram of the 0.076 m and 0.152 m spouted beds.....	131
Fig. 3.	Schematic diagram showing the positions of 14-detectors arranged around the 0.152 m spouted bed.	132
Fig. 4.	Azimuthally and axially averaged radial profiles of the axial particle velocity for the conditions of the reference Case (Case A), the case with matched dimensionless groups (Case B), and the case with mismatched dimensionless groups (Case C) for 0.152 m and 0.076 m spouted beds in the spout/annulus and the fountain regions.....	133
Fig. 5.	Azimuthally and axially averaged radial profiles of the dimensionless axial particle velocity for the conditions of matched and mismatched dimensionless groups for 0.152 m and 0.076 m spouted beds in the spout/annulus and the fountain regions ($U_{ms} = 89, 61, 68$ cm/s, respectively for Cases A, B, and C).....	134
Fig. 6.	Azimuthally and axially averaged radial profiles of the radial particle velocity for the conditions of matched and mismatched dimensionless groups for 0.152 m and 0.076 m spouted beds in the spout/annulus and the fountain regions.....	135
Fig. 7.	Azimuthally and axially averaged radial profiles of the dimensionless radial particle velocity for the conditions of matched and mismatched dimensionless groups for 0.152 m and 0.076 m spouted beds in the spout/annulus and the fountain regions ($U_{ms} = 89, 61, 68$ cm/s, respectively for Cases A, B, and C).....	136
Fig. 8.	Azimuthally and axially averaged radial profiles of (a) the axial normal stresses and (b) the dimensionless axial normal stresses with respect to the squared minimum spouting velocity, in the spout/annulus and the fountain regions for the conditions of matched and mismatched dimensionless groups for 0.152 m and 0.076 m spouted beds ($U_{ms} = 89, 61, \text{ and } 68$ cm/s, respectively for Case A, B, and C).....	137
Fig. 9.	Azimuthally and axially averaged radial profiles of the radial normal stresses in (a) and (b) the dimensionless radial normal stress, in the spout/annulus and (d) the fountain regions for the conditions of matched and mismatched dimensionless groups for 0.152 m and 0.076 m spouted beds ($U_{ms} = 89, 61, \text{ and } 68$ cm/s, respectively for Case A, B, and C).....	138

Fig. 10.	Azimuthally and axially averaged radial profiles of (a) the azimuthal normal stresses, and (b) the dimensionless azimuthal normal stresses, in the spout/annulus and the fountain regions for the conditions of matched and mismatched dimensionless groups for 0.152 m and 0.076 m spouted beds ($U_{ms} = 89, 61, \text{ and } 68 \text{ cm/s}$, respectively for Case A, B, and C).....	139
Fig. 11.	Azimuthally and axially averaged radial profiles of the shear stresses for the conditions of matched and mismatched dimensionless groups for 0.152 m and 0.076 m spouted beds in the spout/annulus and the fountain regions.	140
Fig. 12.	Azimuthally and axially averaged radial profiles of the dimensionless shear stresses in the spout/annulus and the fountain regions for the conditions of matched and mismatched dimensionless groups for 0.152 m and 0.076 m spouted beds ($U_{ms} = 89, 61, \text{ and } 68 \text{ cm/s}$, respectively for Case A, B, and C).	141
Fig. 13.	Azimuthally and axially averaged radial profiles of turbulent kinetic energy (per unit bulk density), And (b) the dimensionless turbulent kinetic energy, in the spout/annulus and the fountain regions for the conditions of matched and mismatched dimensionless groups for 0.152 m and 0.076 m spouted beds ($U_{ms} = 89, 61, \text{ and } 68 \text{ cm/s}$, respectively for Case A, B, and C).	142
 PAPER III		
Fig. 1.	Schematic diagram of spouted beds.....	169
Fig. 2.	Schematic diagram of 0.076 m and 0.152 m spouted beds.....	170
Fig. 3.	Photograph of the DSCT technique, and 6-inch spouted bed inside the setup for scan.	171
Fig. 4.	Cross-sectional distribution and corresponding frequency distribution of gas holdup for the conditions of (a) the reference case of 0.152 m spouted beds at $z/D=1.8$ and (b) similar radial profile of 0.076 m spouted beds at $z/D=1.8$	172
Fig. 5.	Comparison of gas holdup radial profiles at $z/D = 1.8$, for the conditions of reference case (Case A) in 0.152 m spouted bed, and for the conditions that give similar radial profile of gas holdup (called similar ϵ_q) in 0.076 m spouted beds (Table 2.1).....	173
Fig. 6.	Cross-sectional distribution and corresponding frequency distribution of solids holdup for Case A along the bed height of the 0.152 m spouted beds.....	174

Fig. 7.	Cross-sectional distribution and corresponding frequency distribution of the solids holdup for the conditions of similar gas holdup profiles along the bed height of the 0.076 m spouted bed.	175
Fig. 8.	Comparison of solids holdup radial profiles at z/D levels of 0.8, 1.1, 1.8, and 2.4 for the conditions of reference case (Case A), and similar radial profile of gas holdup (called similar ϵ_g) in 0.152 m and 0.076 m spouted beds.....	176
Fig. 9.	Cross-sectional distribution and corresponding frequency distribution of gas holdup for Case A along the bed height of the 0.152 m spouted bed.	177
Fig. 10.	Cross-sectional distribution and corresponding frequency distribution of gas holdup for the conditions of similar gas holdup profiles along the bed height of the 0.076 m spouted bed.	178
Fig. 11.	Comparison of gas holdup radial profiles at z/D levels of 0.8, 1.1, 1.8, and 2.4 for the conditions of reference case (Case A), and similar radial profile of gas holdup (called similar ϵ_g) in 0.152 m and 0.076 m spouted beds.....	179
Fig. 12.	Cross-sectional image and corresponding frequency distribution of solids holdup for Case C along the bed height of 0.076 m spouted bed....	180
Fig. 13.	Comparison of solids holdup radial profiles at z/D levels of 0.8, 1.1, 1.8, and 2.4 for the conditions of reference case (Case A), and Non-similar radial profile of gas holdup (called non-similar ϵ_g) in 0.152 m and 0.076 m spouted beds.....	181
Fig. 14.	Cross-sectional distribution and corresponding frequency distribution of the conditions of similar gas holdup profiles along the bed height of the 0.076 m spouted bed.	182
Fig. 15.	Comparison of gas holdup radial profiles at z/D levels of 0.8, 1.1, 1.8, and 2.4 for the conditions of reference case (Case A), and Non-similar radial profile of gas holdup (called non-similar ϵ_g) in 0.152 m and 0.076 m spouted beds.....	183
Fig. 16.	Comparison of gas holdup profiles measured using CT and Optical probe by [13].	184
 PAPER IV		
Figure 1.	Schematic diagram of spouted beds.....	216
Figure 2.	Schematic diagram of the 3-inch and 6-inch spouted beds.....	217

Figure 3.	Azimuthally and axially averaged radial profiles of the axial particle velocity for the conditions of Case A, similar, and non-similar gas holdup profiles for 6-inch and 3-inch spouted beds in the spout/annulus and the fountain regions.....	218
Figure 4.	Azimuthally and axially averaged radial profiles of the dimensionless axial particle velocity for the conditions of Case A and similar and non-similar gas holdup profiles for 6-inch and 3-inch spouted beds in the spout/annulus and the fountain regions.....	219
Figure 5.	Azimuthally and axially averaged radial profiles of the radial particle velocity for the conditions of similar and non-similar gas-holdup profiles for 6-inch and 3-inch Spouted beds in the spout/annulus and the fountain regions.....	220
Figure 6.	Azimuthally and axially averaged radial profiles of the dimensionless radial particle velocity for the conditions of similar and non-similar gas holdup profiles for the 6-inch and the 3-inch spouted beds in the spout/annulus and the fountain regions.....	221
Figure 7.	Azimuthally and axially averaged radial profiles of (a) the axial normal stresses and (b) the dimensionless axial normal stresses for the conditions of Case A, similar, and non-similar gas holdup profiles for 6-inch and 3-inch spouted beds in the spout/annulus and the fountain regions.....	222
Figure 8.	Azimuthally and axially averaged radial profiles of (a) the radial normal stresses and (b) the dimensionless radial normal stresses for the conditions of Case A, similar, and non-similar gas holdup profiles for 6-inch and 3-inch spouted beds in the spout/annulus and the fountain regions.....	223
Figure 9.	Azimuthally and axially averaged radial profiles of (a) the azimuthal normal stresses and (b) the dimensionless azimuthal normal stresses for the conditions of Case A, similar, and non-similar gas holdup profiles for 6-inch and 3-inch spouted beds in the spout/annulus and the fountain regions.....	224
Figure 10.	Comparison of the azimuthally and axially averaged radial profiles of the turbulent Reynolds shear stress components for the conditions of the reference case (case A), similar gas holdup, and non-similar gas holdup profiles.	225
Figure 11.	Comparison of the azimuthally and axially averaged radial profiles of the dimensionless shear stress components for the conditions of the reference case (case A), similar gas holdup, and non-similar gas holdup profiles.	226

Figure 12. Comparison of the azimuthally and axially averaged radial profiles of (a) the turbulent kinetic energy (per unit bulk density) and (b) dimensionless turbulent kinetic energy for the conditions of the reference case (case A), similar gas holdup, and non-similar gas holdup profiles. 227

LIST OF TABLES

	Page
PAPER I	
Table 1. Dimensional parameters and properties of scale-up verification conditions from the work of (He et al., 1997).	78
PAPER II	
Table 1. Experimental conditions (Dimensions, particle properties, and scaling parameters) for matched and mismatched dimensionless groups; used for the scale-up of spouted beds [13].	128
Table 2. Percentage differences in shear stresses among the studied conditions of Cases A, B, and C.	129
PAPER III	
Table 1. Experimental Conditions for similar and non-similar gas holdup radial profiles for the hydrodynamics similarity of spouted beds identified by Aradhya (2013).	165
Table 2. Mean and standard deviation of the solids holdup distribution for the conditions of the reference case and similar gas holdup profiles listed in Table 1.	166
Table 3. Mean and standard deviation of the gas holdup distribution for the conditions of the reference case and similar gas holdup profiles listed in Table 1.	167
Table 4. Mean and standard deviation of the gas holdup distribution for the conditions of the reference case and Non-similar gas holdup profiles listed in Table 1.	168
PAPER IV	
Table 1. Experimental Conditions for similar and non-similar gas holdup radial profiles for the hydrodynamics similarity of spouted beds identified by (Aradhya, 2013).	212
Table 2. Comparison between the measured and the correlation predictions of the minimum spouting velocity.	213
Table 3. Percentage differences in normal stresses among the studied sets of conditions of the Case A and similar and non-similar gas holdup profiles. .	214

Table 4. Percentage differences in shear stresses among the studied conditions of the reference case, similar and non-similar gas holdup profiles.....	215
--	-----

1. INTRODUCTION

1.1 THE NEED FOR NUCLEAR ENERGY.

Energy involves in every aspect of life, and it is essential factor in all sectors of modern economies. The convention energy sources such as oil, coal, and natural gas effectively have led to the world economic prosperity. On the other hand these fossil fuels also have led to damage the environment, effect human health, and oligopoly in production and distribution. Furthermore fossil fuels are being depleted, and will not satisfy the future needs (Herzog et al., 2001) Before and during the World War II, major focus of nuclear research was on the defense weapons and their development. However, in post World War II, interest was increased in peaceful applications of the nuclear technology. One of the significant uses for the nuclear energy is to generate electricity (Energy et al., 1994).

Figure 1.1 illustrates the distribution of the nuclear power plants for electricity production in the world and shows the nuclear electrical power generated per capita per annum in the world. (IAEA, 2013; Rashad, 2008) reported that a lot of international, national or private establishments are regularly involved in nuclear energy desire and supply projection. These projections were based on the engagement of economic growth and energy utilization. Also efficiency of technology, cost, prices of the fuel in the future, energy policy and physical environmental constrains and availability of energy source has affected these projections.

Nuclear energy is characterized by no carbon emission. It has been increasingly supported to be the alternative to the fossil fuel-based energy production systems in the future. During 52 year 9 nuclear power plants have been used mostly in industrialized countries. Actually there are 439 nuclear power reactors in operation in the world. 403

nuclear power reactors 91% of the total number are distributed between the organization for Economic Cooperation and Development (OCED) countries or countries with economic transition. The nuclear electrical capacity installed in these countries has been generating 349 GWCe around 15.2 % of the world's electricity that is provided by the 439 nuclear reactors in operation in 30 countries (Rashad, 2008).

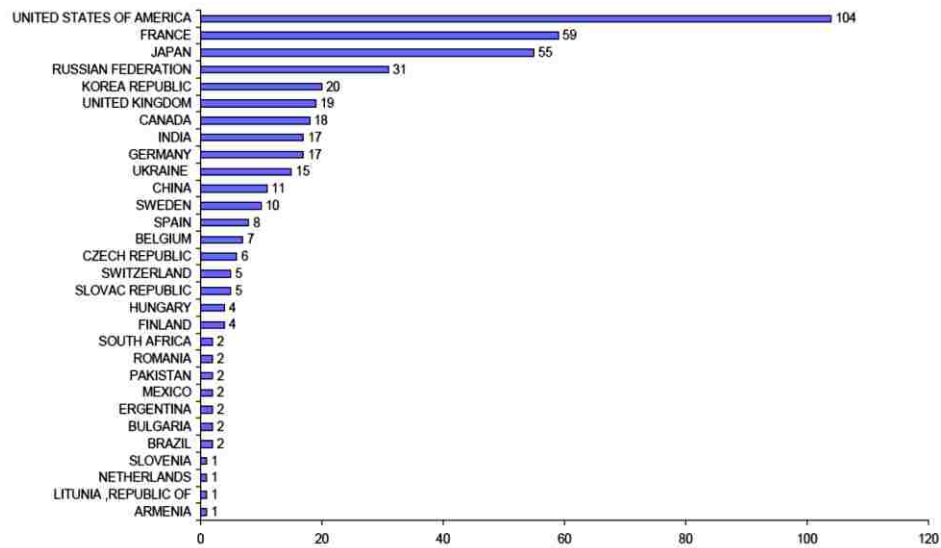


Figure 1.1. The Generation of Electricity globally by Nuclear Power (Rashad, 2008)
Number of Nuclear Power.

Table 1.1. (KW-h/capita/a) The global Generation of Electricity worldwide taken from (Rashad, 2008).

Country	KW-h/capita / a- 2003	Country	KW-h/capita / a- 2003
Ethiopia	33	Russian Federation	6295
Nigeria	148	Italy	6540
Kenya	158	United Kingdom	6731
Ghana	290	Saudi Arabia	6792
Vietnam	503	Republic of Korea	7249
India	597	Brunei Darussalam	7975
Indonesia	526	Austria	8095
African average	593	France	8099
Egypt	1348	Japan	8214
China	1500	Japan	8214
Jordan	1639	OECD average	8612
Latin American average	1911	Belgium	8776
Thailand	1922	Bahrain	10910
Turkey	1996	Australia	11411
Mexico	2113	United Arab Emirates	12259
Islamic Republic of Iran	2307	USA	14040
Brazil	2277	Kuwait	16612
Argentina	2641	Canada	18425
World average	2670	Iceland	29412
Poland	3704	Sweden	16551
Hungary	4056		
South Africa	4997		

United States generates 20 percent of its electricity needs from nuclear energy. Clean, reliable and affordable electricity are generated from nuclear power plants. One in five houses and businesses in United States are getting their electricity from nuclear energy by 104 nuclear reactors in 31 states (Figure 1.2) (NEI, 2008). There are several of nuclear reactors to generate electricity. There are discussed in the following section. The largest source of generating electricity with carbon-free emission is nuclear energy, which represents 70% of all emission-free electricity generated. About one-third of U.S. electricity came from emission-free sources (Lee et al., 2008).

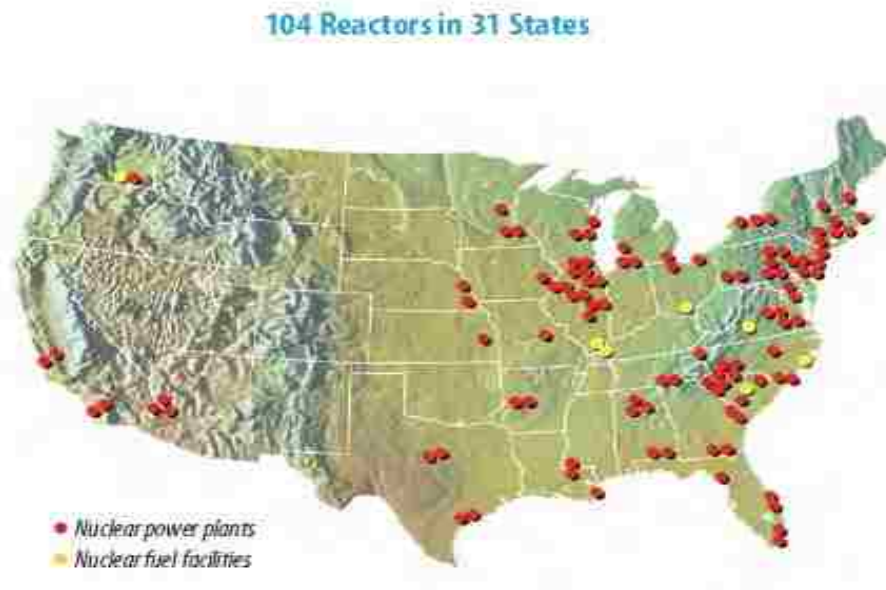


Figure 1.2. The distribution of nuclear power plants and nuclear fuel facilities in 31 States taken from (NEI, 2008).

1.2 NUCLEAR REACTOR TYPES.

The purpose of nuclear power plant is to produce electricity. In general, to produce electricity a source of heat is needed to boil to generate steam, which drives turbines to

produce electricity. The source of heat in the fossil fuel plants is burning coal, oil, or gas. On the other hand the source of heat in a nuclear power plant is nuclear reaction using fuels that utilized in nuclear reactors. In a nuclear reactor the fertile atom (uranium, plutonium, etc.) splits by neutron bombardments, which release heat, neutrons and fission products. As shown in Figure 1.3 many different types of reactors have been developed, but not all of them have been commercialized. Several of these reactors have been developed to prototypes and a number of them have been further developed to commercial scale. There are six types of reactors have been designed for commercial electricity production around the world; Magnox reactor (The name magnox comes from the magnesium-aluminium alloy used to clad the fuel rods inside the reactor), Advanced Gas- Cooled Reactor (AGR), Pressurized Water Reactor (PWR), Boiling water Reactor (BWR), Canada Deuterium Uranium (CANDU), and Light water graphite-moderated reactor (RBMK). Also other types of reactors have been developed to full-scale demonstration step. Currently in the United States, pressurized water and boiling water nuclear reactors have been developed and utilized for electricity production. . As mentioned before United States has 104 nuclear reactors in operation where 69 of them are pressurized water reactors and 35 of them are boiling water reactors. Table 1.2 summaries the general features of these reactors. However, various new technologies of nuclear reactors are being developed to enhance passive safety, increase nuclear reactor thermal efficiency, reduce proliferation, and to make them environmentally benign. The design of these nuclear reactors will be discussed briefly in the following section.

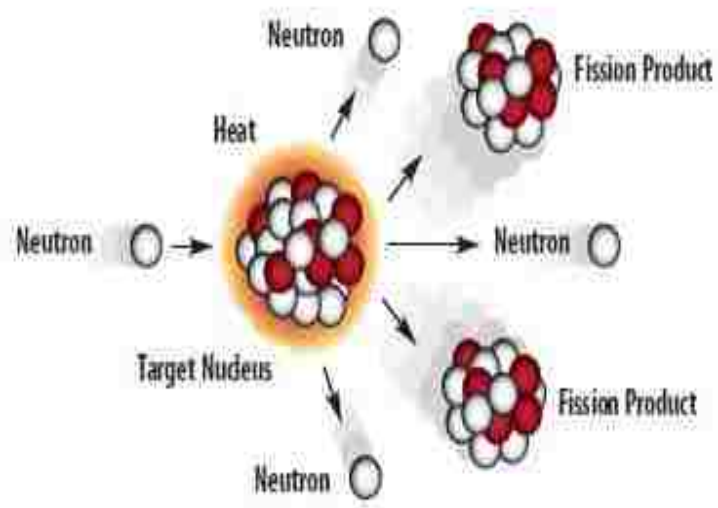


Figure 1.3. Illustration of fission process, (NEI, 2008)

Table 1.2. Schematics and some features of the types of nuclear reactors used in USA for electricity production (NEI, 2008) .

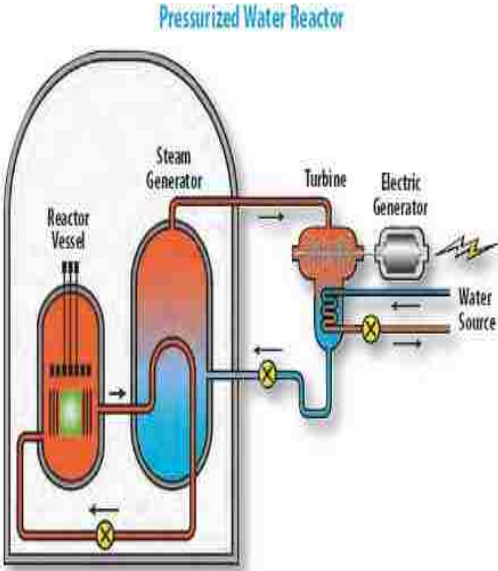
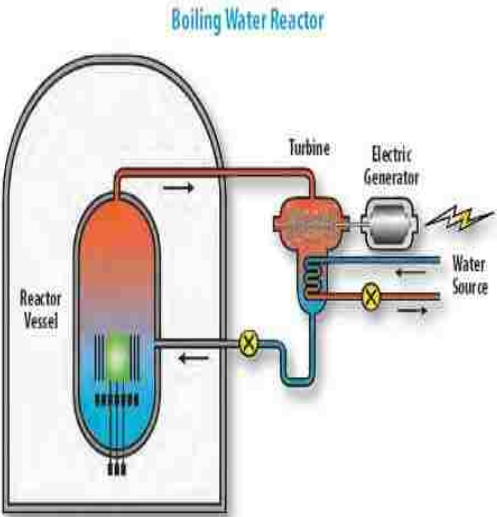
	Reactor	Some Features
Pressurized Water Reactor		<ul style="list-style-type: none"> • The first prevalent reactor used. • Designed by Westinghouse. • Water is inside the core of the reactor under high pressure. • Water boils at very high temperature under high pressure so the water can absorb more energy. • Water moves up the core instead of moving down. • Water is mostly liquid. • At the top of the core the water arrived very hot by absorbing a lot of energy and removing a good amount of heat from the fuel.(primar scale). • The steam that is going through the turbine to generate electricity is generated in the steam generator (secondary cycle) by the hot water coming from the reactor core. • The steam exiting the turbine passes through heat exchanger to deposit its energy to entering the cold water the steam is converted to cold liquid water to be recycled to the steam generator. • The hot water coming out of the steam generator is recycled back to the reactor core at the bottom to repeat the process. (correct reference).

Table 1.2. Schematics and some features of the types of nuclear reactors used in USA for electricity production (NEI, 2008) (cont.)

	Reactor	Some Features
Boiling Water Reactor		<ul style="list-style-type: none"> • Designed by General Electric (currently is GR Hitachi Nuclear Energy). • the water is boiled by pumping into the core. • The water is converted to steam after absorbing the heat from the fuel. • Electricity is generated by passing the steam through the turbine. • After the turbine, the hot water end or cooled to cold liquid water through heat exchanger where the engine deposited into entering cold water. • The cooled water is then pumped to the core of the reactor and the process is repeated.

1.3 GENERATIONS OF NUCLEAR REACTORS.

The nuclear reactor technology passes through various stages of development to advance its performance, safety, efficiency, etc. In today's world, there are three generations of nuclear power production systems are in use. Generation one, two and three were initially derived from the designs originally developed for Naval use that began in the late 1940s. The current reactors in operation are of the third generation, which is characterized in more advancement in performance and in safe operation than of the second and first generations. To enhance and to wide spread the use of nuclear power yet to

enhance and improve their safety, new trends are being proposed and developed such as fourth generation nuclear power plant, Small Modular Reactors technology. (SMRs) that in based on pressurized water reactor (cooled by either forced convection or natural convection) and advanced small modular reactors (molten salt, molten metal, gas) Nuclear energy will be going to be the essential part of energy mix that the world needs. Therefore, there is a need to advance the nuclear energy technology further in terms of improving thermal efficiency, being environmentally benign, having risk free proliferation, and be more safe. The following is an outline of some of the features of the nuclear reactors generations :

1.3.1 First Generation. It is referred to that was employed the civil nuclear, represents the early prototype reactors from the 1950s and 1960s such as “Shipping port (1957–1982) in Pennsylvania, Dresden-1 (1960–1978) in Illinois, and Calder Hall-1 (1956–2003) in the United Kingdom”. The Wylfa Nuclear Power Station in Wales, UK was the last commercial first generation of nuclear power Gen I plant was till December 2012 (Goldberg and Rosner, 2011).

1.3.2 Second Generation. This generation was designed to be economical and reliable, for up to 40 years lifetime. This generation includes boiling water reactors (BWR), pressurized water reactors (PWR), Canada Deuterium Uranium reactors (CANDU). The operation of the second-generation nuclear power plants was initiated in the late 1960s, which represent the world’s 400+ commercial PWRs and BWRs. These reactors are typically called light water reactors (LWRs). They use traditional active safety features in which the electrical or mechanical operations are initiated automatically, but in some cases operators can initiate these operations. However, some of the nuclear reactors of this

generation were passively safe, for example, using pressure relief valves that can be performed without operator control or loss of auxiliary power. The economic efficiency of the existing second-generation plants is satisfactory.

1.3.3 Third Generation. The third generation nuclear reactors are essentially Gen II reactors with evolutionary, state-of-the-art design improvements. The improvements are related to the fuel technology, thermal efficiency, modularized construction, safety systems (especially the use of passive rather than active systems), and standardized design. Such improvements result in a longer operational life, typically 60 years but with a potential to significantly exceed 60 years of operation, before complete overhaul and reactor pressure vessel replacement. Investigating the nuclear plant aging beyond 60 years is required to allow these reactors to operate over such extended lifetimes. Unlike first generation and second generation, 10 CFR Part 52 is used to regulate third generation reactors by NRC. The Westinghouse 600 MW advanced PWR (AP-600) was one of the first third-generation reactor designs. However, GE Nuclear Energy designed the Advanced Boiling Water Reactor (ABWR) and obtained a design certification from the NRC at the same time. Only four reactors of the third generation, all ABWRs, are in operation today. No third generation plants are in service in the United States.

The evolutionary design of the third generation nuclear reactors gave rise to the third generation plus reactor designs. These designs provide significant improvements in safety, which has been certified by the NRC in the 1990s. In the United States, Gen III+ designs must be certified by the NRC pursuant to 10 CFR Part 52. Examples of Gen III+ designs include (Goldberg and Rosner, 2011):

- VVER-1200/392M Reactor of the AES-2006 type
- Advanced CANDU Reactor (ACR-1000)
- AP1000: based on the AP600, with increased power output
- European Pressurized Reactor (EPR): evolutionary descendant of the Framatome N4 and Siemens Power Generation Division KONVOI reactors
- Economic Simplified Boiling Water Reactor (ESBWR) based on the ABWR
- APR-1400: an advanced PWR design evolved from the U.S. System 80+, originally known as the Korean Next Generation Reactor (KNGR)
- EU-ABWR based on the ABWR, with increased power output and compliance with EU safety standards Manufacturers. The major improvement of the third generation plus plants is the incorporation of passive safety features that do not require active controls or operator intervention but instead rely on gravity or natural convection to mitigate the impact of abnormal events. The inclusion of passive safety features, among other improvements, could help expedite the reactor certification review process and thus shorten the construction time duration. These reactors are expected to achieve higher fuel burn up and hence, reduce fuel consumption and waste production.

1.3.4 Fourth Generation. To address the future energy challenges, ten countries have agreed on a framework for international cooperation in research for an advanced generation of nuclear energy systems, known as Generation IV. Six basic concept

of Gen IV nuclear reactors have been proposed which 10 CFR Part 52 must be met to certify by NRC the fourth generation nuclear reactors similar to that of generation three and generation three plus designs in the United States, based on updated regulations and regulatory guides. The U.S. Department of Energy (DOE) Office of Nuclear Energy has taken responsibility for developing the science required for Gen IV technologies.

The Next Generation Nuclear Plant (NGNP) project is considering one of the six models of Gen IV reactor systems that is Very High Temperature Reactor, which was designed to provide high-temperature heat ($\sim 1000^{\circ}\text{C}$) for a variety of co-products, including hydrogen production and process heat besides electricity. The NRC is working with DOE on a licensing approach. In general, fourth generation systems include full actinide recycling and on-site fuel-cycle facilities based on advanced aqueous, pyrometallurgical, or other dry-processing options (Goldberg and Rosner, 2011). Among the six candidate models the very high temperature reactor VHTGR seems to be a promising one, which has been designed into two different types as follows:

- Pebble Bed Reactor (up to 200 MWe).
- Prismatic Block Reactor (up to 600 MWe).

For both of these reactors, the nuclear fuels are made of TRISO nuclear fuel particles, as it will be discussed in the following section. Since these two reactors are promising modular reactors for commercial development. Advancing and scaling up the process of manufacturing TRISO nuclear fuel particles with robustness become critical for the commercialization of these reactors. For pebble bed reactors, China developed a pilot plant pebble reactor and recently, a demonstration unit has been in operation. Work

continues on developing prismatic block reactor. The Six Basic Candidates of the Generation IV Systems are outlined in Table 1.3.

Table 1.3. Some features of the six basic candidates of the Generation IV Systems (Gen IV, 2002).

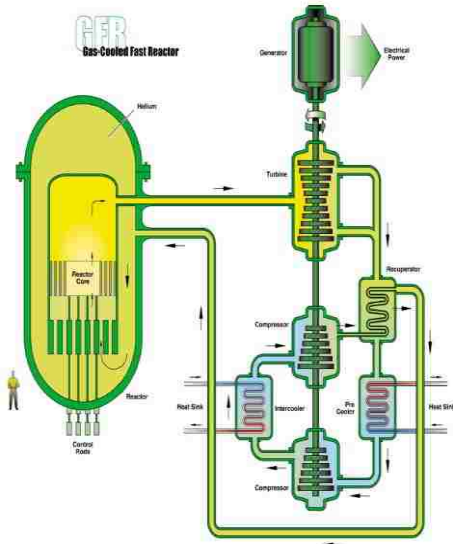
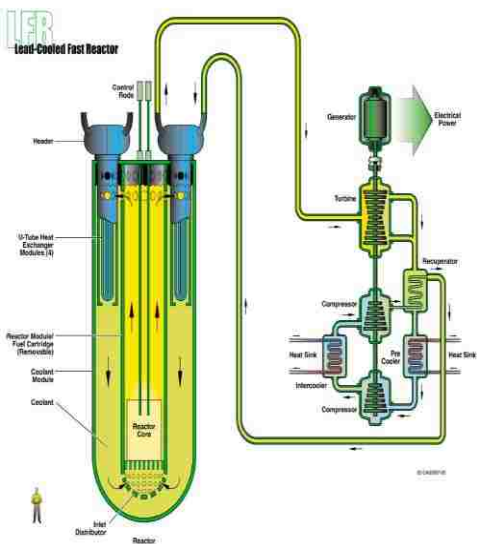
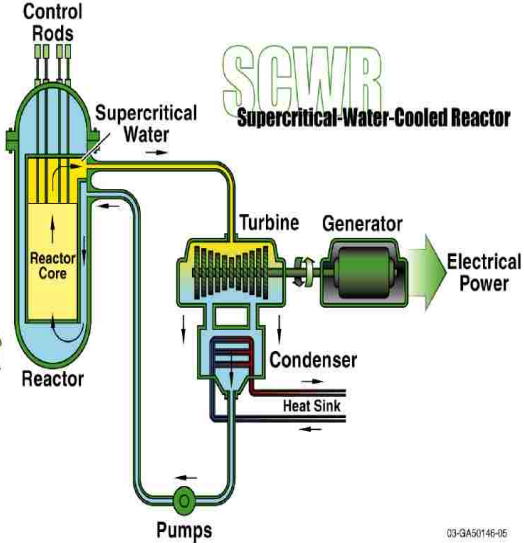
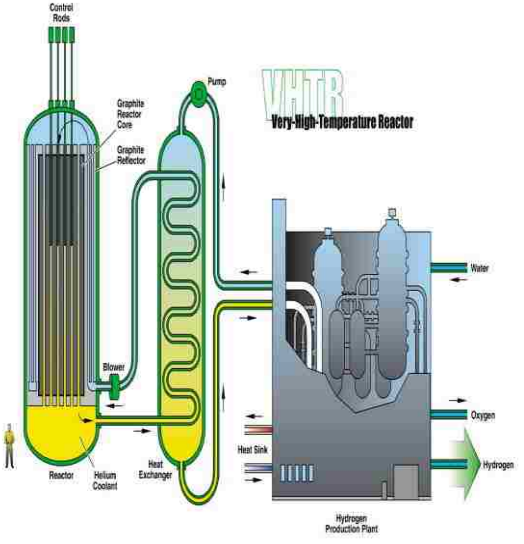
Reactor	Schematic	Features
Gas cooled fast reactor		<ul style="list-style-type: none"> • coolant is He. • Outlet temperature is 850°C • 600 MWth/ 288 MWe, and direct-cycle gas-turbine. • efficient electricity generation. • high U-resource utilization. • waste minimization. • can be used for hydrogen production. • active safety systems needed at targeted power density due to relatively low thermal inertia and poor heat transfer characteristics of coolant at low pressure, fuel and materials development challenges.
Lead-Cooled Fast Reactor (LFR)		<ul style="list-style-type: none"> • coolant is lead (Pb) or lead (Pb), lead-bismuth (Pb-Bi). • outlet temperature is 500°C to 800°C. • plutonium mixed mononitride (U-TRU) nitride fuel 25–200 MWe and 15–30 year core refueled as a cartridge. • small size tailored to needs for remote or distributed generation • no need for on-site fuel storage or local fuel cycle infrastructure. • simplification of design. • control of corrosion. • coolant activation. • seismic safety and the qualification of Russian data.

Table 1.3. Some features of the six basic candidates of the Generation IV Systems (Gen IV, 2002) (cont.)

Reactor	Schematic	Features
Sodium Cooled Fast Reactor (SFR)		<ul style="list-style-type: none"> • Coolant is sodium. • Outlet temperature is 550°C. • Primary system is at atmospheric pressure. • Efficient electricity generation is 1000-5000 MWth. • Advantageous actinide management. • Efficient conversion of fertile uranium. • Metal or MOX fuel with advanced recycling. • Development of oxide fuel fabrication technology. • Sodium leak prevention.
Molten Salt Reactor (MSR)		<ul style="list-style-type: none"> • Fuel is a molten salt fuel mixture. • Power net is 1000 MWe. • Generating electricity efficiently. • Safe. • can be used for hydrodynamic production. • Actinide burning. • Efficiently using the fuel. • Reducing the low pressure stress on vessel and piping.

Table 1.3. Some features of the six basic candidates of the Generation IV Systems (Gen IV, 2002) (cont.)

Reactor	Sechmatic	Features
Supercritical-Water-Cooled Reactor		<ul style="list-style-type: none"> • Coolant is water above critical point (374 °C, 22.1 MPa) • Direct cycle cooling • System is simple • Less components • thermal efficiency approaches 44%. • Stability of the coolant flow against oscillations • Safe. • Applicable fuel design.
Very High Temperature Reactor (VHTR)		<ul style="list-style-type: none"> • core is prismatic block or pebble bed. • fuel is TRISO particle. • coolant is helium. • outlet temperature is up to 1000°C. • modular is 300-600 MWth. • more safe. • more efficient with conversion cycle of Helium Brayton. • hydrogen production is clean and efficient. • usability of high temperature material. • high performance and dependable fuel. • can be used for hydrogen production.

1.4 TRISO NUCLEAR FUEL PARTICLES.

TRISO is abbreviation of TRIstructural-ISOtropic. The TRISO particle fuel consists of fuel kernel made of UO_2 or UCO , or other type of fertile material coated by four layers of isotropic materials for protection and containment. The TRISO coated particle fuel which is to be used in the next generation of the gas cooled reactor has significant features such as the ability to operate at high temperatures, to achieve high burn up, and to survive adverse conditions. (World Nuclear Association report, Page. 5, 2009). Size from approximately $920\ \mu\text{m}$ to $1000\ \mu\text{m}$, the particles are durable and impervious to moisture for long term, and that would make them an attractive alternative to recent metallic fuel containers. Also this type of fuel has been known for decades. The Germans first developed it in the 1980s and some countries have considered it for different next generation reactors.

TRISO fuel functions admirably in high temperature gas cooled reactors HTGRs by means of permitting much higher temperatures and substantially more compelling utilization of the uranium within the tiny sphere. Figure 1.4 shows the structure of the TRISO nuclear fuel particle, which consists of the following:

- Fuel kernel: it consists selected fertile material ($\sim 350\ \mu\text{m}$ to $500\ \mu\text{m}$).
- Buffer layer: it spicily made of pyrolytic carbon ($60\ \mu\text{m}$ to $100\ \mu\text{m}$) that attenuates fission product recoils from kernel and provides space for the fission gases.
- Inner pyrocarbon (IPyC): it is made of pyrocarbon (IPyC) which is ($30\ \mu\text{m}$ to $40\ \mu\text{m}$) size. It traps the fission gases inside the particle, protects kernel from chlorine- during SiC deposition, and provides support for SiC.

- Silicon carbide (SiC): it is made of silicon carbide (35 μ m). It represents the primary component, the strongest layer, and impervious to gaseous fission products.
- Outer pyrocarbon (OPyC): it is made of pyrocarbon. It protects SiC from surroundings, and holds SiC in compression.

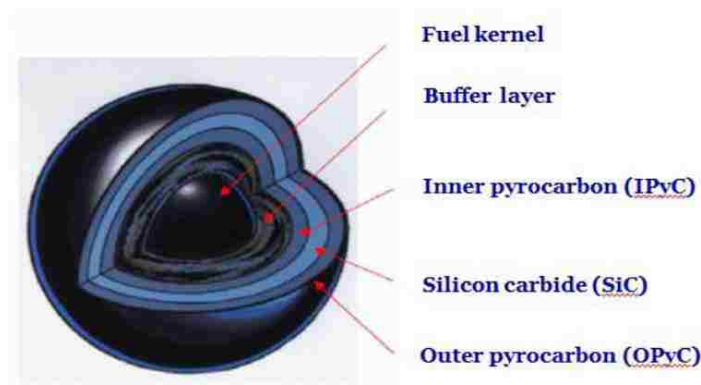


Figure 1.4. TRISO Fuel Particle Using in Generation IV Nuclear Reactor (Mykle Schneider, 2009).

1.5 TRISO NUCLEAR FUEL PARTICLES COATING PROCESS.

Fuel-coating technology and the related processes are the key for the commercialization of the Gen IV- VHTRs and hence for the future of nuclear power production as alternative sources of energy. The advancement and commercialization of nuclear energy produced by the 4th generation advanced gas reactors (AGRs) are dependent on The TRI structural-ISotropic (TRISO) fuel particles coating process which is based on chemical vapor deposition performed in gas-solid spouted beds. The acceptable level of defective coated particles is ultimately zero whether the coating is uniform or non-uniform. Recently, it has been reported that non-uniform coating of the TRISO particles

would be acceptable. The quality of nuclear fuel particles produced is strongly impacted by the hydrodynamics of the gas-solid spouted bed, solids flow field and flow regime characteristics. Figure 1.5 shows the schematic of the 2-inch TRISO particles spouted bed at Oak Ridge National laboratory (ORNL). The current spouted bed coating technology and its scaling up and development rely on trial and error and is based on empirical approaches. This makes the robustness of the process and the change in coating characteristics needed for the VHTGRs challenging tasks. Accordingly, fundamental understanding of the underlying phenomena of the gas-solid spouted bed TRISO coater is essential. TRISO fuel particles are designed not to crack due to the stresses from processes (such as differential thermal expansion or fission gas pressure) at temperatures up to and beyond 1600°C, and therefore can contain the fuel in the worst of accident scenarios in a properly designed reactor. Two reactor designs that use TRISO particles are the pebble bed reactor (PBR), in which thousands of TRISO fuel particles are dispersed into graphite pebbles, and the prismatic-block gas-cooled reactor (such as the GT-MHR), in which the TRISO fuel particles are fabricated into compacts (pellets) and placed in a graphite block matrix. Both of these reactor designs are high temperature gas reactors (HTGRs). These reactors represent the very high temperature reactors (VHTRs), as one of the six candidates for the Generation IV nuclear reactors that is attempting to reach even higher HTGR outlet temperatures to enhance thermal efficiency (Verfondern et al., 2007).

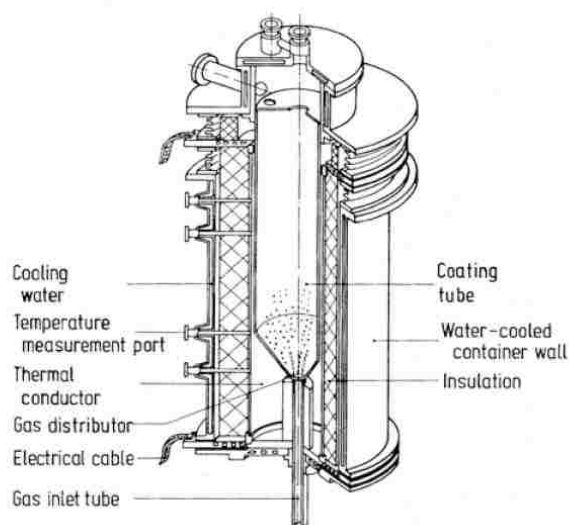


Figure 1.5. Schematic drawing of the 2-inch (5.08-cm)-diameter laboratory TRISO nuclear fuel particle coater used in experiments at ORNL.

1.6 GAS-SOLID SPOUTED BED FOR COATING TRISO NUCLEAR FUEL PARTICLES.

Gas-Solid spouted bed technology has been established as an effective way of contacting between gas and solid particles. Spouted beds are gas-solids granular contactors suitable to handle heavy, coarse, sticky and/or irregularly shaped solids through cyclic flow patterns, to perform well various processes particularly physical transformations processes, such as coating, drying and granulation (Mathur and Epstein, 1974). As high gas velocity arises through the inlet nozzle at the base of the spouted bed, gas forms a jet that picks the particles up and carries them to the top of the bed where the particles returns back to the bed in a continuous circulation. The spouted bed usually contains three distinct regions as illustrated in Figure 1.6: the central spout region, the annulus region and the fountain region. The concentration of particle differs from region to region. In the central spout region, solid particles are pulled from the annulus region and are carried with gas to the

fountain region. In the annulus region the particles move downward as packed bed and their concentration at the maximum. At the top of the bed the particles form fountain where they fall down to the annulus region. It is clear that such flow pattern leads to a complex recirculation flow and gas-particle interactions.

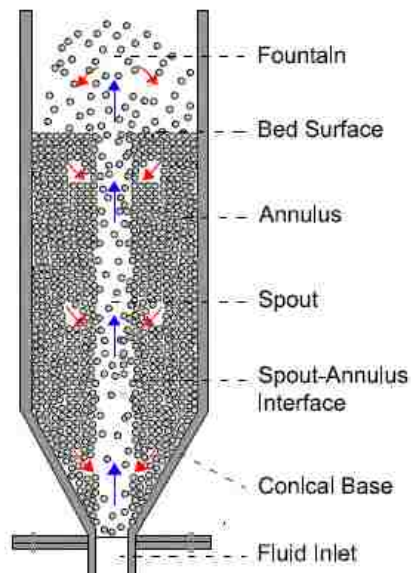


Figure 1.6. Schematic of a cylindrical with cone based and conical spouted bed and the three distinct regions.

1.7 MOTIVATION

As mentioned earlier TRISO nuclear particle is the nuclear fuel for very high temperature reactor (modular reactor, pebble bed reactor, and prismatic bed reactor). These are promising and are being developed for generation four nuclear reactor. They use TRISO nuclear fuel particle, manufacture as mentioned earlier in gas-solid spouted beds. However, currently TRISO nuclear fuel particles have been manufactured in small spouted bed. Spouted bed (3" up 8" inch) has been studied in various literature studies (computation

and experimentation), and due to the need for commercialized in larger scale spouted bed, scale-up approaches and methodologies have been proposed. Spouted beds have plenty complex features making the scale-up from laboratory to full scale systems are very challenging. Initially, (Glicksman, 1984) investigated the scaling relationship of fluidized beds reactor based on dimensional analysis. (Glicksman, 1984) derived his set of scaling groups by non-dimensionalize the combined of two fluid equations of motion. (He et al., 1997) investigated two different sizes of spouted bed at two different temperatures, the ambient temperature and the elevated temperature. (He et al., 1997) also modified the first scale up methodology of the original fluidized bed (Glicksman, 1984) to have a new full set of scaling groups of spouted bed. The complex behavior of solids dynamic in spouted bed creates three different regions (the spout, the annulus, and the fountain); make the need to add two new dimensionless parameters, the internal friction angle and the loose packed voidage to the initial scale up groups of fluidized bed. The dimensionless fountain heights, the dimensionless spout diameter, and the dimensionless pressure profile. (Du et al., 2009) added more progress on the scale up study by investigating the scaling parameters experimentally on two different sizes of spouted bed, 80 mm and 120 mm in diameter. Solid stress analysis used to change the has been made for (He et al., 1997) primarily set of parameters to come up with new set of scale up parameters. The new set of parameter has been presented in (Du et al., 2009) work is the coefficient of restriction of particles that values for the effect of particle- particle collisions in the spout region of a spouted bed. (Aradhya, 2013) assessed the study of the first proposed scaling groups of spouted beds by (He et al., 1997). Optical probe was used in this study to evaluate limited parameters of hydrodynamics of spouted beds. Moreover, new scale up method was proposed and

investigated in this study. (Aradhya, 2013) counts on the similarity of the gas holdup radial profile. In spite of the meaningful and valuable study of (Aradhya, 2013), there are a number of short coming in this study:

- A point measurements using optical fiber probe, produced limited information (velocity up word, velocity down word, and local solid consecration which is converted to solid hold up by calibration method).
- Invasive technique.

The needs are to asses this mechanistic methodology that developed by Dr. Al-Dahhan (Al-Dahhan, DOE Proposal DEFC07-07ID14822) and (Aradhya, 2013) in more detailed solid dynamic. Which means that 3D structure of the solid dynamics and flow pattern (solids hold up distribution, solids velocity component and resultant velocities and their time series fluctuation, turbulent parameters, Reynolds stress, turbulent kinematics, etc) to do this advanced non-invasive measurement techniques that can operate in opaque system which has not been yet implemented. Such technique for assessing and studying the newly developed scale up methodology by (Aradhya, 2013) and Dr. Al-Dahhan (Al-Dahhan, DOE Proposal DEFC07-07ID14822) that mentioned above. Therefore this is the focus of this thesis work.

1.8 OBJECTIVES

The main objectives of this work are to asses and to validate for the first time in details using non-invasive gamma ray commuted tomography (CT) and radioactive particle tracking techniques (RPT) for the following scale-up methodologies for hydrodynamic similarity of gas-solid spouted beds:

1. The newly developed mechanistic scale-up methodology of (Aradhya, 2013) based on matching the radial profile or cross sectional distribution of gas hold-up which dictate the dynamics of the gas-solid spouted bed.
2. The reported methodology of the work of (He et al., 1997) and (Du et al., 2009) based on matching selected dimensionless group.

The objectives are outlined below:

1. Implementing gamma ray computed tomography (CT) technique to measure the cross sectional distribution and the radial profile of the gas and solids holdups along the bed height of the studied gas-solid spouted beds (3 and 6 inch in diameters). This includes the following evaluation and analysis:
 - 1.1. Evaluating the cross sectional distributions and radial profiles of the gas and solids holdups according to the conditions proposed by for matching the radial profiles of the gas and solids holdup which were measured by optical fiber probe at the cylindrical section of the spouted beds. Matching the radial profiles or cross-sectional distribution of the gas and solids holdups represents the basis for the newly developed scale-up methodology for hydrodynamics similarity. If needed, the conditions of the experiment could be adjusted to obtain closer holdups profiles or cross-sectional distribution based on the CT measurements.
 - 1.2. Assessing and validating the newly developed mechanistic scale-up methodology based on comparing the dimensionless spout diameter along the bed height, fountain structure in terms of radial profile and cross-sectional distribution of solids holdups.

2. Assessing the scale-up methodology based on matching the dimensionless groups of (He et al., 1997) and (Du et al., 2009) by utilizing two conditions; one consists of pair of conditions with matching dimensionless groups and another consists of pair of conditions with non-matching dimensionless groups. The following measured parameters will be used for assessment:
 - 2.1. Radial profile and cross-sectional distribution of the gas and solid holdups along the bed height including the fountain region.
 - 2.2. Dimensionless spout diameter along the bed height.
3. Implementing Radioactive Particle Tracking (RPT) technique to measure in details the 3D the local solids velocity, field and its components, flow pattern, turbulent kinetic energy, shear stresses, and normal stresses of the studied gas-solid spouted beds (3 and 6 inch in diameter). newly developed mechanistic scale-up methodology and the one based on matching dimensionless groups for hydrodynamics similarity. This includes the flowing evaluation and analysis:
 - 3.1. Evaluating and validating the newly developed mechanistic scale-up methodology of (Aradhya, 2013) that is based on matching the radial profiles or cross-sectional distributions of gas holdup to achieve the similarity in the hydrodynamics.
 - 3.2. Evaluating the scale-up methodology of (He et al., 1997) and (Du et al., 2009) that is based on matching selected dimensionless groups to achieve hydrodynamics similarity.

2. LITERATURE REVIEW.

The very high temperature reactors (VHTR's) (such as pebble bed and prismatic bed nuclear reactors) are among the leading nuclear reactors for the fourth generation of nuclear reactors. Fundamental safety and efficient performance of these reactors significantly depend on the TRISO-coated fuel particles. In particular, the quality of the coating layers of the TRISO particles are designed to sustain very high temperatures and to prevent the release of fission products that are produced during the fission process under normal or off-normal operation conditions. Therefore, nuclear industry are required today to manufacture zero failure TRISO fuel particles in the near future to commercialize these reactors and to enhance the level of passive safety to meet strict licensing requirements. At the same time, producing large number of TRISO fuel particles should also be destined for large VHTR plants. Gas-solid spouted beds are the units of choice to manufacture the TRISO fuel particles. Proper gas-solid contacts in spouted beds are required during the coating process, which consists of four layers as outlined earlier. Integrity, quality, and uniformity of the layers during the coating process are significantly impacted by the hydrodynamics of spouted beds. It has been shown that the hydrodynamics of spouted beds vary with the size of the bed. Therefore, it is unknown what would happen to the hydrodynamics of the spouted bed coater and hence to the quality of the coating when these TRISO particles are produced in a commercial scale to fulfill the needs for commercialization of the 4th generation nuclear energy. Accordingly, fundamental understanding of scale-up and hydrodynamics of the spouting phenomena of the spouted beds are essential. Unfortunately, there is a lack in such understanding due the complex interaction between the gas phase and solid particles and the limited applications of

advanced measurement techniques. In addition there is limited number of studies that have been focused on the scale up of spouted beds despite there are many investigations in the literature on these contactors. Since this study focuses on evaluation of scale-up methodologies using advanced measurement techniques where detailed local hydrodynamic parameters can be measured, the literature review in this chapter has been focused on only the scale-up of spouted bed and the related gas-solid systems. In the following subsection, the newly developed scale-up methodology in our laboratory (Aradhya, 2013) will be discussed first. Since, the reported literature on the scale-up of spouted bed was based on the earlier development of scale-up methodologies of gas-solid fluidized beds, the related literature on the scale-up of fluidized beds will be outlined as well.

2.1 REVIEW OF THE NEW SCALE-UP METHODOLOGY.

In our laboratory a new methodology for scale-up of spouted bed has been developed and assessed by (Aradhya, 2013). The method is based on a mechanistic approach. In spouted bed the dynamics of the spouted beds are dictated by the gas dynamics, which is affected by the cross-sectional distribution, or radial profile of the gas hold-up inside the bed. This is similar to its role in fluidized beds and in bubble columns (Shaikh and Al-Dahhan, 2003, 2005; Zaid, 2013). Accordingly, the new methodology of scaling up gas-solid spouted beds is based on having closer radial profile or cross-sectional distribution of the gas holdup in order to achieve close hydrodynamics similarity in form of absolute values or dimensionless parameters. Once the hydrodynamics similarity is achieved, the performance of spouted bed for coating TRISO fuel particles should be maintain similar or closer to the smaller size beds or to the beds that are operated at

different conditions. To assess the newly proposed scale up methodology, (Aradhya, 2013) used newly developed sophisticated optical fiber probes for point measurements local solids hold-up and solids velocity simultaneously and their time series. By extensive experimentation and trials and errors, (Aradhya, 2013) was able to identify the conditions where the radial profile of gas hold-up are closer in 3 inch and 6 inch spouted beds. Also the conditions that provide different magnitudes and profiles (and cross sectional distribution) of gas holdup were identified. Table 2.1 summarizes these conditions. Figure 2.1 and Figure 2.2 illustrate samples of these results. For clarity, these figures were taken from the thesis of (Aradhya, 2013).

Table 2.1. Experimental Conditions for similar and non-similar gas holdup radial profiles for the hydrodynamics similarity of spouted beds identified by (Aradhya, 2013).

Condition/Case	A (Reference case) He et al. (1997)	Similar gas-holdup profiles (ϵ_g) _r	Non-similar gas-holdup profiles (ϵ_g) _r
D_c (m)	0.152	0.076	0.076
D_i (mm)	19.1	9.5	9.5
L (m)	1.14	1.14	1.14
H (m)	0.323	0.16	0.16
T (K)	298	298	298
P (kPa)	101	364	101
Particles	Glass	Steel	Glass
d_p (mm)	2.18	1.09	1.09
ρ_s (kg/m ³)	2400	7400	2450
ρ_f (kg/m ³)	1.21	3.71	1.21
μ (x 10 ⁵) (Pa.s)	1.81	1.81	1.81
U (m/s)	1.08	0.64	0.74

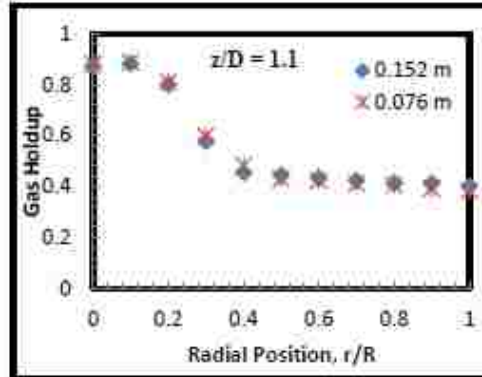


Figure 2.1. Gas holdup profiles for the conditions for similar radial profile of gas holdup in 0.152 m and 0.076 m spouted beds at $z/D = 1.1$ measurement level. $z/D = 1.1$ (means $z = 83.6$ mm from the inlet of ID = 0.076 m and $z = 167$ mm from the inlet of ID = 0.152 m of used spouted beds).

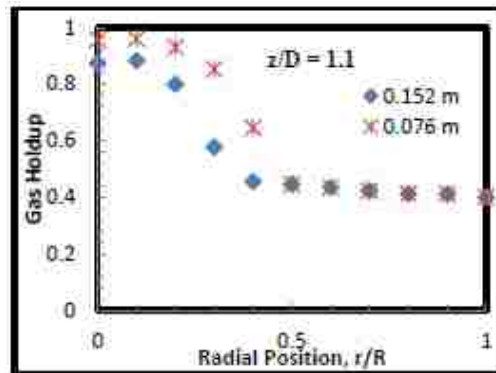


Figure 2.2. Gas holdup profiles for the conditions for non similar radial profile of gas hold-up in 0.152m and 0.076m spouted bed at $z/D = 1.1$ measurement level. $z/D = 1.1$ (means $z = 83.6$ mm from the inlet of ID = 0.076 m and $z = 167$ mm from the inlet of ID = 0.152 m of used spouted beds).

The newly developed optical probe was implemented on these conditions to measure the local solids velocity at selected locations along the radius of the bed to assess and to confirm the proposed methodology (Aradhya, 2013). Figure 2.5 and Figure 2.6 demonstrate the success of such new mechanistic methodology. It is obvious due to the properties of the bed and its dimensions, the absolute values of the solids velocities in spout region vary between 3 inch and 6 inch spouted beds as shown in Figure 2.3 and Figure 2.4.

In the annular region the values of the velocities are the same since the solids are moving downward at slow velocity as a moving bed. However, if these values of the absolute velocities are non-dimensionalized based on minimum spout velocity, the hydrodynamics similarity is achieved as shown Figure 2.5. Figure 2.6 shows that when the profile of gas holdup and magnitudes differ the local solids velocities vary.

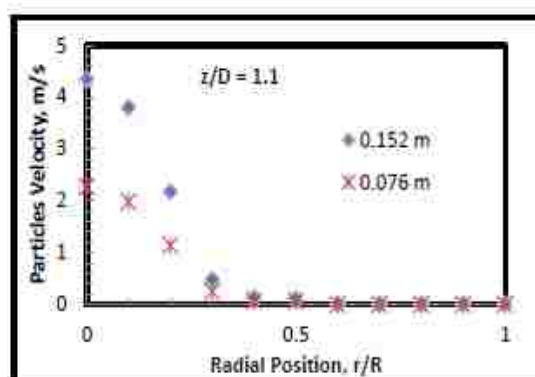


Figure 2.3. Particle velocity profiles for the conditions for similar radial profile of gas hold-up of 0.152 m and 0.027 m of spouted beds at $z/D = 1.1$ measurement level.

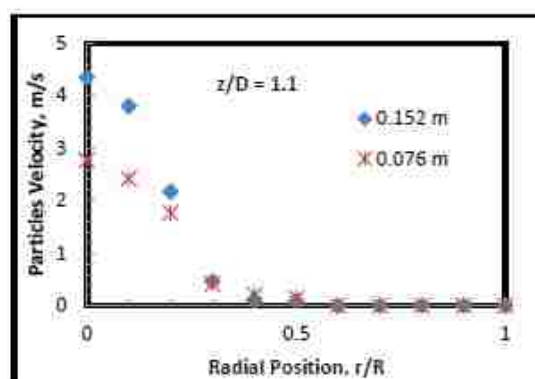


Figure 2.4. Particles velocity profiles for the conditions for the non-similar profile of gas hold-up in 0.152 m and 0.076 m spouted beds at $z/D = 1.1$ measurement level.

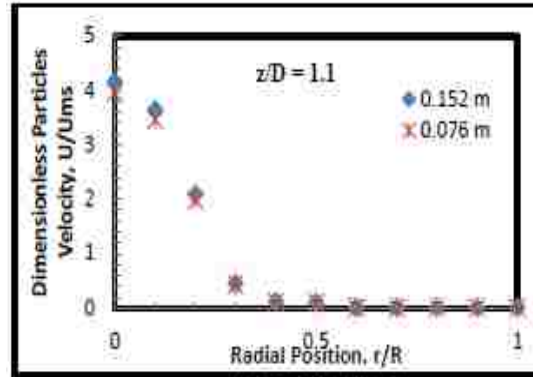


Figure 2.5. The dimensionless particles velocity profiles for the conditions for similar radial profile of gas hold-up in 0.152 m and 0.076 m spouted beds at $z/D = 1.1$ measurement level.

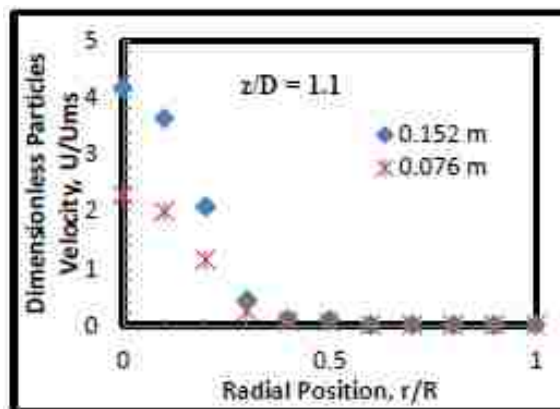


Figure 2.6. Dimensionless particles velocity radial profile for the conditions for non-similar gas hold-up profile in 0.152 m and 0.076 m spouted beds at $z/D = 1.1$ measurement level.

Furthermore, (Aradhya, 2013) demonstrated the similarity in dimensionless spout diameter, dimensionless fountain height, dimensionless bed height, etc. (Aradhya, 2013). However, there are some limitations in the work of (Aradhya, 2013) which is summarized as follows:

- The optical fiber probe is a point measurement and despite it is small it is intrusive and could affect the local measurements of solids holdup and solids velocities.
- It provides only instantaneous solids velocities and time average velocities in the axial direction in upward and downward. It does not provide the solids velocities in radial and angular directions (i.e., 3D velocity field and the resultant and components velocities cannot be found).
- It does not provide any solids turbulent parameters such as normal stresses, shear stresses and kinetic energy in the three regions (the spout, the annulus, and the fountain), which are essential for evaluating the scale-up methodologies and in providing benchmarking data to computational fluid dynamics (CFD).
- It provides only point measurements of spout diameter and it does measure the fountain height and the spout height.

(Aradhya, 2013) measurements despite are invasive, local, and have limitations they are really an important step forward in validating this methodology and to provide some local knowledge about spouted beds. However, in order to truly assess in details the new methodology of scale up and to provide also data for detailed assessment and validation of CFD there is a need to apply non-invasive advanced measurement technique that can provide in 3D detailed local hydrodynamic parameters. Accordingly, this study addresses these needs and overcomes the above limitations by implementing gamma ray computed tomography (CT) technique to image the cross sectional distribution of solids and gas holdups and to obtain radial or diameter holdups profiles and radioactive particle tracking (RPT) technique to measure in 3D the velocity fields and turbulent parameters mentioned above.

2.2 LITERATURE REVIEW OF THE REPORTED SCALE-UP METHODOLOGY BASED ON MATCHING DIMENSIONLESS GROUPS.

(He et al., 1997) extrapolated the (Glicksman, 1984)'s proposed dimensionless groups for scaling up gas-solid fluidized beds to scale up gas-solid spouted beds despite there are significant differences between them particularly in the flow patterns of the solid and the gas phases. Thus, (He et al., 1997) suggested the following dimensionless groups for scaling up and for the hydrodynamic similarity of gas-solid spouted beds:

$\frac{gd_p}{U^2}, \frac{\rho_s d_p U}{\mu}, \frac{\rho_f}{\rho_s}, \frac{H}{d_p}, \frac{D_c}{d_p}, \phi_s, \varphi, \varepsilon_o$ Dimensionless particle size distribution, and dimensionless bed geometry.

Where, gd_p/U^2 is Froude number, $\rho_s d_p U/\mu$ is Reynolds number, ρ_f/ρ_s is ratio of fluid density to particle density, H/d_p is ratio of bed height to particle diameter, D_c/d_p is ratio of column diameter to particle diameter, ϕ_s is sphericity of particles, φ is inertial friction angle of particle, °, and ε_o is loose packed voidage.

These dimensionless groups cover the low, intermediate and high Reynolds number ($Re = \rho_f d_p U/\mu$) (Glicksman, 1984; He et al., 1997). In spouted beds, Re could be in the order of 100. However, in the spout region and in large columns, Re can be as high as 3000. With such wide range of Re in various regions of the spouted beds (spout, annulus and fountain), it is not suitable to eliminate dimensionless groups of the list above based on low, high and intermediate Re number as (Glicksman, 1984) proposed. This in fact represents one of the uncertainties in extrapolating the dimensionless groups for scaling up fluidized beds to scaling up spouted beds. (He et al., 1997) added two additional dimensionless parameters which are the internal friction angle (φ) and the loose packed bed voidage (ε_o), to achieve mechanical similarity in the annular region of the spouted bed

based on the findings of (Sokolovskii, 1965). Since the particles in the spouted beds are always larger than 1 mm, the non-dimensional coefficient of cohesion, which was also proposed by (Sokolovskii, 1965) for small particles, is neglected (He et al., 1997).

Furthermore, (He et al., 1997) also adopted the simplified set of dimensionless groups proposed by (Glicksman, 1984) for fluidized beds where the group of $(\rho_s d_p U/\mu)$ in the list of the dimensionless group above is replaced by (U/U_{mf}) . Hence, the other list of the simplified dimensionless groups are as follows (He et al., 1997):

$$\frac{U^2}{gD_c}, \frac{U}{U_{mf}}, \frac{\rho_f}{\rho_s}, \frac{H}{d_p}, \frac{D_c}{d_p}, \phi_s, \varphi, \varepsilon_o$$

dimensionless particle size distribution, and dimensionless bed geometry.

(He et al., 1997) reported that matching (U/U_{mf}) is much easier than match $(\rho_s d_p U/\mu)$. Therefore, these two sets of dimensionless groups (Eqs. 8 and 12) were investigated by (He et al., 1997).

To experimentally evaluate this methodology of scale up of spouted bed, they used two different sizes of spouted bed at ambient and elevated pressure. Using these spouted beds, (He et al., 1997) employed conditions where the above dimensionless groups are matched and conditions where various dimensionless groups are varied to examine the effect of such mismatching on the selected dimensionless groups on the similarity of the hydrodynamics. For example Table 2.2 illustrates the conditions that are identified and utilized by (He et al., 1997) at ambient temperature which provide matching and mismatching the above two sets of the dimensionless group (Eqs. 8 and 12). Selected conditions of Table 2.2 (Cases A, B and C) have been employed in this study to evaluate this methodology against the detailed local hydrodynamic parameters measured by the above mentioned non-invasive techniques (i.e., CT and RPT). The condition of the case A

(column A of Table 2.2) is the base case or base conditions. This base condition Case (A) is similar to the case conditions used by (Aradhya, 2013) listed in Table 2.1 above. The conditions of Case B represents the conditions where the dimensionless groups are matched with Case A to validate this proposed methodology and the suggested dimensionless groups for gas-solid spouted beds. Cases C, D, E, F and G represent the conditions where selected dimensionless groups were varied to evaluate their effects on the scale up and hydrodynamics similarity.

Under all these conditions, the spouted beds were operated under stable spouting where (He et al., 1997) reported the following criteria for stable spouting (Chandnani and Epstein, 1986; Epstein, 1968; He et al., 1992; Mathur and Epstein, 1974a). The first criterion was based on the ratio of the inlet orifice diameter to the particle diameter (D_i/d_p) which should be smaller than ($<$) 25~30 (Chandnani and Epstein, 1986)). After (Lim and Grace, 1987) extended the work on a 0.91 m diameter column, they found it is essential to operate with inlet orifice diameters less than about 30 times the mean particle diameter in order to maintain a stable spouting mode within the spouted bed. The second criterion was based on the ratio of the column diameter for small columns to the inlet orifice diameter (D_c/D_i) which should be smaller than ($<$) 3~12 (Mathur and Epstein, 1974b). The third criterion is that the height of the static bed (H) should be smaller than ($<$) the maximum height of the spoutable bed (He et al., 1992).

Table 2.2. The conditions that provide matching and mismatching dimensionless groups identified and used by (He et al., 1997) at ambient temperature.

Condition/run	A	B	C	D	E	F	G
D_c (m)	0.152	0.076	0.076	0.076	0.076	0.076	0.152
D_i (mm)	19.3	9.5	9.5	9.5	9.5	9.5	19.3
L (m)	1.38	1.14	1.38	1.14	1.38	1.14	1.38
H (m)	0.333	0.16	0.333	0.16	0.333	0.16	0.333
T (K)	298	298	298	298	298	298	298
P (kPa)	101	312	101	101	101	101	101
Particles	Glass	Steel	Glass	Glass	Glass	Glass	Steel
d_p (mm)	2.18	1.09	1.09	1.09	2.18	2.18	2.18
ρ_s (kg/m^3)	2450	7400	2450	2450	2450	2450	2450
ρ_f (kg/m^3)	1.21	3.71	1.21	1.21	1.21	1.21	1.21
μ ($\times 10^{-5}$) (Pa s)	1.81	1.81	1.81	1.81	1.81	1.81	1.81
U (m/s)	1.12	0.75	0.75	2.15	1.12	1.12	1.12
Scaling groups							
ϕ_s	1	1	1	1	1	1	0.88
ϕ ($^\circ$)	36	28	36	27	26	26	38
\mathcal{E}_{mf}	0.41	0.42	0.41	0.42	0.41	0.41	0.41
H/D_c	2.1	2.1	2.1	2.1	2.1	2.1	2.1
D_c/D_i	8	8	8	8	8	8	8
D_c/d_p	69.9	69.9	69.9	69.9	35.0	35.0	69.9
ρ_s/ρ_f	1994	1995	2029	2029	648	1994	2003
$Re = \rho_f d_p U / \mu$	168	168	54	157	474	161	162
$U^2 / g d_p$	52.6	52.6	52.6	432	52.6	57.6	52.6
$\rho_s d_p U / \mu$ ($\times 10^{-3}$)	334	334	109	317	317	324	334
$U^2 / g D_c$	0.75	0.75	0.75	6.18	0.75	1.65	0.75
U / U_{mf}	0.92	0.92	0.92	3.37	0.92	0.98	0.92
U / U_{ms}	0.92	0.92	0.92	2.63	0.92	0.66	0.92

It is noteworthy that (He et al., 1997) used the measurement of the global parameters to validate and assess their proposed methodology. These parameters are: H_m , H_m/D_c , dimensionless height (z/H), dimensionless pressure along the bed height (pressure drop at a certain height/overall pressure drop of the bed) (where the pressure was measured at the wall), fountain height (HF), and dimensionless fountain height (HF/ D_c). With these measurements, (He et al., 1997) demonstrated the validation of the full set of the

dimensionless groups listed above (Eqs. 8 and 12) when they are matched between Case B and Case A. When one of the dimensionless groups varied the measured parameters mentioned above varied. The following are selected results taken from (He et al., 1997) (Figure 2.7, Figure 2.8, and Table 2.3) to demonstrated some of their findings and the validation based on the measurement of the global parameters.

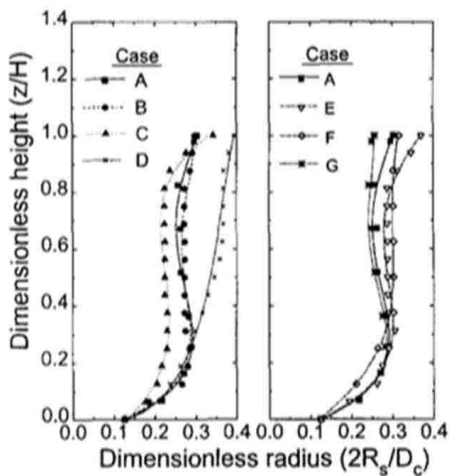


Figure 2.7. Dimensionless spout diameters as a function of dimensionless height for smaller columns (He et al., 1997).

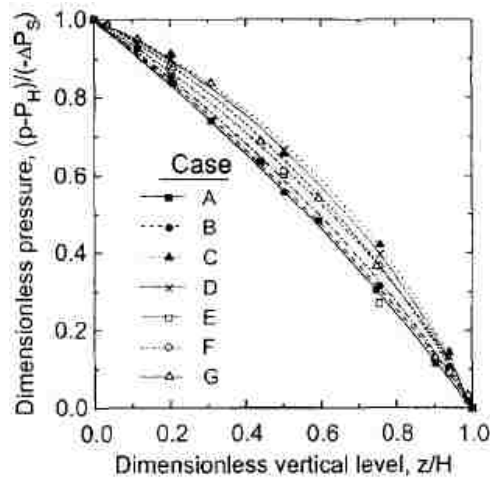


Figure 2.8. Longitudinal pressure profiles in the annulus for columns of diameter 0.076 m and 0.152 m spouted beds.

Table 2.3. Fountain heights for the seven cases outlined in Table 2.2 (He et al., 1997).

Case	Bed height H(mm)	Fountain height H_f (mm)	Dimensionless fountain height, H_f/D_c	Deviation (%)
A	325	135	0.89	-
B	160	59	0.78	- 13
C	160	40	0.53	- 41
D	160	250	1.56	+ 75
E	160	84	1.11	+24
F	160	45	0.59	-34
G	325	300	1.97	+ 122

It is obvious that the experimentation of (He et al., 1997) to validate their proposed scale up methodology has major shortcomings due to relying on global parameters for evaluation, lack of using advanced or sophisticated measurement techniques for local parameters measurements, and limited type of parameters to compare with for validations as mentioned above. Such shortcomings will be overcome by this study as stated earlier. (Shirvanian and Calo, 2004) modified (He et al., 1997)'s scaling up relationships for two dimensional (2D) (rectangular) liquid-solid spouted bed with a draft duct. They found that in the spouted bed, the coefficients of restitution ($e_{ss}= 0.97$) and friction of the particles need to be matched in addition to the other dimensionless groups of (Glicksman, 1984) to maintain hydrodynamics similarity. The friction of the particles is represented by $\tan(\varphi)= 0.092$, where φ is the angle of internal friction. They validated the modified scaling up dimensionless parameters using CFD for a standard case and for small (1/10 of the standard case) and large (10 times the standard case) sizes. They validated the method using the CFD results of the three studied scales in terms of the radial profiles of the dimensionless solids velocity

(solids velocity/inlet fluid velocity), dimensionless fluid velocity (measured by pitot tube), solids volume fraction and fluid volume fraction. However, these hydrodynamic parameters were not measured locally for such validation or to validate the CFD results for small and large scales rectangular spouted beds which represent major shortcomings to adopt such methodology for industrial practice.

According to the above findings, (Xu et al., 2007) modified the (He et al., 1997) dimensionless groups by adding the restitution coefficient (e_{ss}) which is measured experimentally by dropping the particles from a certain height (H_o) and measured by high speed camera the rebounding height (H_1), where $e_{ss}=(H_o/H_1)^{1/2}$. The suggested parameter was based on the analysis of the kinetic energy of colliding particles in the spout and annulus region in spouted bed. They experimentally verified this new set of scaling dimensionless parameters by having spouted beds with matching e_{ss} and spouted beds with mismatching e_{ss} . They used optical probe to measure void and solids fractions, and also they measured dimensionless fountain height and dimensionless spout diameter. Figure 2.9 illustrates the comparison between the conditions of match e_{ss} (Cases A and C) and the conditions of mismatching e_{ss} (Cases A and E). It is obvious that there are some differences and moreover the local solids velocities and turbulent parameters were not measured. This indicates the shortcoming of such validation.

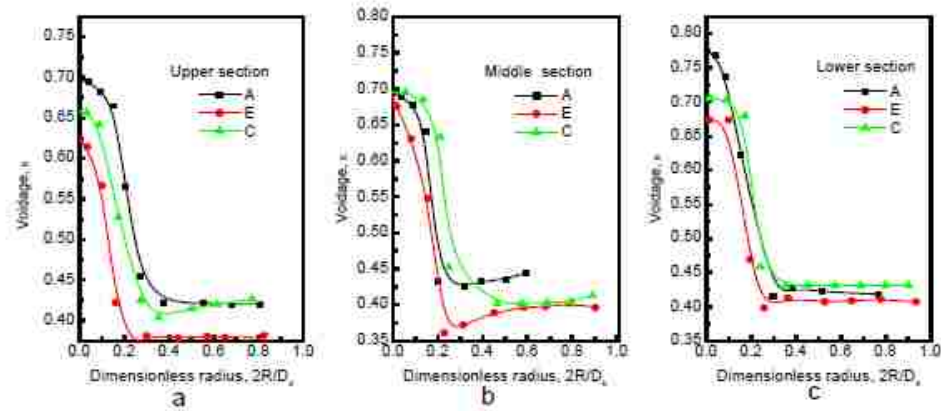


Figure 2.9. Selected results taken from (Xu et al., 2007) that shows the verification of the modified set of scaling dimensionless groups by matching e_{ss} (Cases A and C) and mismatching e_{ss} (Cases A and E).

(Du et al., 2009) proposed the same modification of (Xu et al., 2007) by adding the particles restitution coefficient e_{ss} to the set of the scaling dimensionless group of (He et al., 1997) to be matched in order to attain the hydrodynamics similarity. They reported the same results and findings of (Xu et al., 2007). As mentioned above the results of this research group ((Xu et al., 2007) and (Du et al., 2009)) showed that when all the set of the modified dimensionless groups are closer to each other among the studied cases and condition, the hydrodynamics are closer and when these are a part (not closer to each other) the hydrodynamics are not similar (a part). However, they validated these by measuring the radial profiles of the voidage, the dimensionless fountain height and the dimensionless spout diameter. In this case, the hydrodynamic characteristics like the fountain height, spout diameter, and voidage are closely connected to the coefficients of restitution. Hence, they reported that the coefficient of restitution should be included in the whole set of scale-up relationships of spouted beds. Despite there are some differences (as shown in Figure 2.9 above), they didn't measure the local solids velocities and the turbulent parameters

which are needed for proper verification or assessment. Therefore, such addition of the e_{ss} to the set of the scaling parameters is not yet fully verified.

(Rojas and Deytia, 2011) studied the minimum spouting velocity, fountain height and overall bed pressure drop in shallow spouted beds with dense particles using different spouted bed diameters, bed heights, particles densities and sizes, gas density, and gas flow in ambient temperature and pressure. (Rojas and Deytia, 2011) didn't address or focused on scale up methodology but developed empirical correlations for the above mentioned parameters in terms of selected dimensionless groups that cover different studied bed sizes. In general the dimensionless groups that are used in these correlations to cover various bed sizes of shallow spouted beds are:

$$\text{Archimedes number } Ar = \frac{d_p \rho_f (\rho_g - \rho_f) g}{\mu_g^2}, \text{ Froude number } Fr = \frac{U^2}{gd_p}, \text{ ratio of}$$

static bed height to particle diameter, ratio of particle diameter to bed diameter, ratio of particle density to fluid density, terminal velocity, Reynolds number $Re = \frac{d_p \rho_s U}{\mu_g}$, fluid velocity or dimensionless velocity with respect to the minimum spouting velocity.

It is obvious that these dimensionless groups are directly or indirectly represented in the set of the scaling dimensionless groups proposed by (He et al., 1997). Since these correlations with selected of these dimensionless groups predicted well the minimum spouting velocity, fountain height and over all pressure drop, they could be considered as scaling parameters or scaling relationships for the spouted beds. However, these correlations do not include restitution coefficient (e_{ss}) which was added by ((Xu et al., 2007) and (Du et al., 2009)) to the set of the dimensionless groups of (He et al., 1997). Also these correlations of (Rojas and Deytia, 2011) do not include other parameters listed

in the scaling set of dimensionless groups of (He et al., 1997) such as dimensionless particle size distribution, internal friction angle, loose packed void, and sphericity. This could be due to that these scaling parameters may not be critical for the correlations to predict the minimum spouting velocity, overall pressure drop and fountain height.

In assessment of the dimensionless groups for scaling up to relatively large scale, (Sanderson et al., 2007) evaluated the simplified scaling dimensionless groups of (Glicksman, 1984) and (Horio et al., 1986) in bubbling fluidized beds using ten fold increases in the bed size. Pressure fluctuations were measured at various axial and radial local locations inside the bed. They found that at high gas velocity the local pressure fluctuations obtained in a largest (1.56 m diameter) bed size do not mimic the local pressure fluctuations in a smaller size despite the matching of the dimensionless groups. show these results taken from (Sanderson et al., 2007). These results indicate that this dimensionless group does not capture all the governing phenomena particularly at larger diameter. This means that additional dimensionless groups would be needed. Such finding could be extended to spouted beds where detailed local measurements have not yet been performed. However, the major shortcoming of having large number of dimensionless groups to be matched is that it is difficult to achieve such matching even if it is true for capturing the key phenomena. Therefore, having mechanistic approach as it has been proposed by (Al-Dahhan et al., 2014) could overcome these shortcomings.

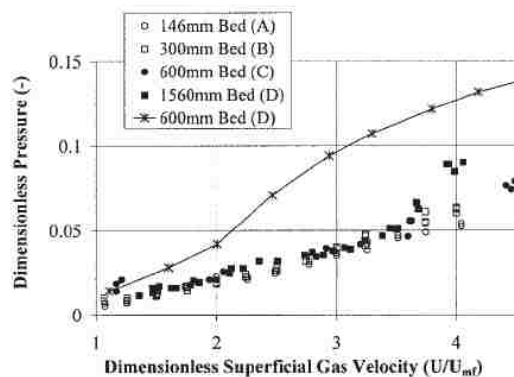


Figure 2.10. Comparison of the dimensionless average absolute deviation of pressure measured from pressure probes located at $h/H_s = 0.77$ and $r/R = 0$ in all five fluidized beds for a range of dimensionless gas velocities.

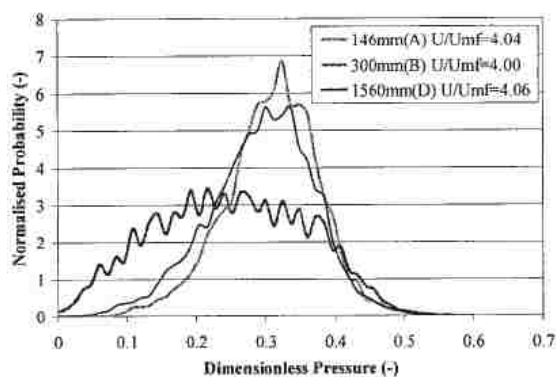


Figure 2.11. Comparison of the normalized probability distributions for the correctly scaled beds (146 mm, material A= 300 mm, material B=1560 mm, material D) at high gas velocity for the probe located at $r/R = 0$ and $h/H = 0.77$.

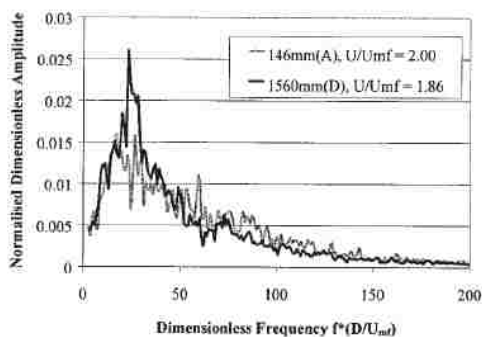


Figure 2.12. Comparison of the dimensionless amplitude spectra from the correctly scaled 146-mm and 1560-mm beds at low gas velocity, with probe located at $r/R = 0$ and $h/H = 0.2$.

It is worth to mention that the experimental work that has been performed so far to assess the proposed scaling dimensionless relationships were based on measuring the global parameters (Du et al., 2009; He et al., 1997; Xu et al., 2007) or measuring local but limited point measurements of solids velocity and holdups (Aradhya, 2013).

Unfortunately, there has been no experimental work that uses advanced measurement techniques to measure in details the three dimensional (3D) distribution in a noninvasive manner the solids and gas holdup , solids velocities, flow field and pattern, solids turbulent parameters which will be addressed in this work.

Furthermore, there is a number of studies in the literature that implemented computational fluid dynamics (CFD) and discrete element method (DEM) to simulate various scales (sizes) of spouted beds. Unfortunately there is either no validation or limited validation to these simulations using limited measurements of global parameters (Béttega et al., 2009; Du et al., 2006a, b; Duarte et al., 2005; Duarte et al., 2009; Gryczka et al., 2009a; Gryczka et al., 2009b; Hosseini et al., 2013; Lan et al., 2012; Li et al., 2012; Moradi et al., 2013; Ren et al., 2011; Rong and Zhan, 2010; Shuyan et al., 2009; Wang et al., 2012; Wang et al., 2013; Wang et al., 2006; Yang et al., 2014; Zhonghua and Mujumdar, 2008). Thus, the detailed local measurements of the hydrodynamics mentioned above to assess properly the reported scaling up methodologies will be in addition valuable benchmarking data and knowledge to properly and reliably evaluate and validate these CFD and DEM simulations which are lacking at this time and hence will be as well addressed in this work.

PAPER**I. Demonstrating the non-similarity in local holdups of gas-solid spouted beds obtained by CT with scale-up methodology based on dimensionless groups.****(CT)**Neven Ali^a, Thaar Al-Juwaya^a, Muthanna Al-Dahhan^{ab*}^aNuclear Engineering,^bChemical and Biochemical Engineering,

Missouri University of Science and Technology (Missouri S&T) – Rolla

Rolla, MO 65409

Abstract

The common scale-up methodology for gas-solid spouted bed that has been reported in the literature is based on matching dimensionless groups. This methodology has been validated by measuring global hydrodynamic parameters and non-validated by limited point measurements of solids holdup and velocity. Therefore, the purpose of this work is to implement our advanced non-invasive gamma-ray computed tomography (CT) technique to assess and to demonstrate that the reported set of the dimensionless groups are not adequate in capturing all the interplay phenomena for achieving similarity in local solids and gas holdups cross-sectional distributions and their radial profiles along the bed height measured in 0.076 and 0.152 m spouted beds. The results clearly identified the three regions (spout, annulus, and fountain) of gas–solid spouted beds and their solids structure. In addition, the reported results are valuable as a benchmarking data for CFD and DEM simulations.

*Corresponding author:

Tel.: +1 573 341 7518; fax: +1 573 341 4377.

E-mail addresses: aldahhanm@mst.edu

Keywords Scale-up; Spouted beds; Gamma ray computed tomography (CT); Cross sectional distribution; phase holdup

1. Introduction

Spouted beds are gas-solid granular contactors suitable to handle heavy, coarse, sticky, and/or irregularly shaped solids through cyclic flow patterns. Gas-solid spouted beds have various industrial applications, particularly physical transformation processes such as coating, drying, and granulation and chemical transformations such as gasification and other reaction processes (Mathur and Epstein, 1974a). These contactors have recently been applied in manufacturing TRISO (tristructural-isotropic) nuclear fuel particles for the 4th generation of nuclear energy using chemical vapor deposition (Lee et al., 2008; Liu et al., 2012; Sawa and Ueta, 2004; Tang et al., 2002). The gas-solid interactions in these spouted beds are complex. The gas is introduced through the inlet nozzle at the base of the spouted bed to form a jet that picks the particles up from the annulus region and carries them to the top of the bed forming fountain where the falling particles return to the annulus region of the bed in a continuous circulation. Hence, three distinct regions, as illustrated in [Figure 1](#), exist in gas-solid spouted beds: the central spout region, the annulus region, and the fountain region. In general, the spouted beds consist of a conical base and a cylindrical column or the whole bed is a conical configuration.

Due to the complex interactions among the phases (gas-solid, solid-solid), the scale-up and design of these contactors/reactors are challenging. Furthermore, most of the studies have focused on measuring the global parameters due to the lack of availability and

implementation of advanced non-invasive measurement techniques that can measure local hydrodynamics. Thus, the knowledge and understanding of the interplay hydrodynamics of the spouted beds are limited. Accordingly, the scale-up approaches and methodologies that have been proposed in the literature are based on matching dimensionless groups. He et al. (1997) extrapolated the dimensionless groups proposed by (Glicksman, 1984) for scaling up gas-solid fluidized beds to scale-up gas-solid spouted beds despite their significant differences of the flow patterns of the solids and gas phases. He et al. (1997) suggested the following dimensionless groups for scaling up and for the hydrodynamic similarity of gas-solid spouted beds:

gd_p/U^2 , $\rho_s d_p U/\mu$, ρ_f/ρ_s , H/d_p , D_c/d_p , ϕ_s , ϕ , ϵ_o , dimensionless particle size distribution and dimensionless bed geometry.

He et al. (1997) added two additional dimensionless parameters which are the internal friction angle (ϕ) and the loose packed bed voidage (ϵ_o), to achieve mechanical similarity in the annular region of the spouted bed based on the findings of (Sokolovskii, 1965). Since the particles in the spouted beds are always larger than 1 mm, the non-dimensional coefficient of cohesion, which was also proposed by (Sokolovskii, 1965) for small particles, is neglected (He et al., 1997).

He et al. (1997) evaluated experimentally this methodology by using two different sizes of spouted beds at ambient and elevated pressure. They employed conditions where the above dimensionless groups were closely matched and conditions where the dimensionless groups were varied to examine the effect of mismatching of the selected dimensionless groups on the similarity of the hydrodynamics. The spouted beds were operated under all these conditions and at stable spouting. It is noteworthy that (He et al.,

1997) used the measurement of the global parameters to validate and assess their proposed methodology. These parameters were maximum spoutable depth (H_m), dimensionless maximum spoutable depth (H_m/D_c), dimensionless height (z/H), dimensionless pressure along the bed height (pressure drop at a certain height/overall pressure drop of the bed where the pressure was measured at the wall), fountain height (H_F), and dimensionless fountain height (H_F/D_c). With these measurements, (He et al., 1997) demonstrated the validation of their set of the dimensionless groups mentioned above. In this study, we have overcome the shortcoming of the evaluation by measuring the global parameters.

Du et al. (2009) modified the scaling of dimensionless groups of (He et al., 1997) by adding the restitution coefficient (e_{ss}) which was estimated experimentally by dropping the particles from a certain height (H_o) and measured by high speed camera the rebounding height (H_1), where $e_{ss} = (H_o/H_1)^{1/2}$. The suggested parameter was based on the analysis of the kinetic energy of colliding particles in the spout and annulus region in spouted beds. They experimentally verified this new set of scaling dimensionless parameters by having spouted beds with matching e_{ss} and spouted beds with mismatching e_{ss} . They used an optical probe to measure voidage profiles, fountain height, and spout diameter and showed that these parameters were closely related to the coefficients of restitution. However, the uncertainty in the measurement of e_{ss} has not been quantified. Furthermore, apart from the measurement of the void profiles, the rest of the measured parameters for the assessment are global parameters. In addition, limited measurement points were taken. Also, the optical probe used would introduce some limitations such as disturbance also the probe's tip, size, design and assembly. These limitations were evident through the experimental results of (Du et al., 2009) where an error was observed on the voidage profiles at the

middle section of the spouted beds. Their complicated voidage distributions in the middle section of the beds may be attributed to the measurement errors (Du et al., 2009). In addition, another disadvantage of their used would be weak light transmission between the tips of the probe when the probe used in dense flow region, which makes this technique ineffective for dense flow system. Since the uncertainty in the estimation of the e_{ss} has not been quantified, it has not been considered as in this work as part of the set of the scaling dimensionless groups.

Aradhya (Aradhya, 2013) demonstrated the non-similarity of the solids hold up by limited local point measurements using a new small optical fiber probe when the dimensionless groups proposed by (He et al., 1997) were matched. In spite of the meaningful and valuable efforts of (Aradhya, 2013) to evaluate this methodology, there are still some limitations for in detailed evaluating such method. These limitations include invasiveness of the probe, which would affect the local measurements of the solids and gas holdups, and its point measurement nature of the solids holdup and the spout diameter. Unfortunately, there has been no experimental work that used advanced measurement techniques to measure the distribution of the solid, and gas holdups in detail and in a noninvasive manner to assess properly the scale-up methodology that is based on matching dimensionless groups. Accordingly, the purpose of this work is to address for the first time these needs, overcome the above-mentioned limitations, and to demonstrate the non-similarity in local holdups when the set of dimensionless groups of (He et al., 1997) has been matched, by implementing our gamma-ray computed tomography (CT) technique to image the cross-sectional distributions of solids and gas holdups along the bed height and provide the holdups radial profiles.

It is noteworthy that a number of studies implemented computational fluid dynamics (CFD) and the discrete element method (DEM) to simulate various sizes of gas-solid spouted beds. Unfortunately, assessment for validation of these simulations was made using limited measurements of global parameters (Béttega et al., 2009; Du et al., 2006; Duarte et al., 2005; Duarte et al., 2009; Gryczka et al., 2009a; Gryczka et al., 2009b; Hosseini et al., 2013; Lan et al., 2012; Li et al., 2012; Moradi et al., 2013; Ren et al., 2011; Rong and Zhan, 2010; Shuyan et al., 2009; Wang et al., 2014; Wang et al., 2006; Yang et al., 2014; Zhonghua and Mujumdar, 2008). Therefore, our detailed local measurements of the cross-sectional distribution and radial profiles of solids and gas holdups will be valuable benchmarking data to evaluate and validate these CFD and DEM simulations.

2. Experimental Work

2.1 Experimental Set-up of Spouted Beds

The experimental works were carried out in two spouted bed cylindrical columns with a conical base made of Plexiglas with inner diameters of 0.076 m and 0.152 m. The schematic diagrams of the two spouted beds are shown in [Figure 2](#). We designed both columns to be geometrically similar with a height of 1.14 m and a conical base at a 60-degree angle. The two columns were designed without any ports or connections on the wall to eliminate the possibility of any non-symmetric problems that complicate the CT reconstruction process. A high open area gas distributor made of stainless steel was placed at the bottom of the conical base to hold the particles and at the mean time to pass the jet of the gas through the bed. The diameters of the inlet orifice were 9.5 mm for the 0.076 m

spouted bed, and 19.1 mm for the 0.152 m spouted bed. The gas used was dry compressed air supplied from an industrial compressor with a capacity of up to 735 CFM and 200 Psig. The gas flow rate was regulated using a pressure regulator and a rotameters setup that consisted of two rotameters connected in parallel.

It is very important to sustain stable spouting in the spouted bed by satisfying a three criteria or conditions in the operation of the spouted beds. The first criterion was based on the ratio of the inlet orifice diameter to the particle diameter (D_i/d_p) which should be smaller than ($<$) 25~30 (Chandnani and Epstein, 1986)). After (Lim and Grace, 1987) extended the work on a 0.91 m diameter column, they found it is essential to operate with inlet orifice diameters less than about 30 times the mean particle diameter in order to maintain a stable spouting mode within the spouted bed. The second criterion was based on the ratio of the column diameter for small columns to the inlet orifice diameter (D_c/D_i) which should be smaller than ($<$) 3~12 (Mathur and Epstein, 1974b). The third criterion is that the height of the static bed (H) should be smaller than ($<$) the maximum height of the spoutable bed (He et al., 1992).

2.2 Experimental conditions

Three different sets of experimental conditions were selected from (He et al., 1997) study which provide matching and mismatching scaling dimensionless groups. This is to evaluate the methodology of achieving hydrodynamics similarity in two different flow fields when the above-mentioned independent dimensionless groups are matched provide that the two flow fields are geometrically similar. The selected experimental conditions include the properties of the particles used and the operating conditions, which are listed

in Table 1. Case A was proposed as the reference case. Hence, the conditions of Cases A and B were taken to match as close as possible the dimensionless groups between the two cases to examine the validity of the scaling dimensionless groups. The conditions of Case C were selected to examine the influence of mismatched scaling groups. The initial bed height (H) and the inner column diameter (D_c) in Case C were 0.16 m and 0.076 m, respectively, in order to achieve similarity with Case A only on the bed dimensionless groups. The values of scaling groups H/D_c , D_c/D_i , and D_c/d_p of Case C were equal to those of Case A. However, two important groups of Case C were not matched with those of Case A: Reynolds number and Froude number. The Reynolds numbers for Cases A and C were 157 and 54, respectively. The Froude numbers for Cases A and C were 54.5 and 51.2, respectively. Subsequently, Cases A and B were designated as Cases of matching dimensionless groups, and Cases A and C were designated as Case of mismatched dimensionless groups.

2.3 Dual Source Gamma Ray Computed Tomography (DSCT).

Our single and dual gamma-ray computed tomography techniques have been used to visualize various multiphase flow systems (Al-Dahhan, 2009; Al-Dahhan et al., 2007; Bhusarapu et al., 2006; Chen et al., 1999; Kemoun et al., 2001; Kumar et al., 1995; Liu et al., 2011; Luo and Al-Dahhan, 2010; Prasser et al., 2003; Rados et al., 2005; Roy and Al-Dahhan, 2005; Roy et al., 2005; Shaikh and Al-Dahhan, 2005; Varma et al., 2008). In this work, we used single source (Cs-137) gamma-ray computed tomography, which is part of the dual source gamma-ray computed tomography (DSCT) technique available in our laboratory. For two-phase flow (e.g., gas-solid, liquid-gas, or liquid-solid) systems, only

single source is needed to distinguish between the two phases, which is termed here as gamma ray computed tomography (CT) technique. However, (gas, liquid and solid) the two sources of the DSCT technique are used to determine the phases volume fraction distributions of three phases which are in dynamic movement. [Figure 3](#) shows the DSCT and the related CT techniques. The details of the mechanical assembly, the electronics data acquisition and the setup, and the operation are not presented here but they can be found elsewhere (Varma, 2008).

The source is collimated to have a fan beam shape with a fan angle of 40° . In the opposite of the source, 15 sodium Iodide (NaI) scintillation detectors are arranged in an arc plate. The CT technique can accommodate a column with a diameter up to 0.762 m. The detectors are collimated using a 2 mm width and 5 mm height slit collimator device attached to each detector. The detectors are 802 Canberra model, consisting of 5.08×5.08 centimeters of cylindrical NaI scintillation crystal, a photomultiplier tube (PMT), an internal magnetic or light shield, aluminum housing, and a 14-pin connector. Each detector is followed by a Canberra preamplifier, which is excited at 900V from a high power supply. The detected signal, from the preamplifier is then amplified using a timing amplifier. The signal is processed and recorded using a multilevel discriminator and a scaler. The detectors arrays are used to collect the unattenuated photons of the gamma rays that pass through the multiphase experimental setup. The source and the detectors array are both mounted on a rotational plate that moves them 360° around the investigated column, offering 197 views in each scan and 21 projections in each view. This rotational plate is connected to another plate that moves axially to selected level position to take the scan along the bed height to produce 2-dimensional and 3- dimensional images. The Cs-137

sealed source (with gamma photon energy of 0.662 MeV) was used for the spouted bed experiments. The activity of Cs-137 was about 200 mCi at the time of the experiments. The counts for each projection were collected by the collimated detectors for 60 samples at 20 Hz to collect enough counts and to reduce noise to signal ration. The means for the data points of each projection, for each sampling method and all scans performed are obtained. The mean value for all the counts based on multiple samples of a given projection is used to process the data.

To acquire the data needed for the CT reconstruction; complete sets of CT scans are performed in each experiment that aims to obtain the phase holdup distribution. These scans include those when the column is under the desired conditions of the gas-solids spouted bed operation (i.e. the actual test), the column is filled with solids as a packed bed (i.e. spouting gas is absent), and a reference one that is made up when the column is empty (i.e. full of air only). The data obtained from the scans are interpreted in terms of Beer-Lambert's law (equation (1)) and used in the reconstruction process.

$$I(y) = I_o(y) \exp \left[\sum_{x \in X} -h(y | x) \mu(x) \right] \quad (1)$$

The reconstruction domain of the bed was discretized by pixels. Cross-section of a given spouted bed column is encompassed by a square matrix of pixels with dimensions of (n) rows x (m) columns pixels. The size of the pixels depends on the size of spouted bed column and the achievable spatial resolution of the CT scanner (i.e. the detector collimator width). An even number of pixels is needed on each side of the matrix, and hence a suitable number of pixels were selected. The corresponding size of pixels were respectively, 80 x 80 and 40 x 40 for 0.152 m and 0.076 m spouted beds.

For image reconstruction, an alternating minimization (AM) algorithm was applied to reconstruct the effective attenuation coefficient $\hat{\mu}_{s-g}(x)$ in equation (2) for gas-solid spouted beds. The index x in $\hat{\mu}_{s-g}(x)$ refers to each pixel in the image domain. The AM was developed by (O'Sullivan and Benac, 2007) and implemented by (Varma, 2008; Varma et al., 2008) for imaging two-phase systems when a single gamma source is used. The target throughout the AM algorithm is to reformulate the maximum-likelihood estimation problems into the minimum Kullback-Leibler divergence (I-divergence or information divergence) (Csiszár, 1975) and tackle it algorithmically in iterative process. More details and mathematical proofs regarding the AM algorithm are not discussed here but they can be found elsewhere (O'Sullivan and Benac, 2007; Varma et al., 2008).

Algorithmically, the AM is an iterative process, and should start with some initial values in each pixel, and then iteratively adjust them to explore for the effective attenuation coefficient $\hat{\mu}_{s-g}(x)$ values for the pixels. For the pixels outside the spouted bed domain, zero is assigned as shown in [Figure 4](#). With the aid of equation (1) and the AM algorithm, the effective attenuation coefficient is obtained from the transmission ratio $(I(y)/I_o(y))$ and the known chord length $h(y/x)$ for each pixel. Once $\hat{\mu}_{s-g}(x)$ for each pixel is obtained by reconstructing the image from the entire set of projection measurements, the next step is to calculate the phase volume fractions or phase holdups for gas-solid spouted beds as outlined below.

For holdup calculation of a two-phase system, gas-solid spouted bed in this case, $\mu(x)$ in equation (2) below represents the attenuation value, and ε represents the holdup fraction for each phase. The total mass attenuation coefficient in equation (2) equals the

sum of the individual phase mass attenuation coefficients weighted by the respective volume fraction. Consequently,

$$\hat{\mu}_{s-g}(x) = \hat{\mu}_s(x)\varepsilon_s(x) + \hat{\mu}_g(x)\varepsilon_g(x) \quad (2)$$

Where, x is the index of pixel (image coordinate), $\hat{\mu}_{s-g}(x)$ is the effective attenuation value for the gas-solids when the system is dynamic at the desired operating condition, $\hat{\mu}_s(x)$ is the attenuation value for pure solids phase (column contains solids only and spouting gas is absent), $\hat{\mu}_g(x)$ is the attenuation value for pure gas phase (empty column), $\varepsilon_s(x)$ is the solids phase fraction (or solids holdup), and $\varepsilon_g(x)$ is the gas holdup fraction (or gas holdups). Then if we assume $\hat{\mu}_g(x)$ is neglected (attenuation for gas is very small at 0.662 MeV). Hence, equation (2) will become,

$$\hat{\mu}_{s-g}(x) = \hat{\mu}_s(x)\varepsilon_s(x) \quad (3)$$

The sum of the phase holdups is equal to unity ($\varepsilon_s + \varepsilon_g = 1$). if we replace ε_s by $1 - \varepsilon_g$, the gas holdup becomes equal to

$$\varepsilon_g(x) = \frac{\hat{\mu}_s(x) - \hat{\mu}_{s-g}(x)}{\hat{\mu}_s(x)} \quad (4)$$

And the solids holdup is equal to

$$\varepsilon_s(x) = 1 - \frac{\hat{\mu}_s(x) - \hat{\mu}_{s-g}(x)}{\hat{\mu}_s(x)} \quad (5)$$

The $\hat{\mu}_s(x)$ value is constant for all pixels in the domain and was obtained using the Beer-Lambert's law after measuring the transmitted energy when the column is filled with solids and the column is empty. The $\hat{\mu}_{s-g}(x)$ values were determined using the AM form scans taken when the column is under the desired conditions of the gas-solids spouted bed

operation and the column is empty. Before scans were taken, the gas flow rate was introduced into the column, and the bed pressure was set at the desired operating conditions. At least 30 minutes were given for the entire system to allow the flow inside the spouted bed to be stabilized. Once the desired operating condition is achieved, the CT system is employed to take the scan at four vertical locations. For convincing comparisons between the two beds, those vertical locations were non-dimensionalized (i.e. dimensionless heights z/D) as shown in [Figure 4](#). Where z refers to the actual height from the gas distribution and D refers to the column diameter of the spouted beds. The z/D scan levels for the two beds were; 0.8 at the cone section, 1.1 above the cone section, 1.8, at the middle section and below the bed surface, and 2.4 at the fountain region.

3. Results and Discussion

3.1 The accuracy and reproducibility of the results

The accuracy of our CT technique results has been confirmed using phantom, which consists of two concentric Plexiglas cylinders where one of them was filled with water. The results have shown the measured linear attenuation of water and the dimensions of the cylinders compared to the actual value were within up to 1% (Ahmed, 2014; Mesfer, 2013). To ensure the reproducibility of the results obtained using the CT as well as for accurate comparability between the conditions, a repeated set of scans was performed at selected z/D level and the same operation conditions for each case in [Table 1](#). For the purpose of brevity, just the reproducibility results for the 0.152 m spouted bed (Case A in [Table 1](#)) are demonstrated here. [Figure 5](#) shows the solids holdup cross-sectional distributions and their

radial profiles (solids holdup versus the dimensionless radius (r/R)) with the associated error bars for three CT scans at level of $z/D=1.8$. The results indicate the excellent reproducibility as indicated by the agreement between the profiles at all radial positions in the bed. The error bars are small and the standard error obtained is 0.021, which is very small, and here we confirm that the data from the CT are reproducible.

3.2 Solids and gas holdups of Case A

3.2.1 Solids holdups profiles for the Reference case (Case A).

Figure 6 shows the radial profiles of solids holdup of Case A along the dimensionless heights (z/D) for the 0.152 m spouted bed. These profiles are obtained by azimuthally averaging the time-averaged cross-sectional distribution of the measured solids holdup (Figure 7). It is pronounced that the solids holdup in the spout and the annulus regions of spouted bed is different. The annulus region remains unchanged and has similar solids holdup profiles along the bed height of the spouted beds. The reason for this is that the solids move gradually and slowly downward by gravity in the annulus. In this region, the solids holdup radial profiles are nearly flat and have an average value of 0.6. This value is close to the maximum volume fraction of the solids holdup in the packing bed. In addition, those flat profiles suggest that the interaction between the wall and the particles in this region is small or neglected, explaining why this parameter was ignored by (He et al., 1997) in the first scaling relationship. In the spout, which is characterized as a gas-solid riser the solids holdup is lower near the gas inlet and increase as the height increases along the bed. This increase is because some solids enter the spout from the annulus at levels below the bed surface. The average of the solids holdup values in the spout increased by

28.91% from 0.8 to 1.1 z/D , and by 49.8% from 0.8 to 1.8 z/D . The solids holdup is lower near the center of the spout and gradually increases as the radial distance from the axis increases until it reaches the spout-annulus interface where the spout is confined by the annulus. The solids holdup profile in the fountain region is different from those obtained in the other regions of spouted beds. This is because the motion of the particles in this region is unique from the rest of the regions of the spouted bed where the particles are disengaged from the gas phase to recirculate back into the annulus. The amount of solids in the fountain region is important for the solids hydrodynamics and the solids circulation of spouted beds. As a result, the local solids holdup distribution was measured in this region to assess the scaling dimensionless groups. A maximum solids holdup was observed near the center of the fountain and decreased radially with increasing distance from the center. This radial decrease is expected due to the scatter of the particles in the radial direction of the fountain.

3.2.2 Cross sectional distribution of solids holdup for the Reference case (Case A).

Figure 7 presents the measured time-averaged cross-sectional distributions and the corresponding frequency distribution of the solids holdup for the 0.152 m spouted beds at z/D levels of 0.8, 1.1, 1.8, and 2.4. The scale-bar on the right of the images indicates the fractions of the solids holdup. Red is indicative of a higher solids holdup, and blue is indicative of a lower solids holdup. The color distributions of the images clearly highlights the spout and the annulus regions. The cross-sectional images illustrate the unchanged value of the solids holdup in the annulus region for all the z/D levels. As mentioned above, this is because the particles in this region are moving downward in a moving packed bed mode while feeding solids to the spout region. The frequency distribution of solids holdup

is higher at the limit of the solids holdup at the annulus region ($\epsilon_s \sim 0.6$), and is skewed to the left where the frequency distributions are small in the spout region. A skewed distribution is expected for all levels due to smaller and larger solids holdup values in the spout and annulus regions respectively. In addition, the asymmetrical distribution indicates a divergence between the spout and the annulus regions. The cross-sectional distribution and the corresponding frequency distribution of solids holdup at the fountain region show the smaller solids holdup in the outer region of the fountain where particles fall back into the bed surface. This confirms the divergence between the three regions: the spout, the annulus, and the fountain. The frequency distribution in the fountain region, unlike other regions, is skewed to the right and thinner. This indicates that the solids holdup values are closer in the outer region of the fountain and have a small deviation among each other.

3.2.3 Gas holdup profiles for the reference case (case A)

Figure 8 shows the gas holdup profiles of Case A along the bed height of the 0.152 m spouted bed. They were obtained by $\epsilon_g = 1 - \epsilon_s$. It is demonstrated that the gas holdup is higher in the spout region, and has an even higher value near the gas inlet of the spouted bed, as the solids holdup in this level is small (about 0.08). It is observed in the spout region of both the solids holdup (Figure 6) and gas holdup (Figure 8) results that the gas holdup is higher in the bottom section of the bed (the cone) and decreases as the axial level of the bed increases. This decrease in gas holdup is because solids get into the spout from the annulus region along the spout region. In the fountain region, the gas holdup is about 0.72 at the center and becomes higher in the outer region of the fountain where the particles fall back into the bed surface. Indeed, the two-phase flow behavior makes the structure of spouted beds complex. This complex structure significantly affects the movement of the

solids in the entire bed as well as the gas-solids interaction since the three regions (the spout, the annulus, and the fountain) have a different flow structure from each other. Both the dilute region (the spout) and the dense region (the annulus) in spouted beds provide good interactions, contacts, and mixing of gas-solids, which provide evidence that spouted beds are desirable for many industrial applications including the TRISO nuclear fuel particle coating process.

3.3 Demonstrating the non-similarity in local holdups with matching dimensionless groups.

In this section, the cross-sectional distribution of solids holdup, gas holdup, and their radial profiles are the chosen parameters for evaluating the dimensionless groups proposed by (He et al., 1997) for hydrodynamics similarity of spouted beds. By using the gamma ray computed tomography (CT), a fully detailed phase distribution was obtained for Case A, Case B, and Case C. Correspondingly, the profiles for the solids and gas holdups were obtained in the spout, the annulus, and the fountain regions. It is important to note that obtaining the full picture of the phase distribution of spouted beds is not achievable from the use of other measurement techniques. The strategy of assessing the scaling groups for hydrodynamics similarity started with performing the CT scan for Case A (the reference case) and Case B. The conditions of Case A and Case B were originally selected to achieve matching dimensionless groups between the two cases. The dimensionless groups of Case B are matched as closely as possible to those of Case A, and both cases termed as cases of matching dimensionless groups.

The comparison of solids holdup profiles for Case A (0.152 m) and Case B (0.076 m) at different level of measurements are shown in [Figure 9](#). From the figures, there is a

good agreement in the solids holdup profiles between the cases of matching dimensionless groups, Case A and Case B, in the annulus region as anticipated due to the structure of the flow in this region. The differences in the solids holdup profiles between the two cases are found in both the spout and fountain regions. At level $z/D=0.8$, the average relative difference between the two cases for all individual values in the spout region is 26.37%. Near the center of the spout ($r/R=0.025$), the difference is 42.88%; at $r/R=0.125$ it is 49.31%; at $r/R=0.225$ it is 20.03%; at $r/R=0.325$, it is 8.62%; and at $r/R=0.425$, it is 3.95%. Note that near the spout-annulus interface, $r/R \sim 0.425$, the difference is less. The results of the two cases show that the solids holdup is lower near the center of the spout and gradually increases as the radial distance from the axis increases until the spout-annulus interface. At level $z/D=1.1$, the average relative difference for all individual values in the spout region between Case A and Case B is 25.02%. The difference near the center of the spout ($r/R=0.025$) is 39.02%; at $r/R=0.125$ it was 34.71%; at $r/R=0.225$ it is 23.27%; at $r/R=0.325$ it is 14.85%; and at $r/R=0.425$ the difference is 4.33%. At level $z/D=1.8$, which is below the bed surface, the average relative difference in the spout region is 15.26%. Near the center of the spout, the difference is 16.87%; at $r/R=0.125$, it is 21.66%; at $r/R=0.225$, it is 19.95%; at $r/R=0.325$, it is 11.71%; and at $r/R=0.425$ it is 4.24%. The average relative difference between the profiles in the fountain region is 24.92%. Indeed, the average difference for the levels will be enough to indicate the difference among the measured solids holdup for Case A and Case B. Therefore, the similarity in solids and gas holdups (gas holdup = 1-solids holdup) distribution is not achieved despite the matching of these proposed dimensionless groups.

The evolution of solids holdup cross-sectional distribution of spouted beds should provide valuable information concerning the assessment of the scaling relationships. [Figure](#)

10 shows the measured time-averaged cross-sectional distribution and the corresponding frequency distribution of the solids holdup for Case B (0.076 m) at the z/D levels of 0.8, 1.1, 1.8, and 2.4. The maximum of the color scale were kept equal to those of Case A for connivance comparison between the images. The color distribution of the images clearly highlights the spout and the annulus regions for the 0.076 m spouted bed. The cross-sectional images demonstrate the unchanged value of the solids holdup in the annulus region for Case B for all the z/D levels and further confirm the similarity of the solids holdup profiles between Case A and Case B in this region. However, difference can be observed between the images in the spout region (in strict sense) of the two beds. This difference becomes more obvious, if we take into consideration the frequency distribution of the local solids holdup values in terms of mean, standard deviation, and shape for Case A and Case B. At $z/D=0.8$, the mean of the solids holdup frequency distribution is 0.56 and 0.54, for Case A and Case B, respectively. Note that the statistical analysis of the holdups distribution is impacted by the solids holdup values of both the spout and the annulus regions. At $z/D=1.1$, the mean of the solids holdup frequency distribution is 0.57 and 0.56, for Case A and Case B, respectively. At $z/D=1.8$, the mean of the solids holdups frequency distribution is 0.58 and 0.57, for Case A and Case B, respectively. Difference is also found between the two cases in the fountain region. In the fountain, the mean of the solids holdup distribution is 0.07 and 0.1, for Case A and Case B, respectively. By analyzing the above discussion and the data obtained one may draw conclusion that the similarity in the solids and gas holdups distributions in term of mean, standard deviation and shape are not achieved when the dimensionless groups are matched between the two

beds. This indicates that the suggested scale-up methodology based on matching dimensionless groups is inadequate for the successful scale-up of gas-solids spouted bed.

The comparison of gas holdup radial profiles at different axial levels for Case A (0.152 m) and Case B (0.076 m) are shown in [Figure 11](#). It is more evident that the gas holdup near the center of the spout is higher than in the annulus. In the spout, the gas holdup is higher near the gas inlet (cone section) and decreases with increasing the bed height. This decrease is due to the increase in the solids holdup towards the fountain region. Near the center of the spout, the gas holdup is higher and decreases gradually towards the spout-annulus interface. The average value of the gas holdup in the annulus was found to be constant $\varepsilon_g = 0.4$. The absolute percentage differences between the profiles are compared for all the z/D levels. The average relative percentage differences for all the individual values of gas holdup in the spout region for matched dimensionless groups are 7.62%, 12.57%, and 11.88%, at z/D levels of 0.8, 1.1, and 1.8, respectively. The average difference between the profiles in the fountain region is 6.57%. From the results analysis, the similarity in gas holdup profiles is not achieved despite matching the proposed dimensionless groups. This further indicates that the hydrodynamics of spouted beds are not fully predicted by matching these groups.

3.4 The non-similarity in local holdups with mismatching dimensionless groups.

The examination of different operating conditions with mismatch scaling groups is necessary in order to assess the scaling relationships for scale-up of spouted beds. The conditions of Case C are conducted to examine the influence of mismatched scaling groups. Case C is also proposed to study the common unsuitable scale-up criteria through varying

only the bed dimensions to achieve geometrical similarity while other scaling groups are not matched. [Figure 12](#) shows the comparison of solids holdup profiles for Case A (0.152 m) and Case C (0.076 m) at z/D levels of 0.8, 1.1, 1.8, and 2.4. The results show that the solids holdup profiles of the two beds deviate from each other substantially in the spout and fountain regions, and have similar profiles in the annulus region. The absolute percentage differences between the profiles of the two beds have been evaluated. At $z/D=0.8$, the relative average percentage difference between the two cases for all individual values in the spout region is 46.26%. Near the center of the spout ($r/R=0.025$), the difference is 65.92%; at $r/R=0.125$, it is 72.59%; at $r/R=0.225$, it is 55%; at $r/R=0.325$, it is 22.07%; and at $r/R=0.425$, it is 5.08%. At $z/D=1.1$, the average relative difference in the spout region between Case A and Case C is 44.29%. The difference near the center of the spout is 67.3% at $r/R=0.025$; at $r/R=0.125$, it is 68.08%; at $r/R=0.225$, it is 50.46%; at $r/R=0.325$, it is 24.05%; and at $r/R=0.425$, it is 5.17%. At $z/D=1.8$, the average relative difference between the profiles in the spout region is 38.12%. The difference in the spout is 55.75% at $r/R=0.025$; at $r/R=0.125$, it is 55.4%; at $r/R=0.225$, it is 45.8%; at $r/R=0.325$, it is 23.96%; and at $r/R=0.425$, it is 4.9%. The average relative percentage difference between the profiles in the fountain region is 22.43%. By realizing the solids holdup profiles for mismatch dimensionless groups, it is not sufficient to achieve good hydrodynamics similarity between the two beds by matching only the beds and particles dimensionless groups. However, matching all the dimensionless groups of spouted beds is difficult since many parameters are included especially when it comes to industry for those of large columns.

Figure 13 shows the measured time-averaged cross-sectional distribution and the corresponding frequency distribution of the solids holdup for Case C (0.076 m) at z/D levels of 0.8, 1.1, 1.8, and 2.4. The color distribution of the images clearly highlights the spout and the annulus regions for the 0.076 m spouted bed. The cross-sectional images show the unchanged solids holdup value in the annulus region for Case C at all the z/D levels and further confirm the similarity of the solids holdup profiles between Case A and Case C in this region. However, difference can be observed between the images in the spout region (in the strict sense) of the two beds. This difference becomes more obvious, if we consider the frequency distribution of the local solids holdup values in terms of mean, standard deviation, and shape for Case A and Case B. At $z/D=0.8$, the mean of the solids holdups frequency distribution is 0.56 and 0.54, for Case A and Case C, respectively. At $z/D=1.1$, the mean of the solids holdups frequency distribution is 0.57 and 0.55, for Case A and Case C, respectively. While at $z/D=1.8$, the mean of the solids holdups frequency distribution is 0.583 and 0.564, for Case A and Case C, respectively. Difference is also found between the two cases in the fountain region where the mean of the solids holdup distribution is 0.073 and 0.0672, respectively, for Case A and Case C. From the results above, matching only the beds and particles dimensionless groups are not sufficient for achieving good hydrodynamics similarity between the two beds.

Figure 14 shows the comparison of gas holdup profiles for Case A (0.152 m) and Case C (0.076 m) at z/D levels of 0.8, 1.1, 1.8, and 2.4. The relative percentage difference between the profiles of Case A and Case C were evaluated at all z/D levels. The average relative percentage difference for all the individual values of gas holdup in the spout region for mismatched dimensionless groups is 13.47%, 20.53%, and 24.25%, at z/D levels of 0.8,

1.1, and 1.8, respectively. The average percentage between the profiles in the fountain region is 7.36%. The results above indicate the differences in the gas holdup profiles between the two beds for mismatch dimensionless groups.

4. Conclusion

The key conclusion drawn from the results of this work is that the dimensionless groups proposed by (He et al., 1997) are not sufficient to maintain similarity in local solids and gas holdups distributions along the bed height by implementing gamma ray computed tomography (CT) as an advanced non-invasive technique using the studied gas-solid spouted beds of 0.076 m and 0.152 m diameter. Adding more dimensionless groups to match in order to capture the other interplay phenomena will further complicate the scale-up methodology since it will be not easy to define the conditions between two scales to match large number of dimensionless groups. This is because of the complex flow pattern of spouted beds arising from complex interactions among the solids and between the solids and the gas phases. This necessitates the need to measure the other local parameters, such as solids velocity field and the associated turbulent parameters to properly and further evaluate such a method for scale-up of spouted beds. Furthermore, a new mechanistic scale-up methodology needs to be developed which could be based on identifying the key parameter(s) that dictate the dynamics of the bed such as gas holdup radial profiles.

Our results have also demonstrated that in the spout region the solids holdup increases along the height of the spouted bed. This is because the solids are being pulled by the jet of the gas phase at the interface between the spout region and the annulus region

along the spout height. In the annulus region, the solids move downward as a moving bed. Hence, the solids holdup does not change along the bed height. The structure of the solids holdup distributions in the annular region is clearly distinguished from the spout and fountain regions.

It is worth to mention that the reported data is valuable to benchmark CFD and DEM simulations and to validate the selected set models and closures.

Acknowledgments

US Department of Energy - Nuclear Energy Research Initiative (DOE-NERI) grant (NERI DEFC07-07ID14822), the GAANN, chancellor fellowship, and professor Al-Dahhan's Lab Fund are acknowledged for the financial support that made this work possible. The second author would like to thank the Saudi Arabian Cultural Mission (SACM) for sponsoring his Ph.D. studies at Missouri S&T.

Notation

d_p	particle diameter, m
D	inner column diameter, m
D_i	inlet orifice diameter, m
e_{ss}	restitution coefficient of the particles
Fr	Froude number
g	acceleration of gravity, $m\ s^{-2}$
H	static bed height, m
H_o	initial height, m
H_l	particle rebounding height, m
H_F	fountain height, m
H_m	maximum spoutable bed depth, m
$h(y/x)$	length of the segment of projection y in pixel x (cm)
I	the intensity of radiation
$I_o(y)$	the incident radiation intensity
$I(y)$	the radiation intensity detected after passing through the chord length
L	column length, m
l	the chord length of each pixel
P	bed pressure, Pa
Re	Reynolds number
R	column radius, cm
r	radial position, cm
T	bed temperature, K

U	superficial gas velocity, m s^{-1}
U_{mf}	minimums fluidization velocity, m s^{-1}
U_{ms}	minimum spouting velocity, m s^{-1}
x	index for pixel in image domain
y	index for projection or source detector pair
z	axial distance form inlet orifice, m

Greek letters

β	fluid-particle interaction coefficient, $\text{kg m}^3 \text{s}^{-1}$
ρ_s	particle density, Kg m^{-3}
ρ_f	fluid density, Kg m^{-3}
μ	fluid viscosity, $\text{Kg m}^{-1} \text{s}^{-1}$
ϕ_s	sphericity of particles
φ	inertial friction angle of particle, deg
ε_{mf}	bed voidage at minimum fluidization
ε_o	voidage at packed bed state
ε_s	solids phase fraction (or solids holdup)
ε_g	gas holdup fraction (or gas holdup)
$\hat{\mu}(x)$	attenuation values estimated by the AM algorithm for a given pixel x , cm^{-1} .
$\hat{\mu}_s(x)$	attenuation values when the system filled with solids and spouting gas is absent, cm^{-1} .
$\hat{\mu}_g(x)$	attenuation values for pure gas phase (empty column), cm^{-1} .
$\hat{\mu}_{s-g}(x)$	attenuation value for the gas-solids when the system is dynamic at the desired operating condition, cm^{-1} .

References

Ahmed, F.S., 2014. Experimental investigation of the pebble bed structure by using gamma ray tomography. *Masters Theses*. Paper 7317. http://scholarsmine.mst.edu/masters_theses/7317.

Al-Dahhan, M.H., 2009. Radioisotopes applications in industry: an overview. *Atoms for Peace: an International Journal* 2, 324-337.

Al-Dahhan, M.H., Kemoun, A., Cartolano, A.R., Roy, S., Dobson, R., Williams, J., 2007. Measuring gas-liquid distribution in a pilot scale monolith reactor via an Industrial Tomography Scanner (ITS). *Chemical Engineering Journal* 130, 147-152.

Aradhya, S.B., 2013. Scaleup and hydrodynamics study of gas-solid spouted beds, *Doctoral Dissertations*. Paper 2254. http://scholarsmine.mst.edu/doctoral_dissertations/2254/.

Béttega, R., Corrêa, R.G., Freire, J.T., 2009. Scale-up study of spouted beds using computational fluid dynamics. *The Canadian Journal of Chemical Engineering* 87, 193-203.

Bhusarapu, S., Al-Dahhan, M.H., Duduković, M.P., 2006. Solids flow mapping in a gas-solid riser: Mean holdup and velocity fields. *Powder Technology* 163, 98-123.

Chandnani, P.P., Epstein, N., 1986. Spoutability and spout detabilization of fine particles with a gas. Engineering Foundation, United States.

Chen, J., Kemoun, A., Al-Dahhan, M.H., Duduković, M.P., Lee, D.J., Fan, L.-S., 1999. Comparative hydrodynamics study in a bubble column using computer-automated radioactive particle tracking (CARPT)/computed tomography (CT) and particle image velocimetry (PIV). *Chemical Engineering Science* 54, 2199-2207.

Csiszár, I., 1975. I-divergence geometry of probability distributions and minimization problems. *The Annals of Probability* 3, 146-158.

Du, W., Bao, X., Xu, J., Wei, W., 2006. Computational fluid dynamics (CFD) modeling of spouted bed: Assessment of drag coefficient correlations. *Chemical Engineering Science* 61, 1401-1420.

Du, W., Xu, J., Ji, Y., Wei, W., Bao, X., 2009. Scale-up relationships of spouted beds by solid stress analyses. *Powder Technology* 192, 273-278.

Duarte, C.R., Murata, V.V., Barrozo, M.A.S., 2005. Simulation of Spouted Bed Using a Eulerian Multiphase Model. *Materials Science Forum* 498-499, 270-277.

Duarte, C.R., Olazar, M., Murata, V.V., Barrozo, M.A.S., 2009. Numerical simulation and experimental study of fluid-particle flows in a spouted bed. *Powder Technology* 188, 195-205.

Glicksman, L.R., 1984. Scaling relationships for fluidized beds. *Chemical Engineering Science* 39, 1373-1379.

Gryczka, O., Heinrich, S., Deen, N.G., van Sint Annaland, M., Kuipers, J.A.M., Jacob, M., Mörl, L., 2009a. Characterization and CFD-modeling of the hydrodynamics of a prismatic spouted bed apparatus. *Chemical Engineering Science* 64, 3352-3375.

Gryczka, O., Heinrich, S., Deen, N.G., van Sint Annaland, M., Kuipers, J.A.M., Mörl, L., 2009b. CFD modeling of a prismatic spouted bed with two adjustable gas inlets. *The Canadian Journal of Chemical Engineering* 87, 318-328.

He, Y.L., Lim, C.J., Grace, J.R., 1992. Spouted bed and spout-fluid bed behaviour in a column of diameter 0.91 m. *The Canadian Journal of Chemical Engineering* 70, 848-857.

He, Y.L., Lim, C.J., Grace, J.R., 1997. Scale-up studies of spouted beds. *Chemical Engineering Science* 52, 329-339.

Hosseini, S.H., Ahmadi, G., Olazar, M., 2013. CFD simulation of cylindrical spouted beds by the kinetic theory of granular flow. *Powder Technology* 246, 303-316.

Kemoun, A., Cheng Ong, B., Gupta, P., Al-Dahhan, M.H., Dudukovic, M.P., 2001. Gas holdup in bubble columns at elevated pressure via computed tomography. *International Journal of Multiphase Flow* 27, 929-946.

Kumar, S.B., Moslemian, D., Duduković, M.P., 1995. A γ -ray tomographic scanner for imaging voidage distribution in two-phase flow systems. *Flow Measurement and Instrumentation* 6, 61-73.

Lan, X., Xu, C., Gao, J., Al-Dahhan, M., 2012. Influence of solid-phase wall boundary condition on CFD simulation of spouted beds. *Chemical Engineering Science* 69, 419-430.

Lee, Y.-W., Park, J.-Y., Kim, Y.K., Jeong, K.C., Kim, W.K., Kim, B.G., Kim, Y.M., Cho, M.S., 2008. Development of HTGR-coated particle fuel technology in Korea. *Nuclear Engineering and Design* 238, 2842-2853.

Li, Y., Che, D., Liu, Y., 2012. CFD simulation of hydrodynamic characteristics in a multiple-spouted bed. *Chemical Engineering Science* 80, 365-379.

Lim, C.J., Grace, J.R., 1987. Spouted bed hydrodynamics in a 0.91 m diameter vessel. *The Canadian Journal of Chemical Engineering* 65, 366-372.

Liu, M., Shao, Y., Liu, B., 2012. Pressure analysis in the fabrication process of TRISO UO₂-coated fuel particle. *Nuclear Engineering and Design* 250, 277-283.

Liu, Y.-J., Li, W., Han, L.-C., Cao, Y., Luo, H.-a., Al-Dahhan, M., Dudukovic, M.P., 2011. γ -CT measurement and CFD simulation of cross section gas holdup distribution in a gas-liquid stirred standard Rushton tank. *Chemical Engineering Science* 66, 3721-3731.

Luo, H.-P., Al-Dahhan, M.H., 2010. Local gas holdup in a draft tube airlift bioreactor. *Chemical Engineering Science* 65, 4503-4510.

Mathur, K.B., Epstein, N., 1974a. 1 - Introduction, in: Mathur, K.B., Epstein, N. (Eds.), *Spouted Beds*. Academic Press, pp. 1-13.

Mathur, K.B., Epstein, N., 1974b. 6 - Spouting Stability, in: Mathur, K.B., Epstein, N. (Eds.), *Spouted Beds*. Academic Press, pp. 112-124.

Mesfer, M. A., 2013. Effect of Dense Heat Exchanging Internals on the Hydrodynamics of Bubble Column Reactors Using Non-invasive Measurement Techniques. *Doctoral Dissertations*. Paper 27.
http://scholarsmine.mst.edu/doctoral_dissertations/27.

Moradi, S., Yeganeh, A., Salimi, M., 2013. CFD-modeling of effects of draft tubes on operating condition in spouted beds. *Applied Mathematical Modelling* 37, 1851-1859.

O'Sullivan, J.A., Benac, J., 2007. Alternating minimization algorithms for transmission tomography. *IEEE Transactions on Medical Imaging* 26, 283-297.

Prasser, H.M., Baldauf, D., Fietz, J., Hampel, U., Hoppe, D., Zippe, C., Zschau, J., Christen, M., Will, G., 2003. Time resolving gamma-tomography for periodically changing gas fraction fields and its application to an axial pump. *Flow Measurement and Instrumentation* 14, 119-125.

Rados, N., Shaikh, A., Al-Dahhan, M.H., 2005. Solids flow mapping in a high pressure slurry bubble column. *Chemical Engineering Science* 60, 6067-6072.

Ren, B., Zhong, W., Jin, B., Yuan, Z., Lu, Y., 2011. Computational Fluid Dynamics (CFD)–Discrete Element Method (DEM) Simulation of Gas–Solid Turbulent Flow in a Cylindrical Spouted Bed with a Conical Base. *Energy & Fuels* 25, 4095-4105.

Rong, L.-W., Zhan, J.-M., 2010. Improved DEM-CFD model and validation: A conical-base spouted bed simulation study. *Journal of Hydrodynamics, Ser. B* 22, 351-359.

Roy, S., Al-Dahhan, M., 2005. Flow distribution characteristics of a gas–liquid monolith reactor. *Catalysis Today* 105, 396-400.

Roy, S., Kemoun, A., Al-Dahhan, M.H., Dudukovic, M.P., Skourlis, T.B., Dautzenberg, F.M., 2005. Countercurrent flow distribution in structured packing via computed tomography. *Chemical Engineering and Processing: Process Intensification* 44, 59-69.

Sawa, K., Ueta, S., 2004. Research and development on HTGR fuel in the HTTR project. *Nuclear Engineering and Design* 233, 163-172.

Shaikh, A., Al-Dahhan, M., 2005. Characterization of the hydrodynamic flow regime in bubble columns via computed tomography. *Flow Measurement and Instrumentation* 16, 91-98.

Shuyan, W., Xiang, L., Huilin, L., Long, Y., Dan, S., Yurong, H., Yonglong, D., 2009. Numerical simulations of flow behavior of gas and particles in spouted beds using frictional-kinetic stresses model. *Powder Technology* 196, 184-193.

Sokolovskii, V., 1965. *Statistics of granular media*. Pergamon Press, Oxford.

Tang, C., Tang, Y., Zhu, J., Zou, Y., Li, J., Ni, X., 2002. Design and manufacture of the fuel element for the 10 MW high temperature gas-cooled reactor. *Nuclear Engineering and Design* 218, 91-102.

Varma, R., 2008. Characterization of anaerobic bioreactors for bioenergy generation using a novel tomography technique. *Doctoral Dissertations*. Washington University. Dept. of Energy, Environmental and Chemical Engineering.

Varma, R., Bhusarapu, S., Sullivan, J.A.O., Al-Dahhan, M.H., 2008. A comparison of alternating minimization and expectation maximization algorithms for single source gamma ray tomography. *Measurement Science and Technology* 19, 015506.

Wang, S., Zhao, L., Wang, C., Liu, Y., Gao, J., Liu, Y., Cheng, Q., 2014. Numerical simulation of gas–solid flow with two fluid model in a spouted-fluid bed. *Particuology* 14, 109-116.

Wang, Z.G., Bi, H.T., Lim, C.J., 2006. Numerical simulations of hydrodynamic behaviors in conical spouted beds. *China Particuology* 4, 194-203.

Yang, S., Luo, K., Fang, M., Zhang, K., Fan, J., 2014. Parallel CFD–DEM modeling of the hydrodynamics in a lab-scale double slot-rectangular spouted bed with a partition plate. *Chemical Engineering Journal* 236, 158-170.

Zhonghua, W., Mujumdar, A.S., 2008. CFD modeling of the gas–particle flow behavior in spouted beds. *Powder Technology* 183, 260-272.

Table captions

[Table 1](#). Dimensional parameters and properties of scale-up verification conditions from the work of (He et al., 1997).

Figure captions

Figure 1. Schematic diagram of spouted beds.

Figure 2. Schematic diagram of 0.076 m and 0.152 m spouted beds.

Figure 3. Photograph of the DSCT technique, and 0.152 m spouted bed inside the setup for scan.

Figure 4. The computational domain is discretized into cells of size x .

Figure 5. Reproducibility of CT measurements for (a) cross-sectional solids holdup distributions and (b) their radial profiles with the associated error bars for three CT scans at $z/D=1.8$ (Conditions; Case A in [Table 1](#)).

Figure 6. Radial profiles of solids holdup along the bed height of the 0.152 m spouted bed using conditions in Case A (reference case) listed in [Table 1](#).

Figure 7. Cross sectional distribution and corresponding frequency distribution of solids holdup for Case A along the bed height of the 0.152 m spouted bed.

Figure 8. Radial profiles of gas holdup along the bed height of the 0.152 m spouted bed using conditions in Case A (reference case)

Figure 9. Comparison of radial profiles of solids holdup at z/D levels of 0.8, 1.1, 1.8, and 2.4 for Case A (0.152 m) and Case B (0.076 m) spouted beds.

Figure 10. Cross sectional image and corresponding frequency distribution of solids holdup for Case B along the bed height of the 0.076 m spouted bed.

Figure 11. Comparison of radial profiles of gas holdup at z/D levels of 0.8, 1.1, 1.8, and 2.4 for Case A (0.152 m) and Case B (0.076 m) spouted beds.

Figure 12. Comparison of radial profiles of solids holdup at z/D levels of 0.8, 1.1, 1.8, and 2.4 for Case A (0.152 m) and Case C (0.076 m) spouted beds.

Figure 13. Cross sectional image and corresponding frequency distribution of solids holdup for Case C along the bed height of the 0.076 m spouted bed.

Figure 14. Comparison of radial profiles of gas holdup at z/D levels of 0.8, 1.1, 1.8, and 2.4 for Case A (0.152 m) and Case C (0.076 m) spouted beds.

Table 1. Dimensional parameters and properties of scale-up verification conditions from the work of (He et al., 1997).

Condition/Case	A	B	C
D_c (m)	0.152	0.076	0.076
D_i (mm)	19.1	9.5	9.5
L (m)	1.14	1.14	1.14
H (m)	0.323	0.16	0.16
T (K)	298	298	298
P (kPa)	101	312	101
Particles	Glass	Steel	Glass
d_p (mm)	2.18	1.09	1.09
ρ_s (kg/m ³)	2400	7400	2450
ρ_f (kg/m ³)	1.21	3.71	1.21
μ ($\times 10^5$) (Pa.s)	1.81	1.81	1.81
U (m/s)	1.08	0.75	0.74
Scaling groups			
ϕ_s	1	1	1
φ ($^\circ$)	26	28	27
ε_{mf}	0.41	0.42	0.42
H/D_c	2.1	2.1	2.1
D_c/D_i	8	8	8
D_c/d_p	70	70	70
ρ_s/ρ_f	1994	1995	2029
$Re = \rho_f d_p U / \mu$	157	168	54
$Fr = U^2 / gd_p$	54.5	52.6	51.2
$\rho_s d_p U / \mu$ ($\times 10^{-3}$)	313	334	109
U^2 / gD_c	0.78	0.75	0.73
U / U_{mf}	0.95	0.92	0.16
U / U_{ms}	0.93	0.92	0.9

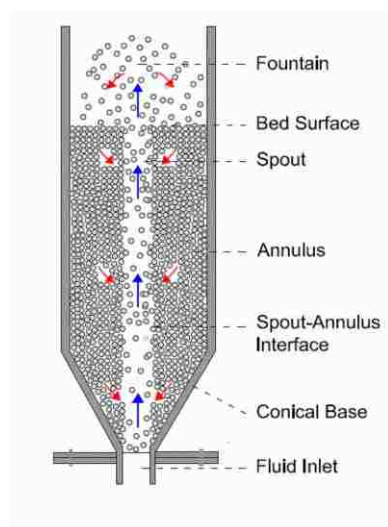


Figure 1. Schematic diagram of spouted beds.

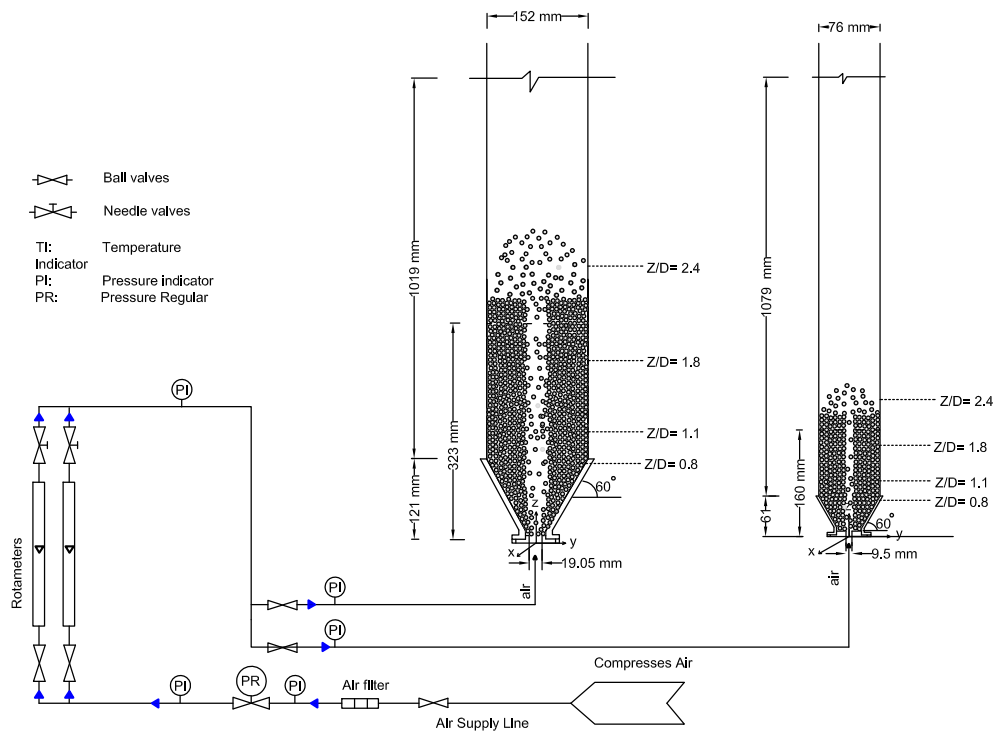


Figure 2. Schematic diagram of 0.076 m and 0.152 m spouted beds.



Figure 3. Photograph of the DSCT technique, and 0.152 m spouted bed inside the setup for scan.

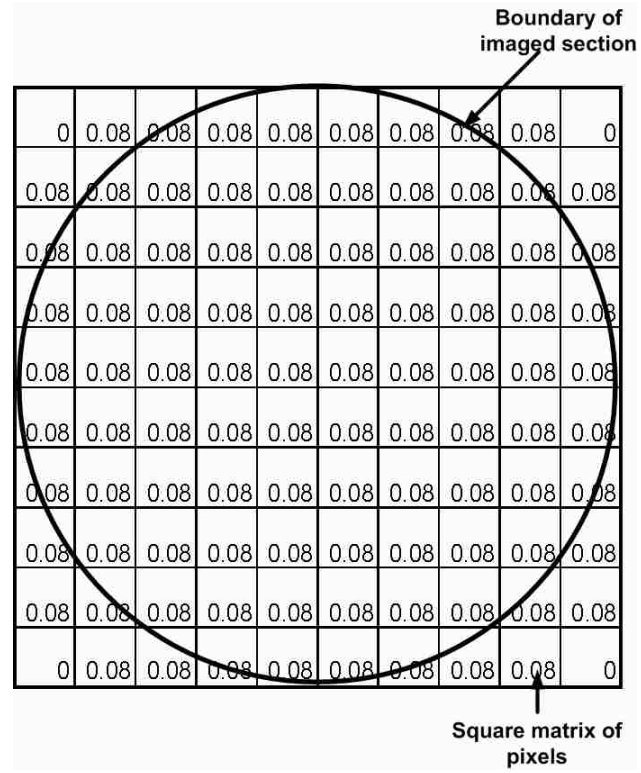


Figure 4. The computational domain is discretized into cells of size x .

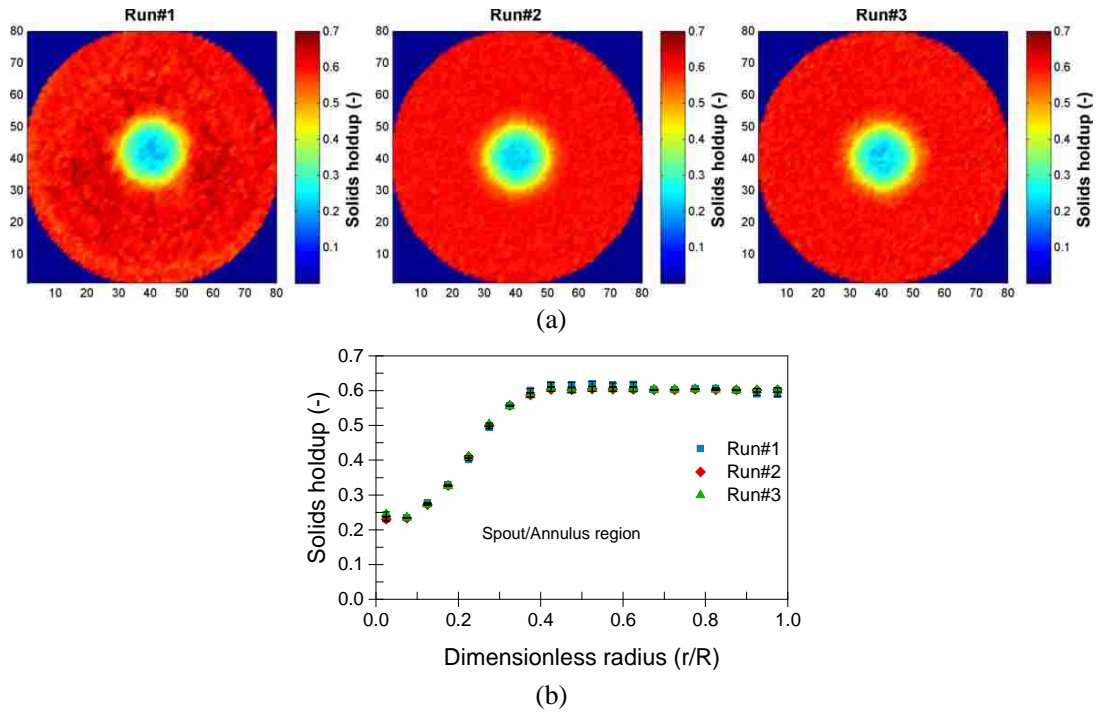


Figure 5. Reproducibility of CT measurements for (a) cross-sectional solids holdup distributions and (b) their radial profiles with the associated error bars for three CT scans at $z/D=1.8$ (Conditions; Case A in Table 1).

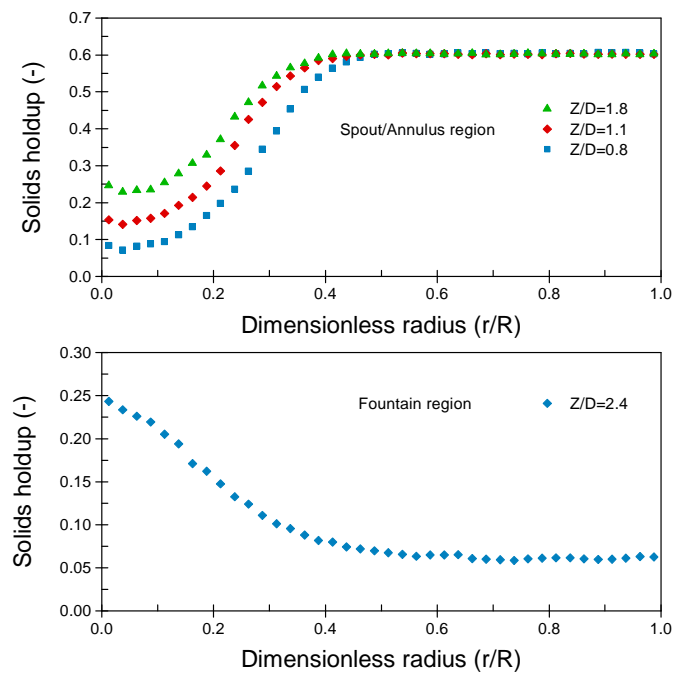


Figure 6. Radial profiles of solids holdup along the bed height of the 0.152 m spouted bed using conditions in Case A (reference case) listed in Table 1.

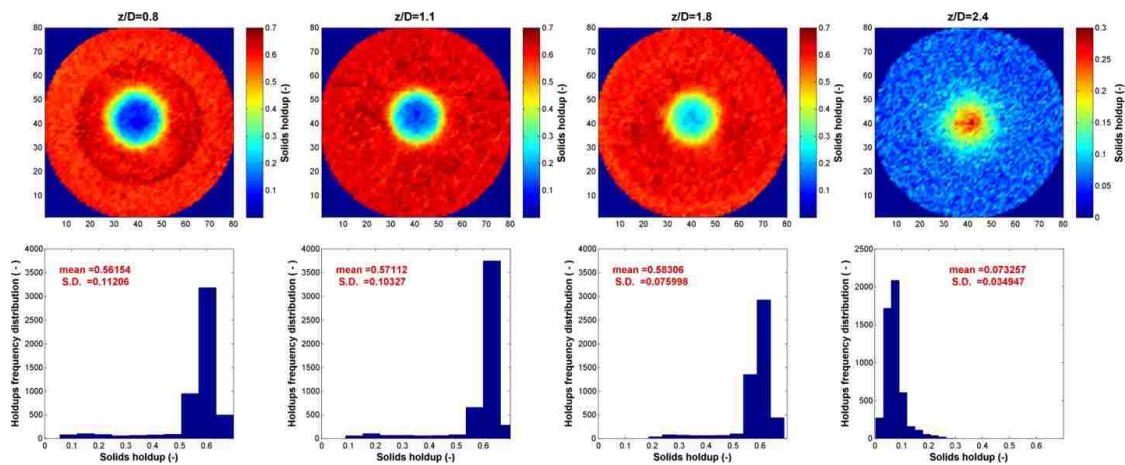


Figure 7. Cross sectional distribution and corresponding frequency distribution of solids holdup for Case A along the bed height of the 0.152 m spouted bed.

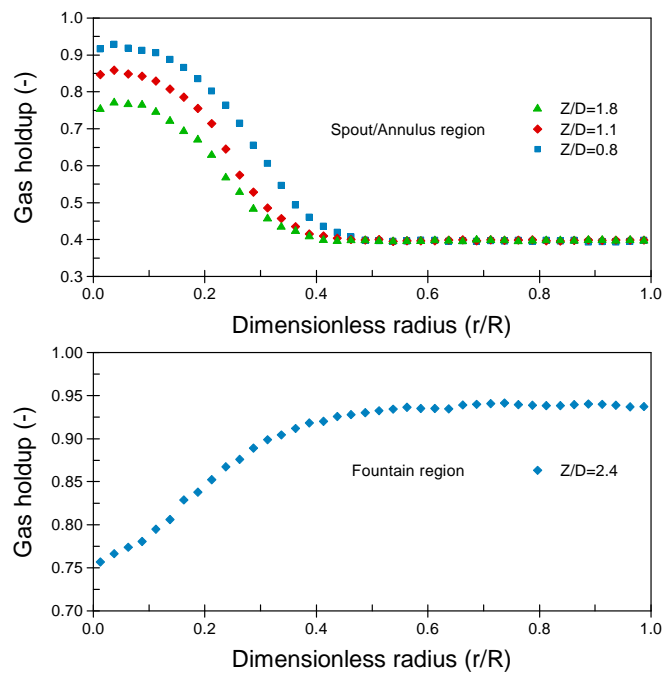


Figure 8. Radial profiles of gas holdup along the bed height of the 0.152 m spouted bed using conditions in Case A (reference case) listed in Table 1.

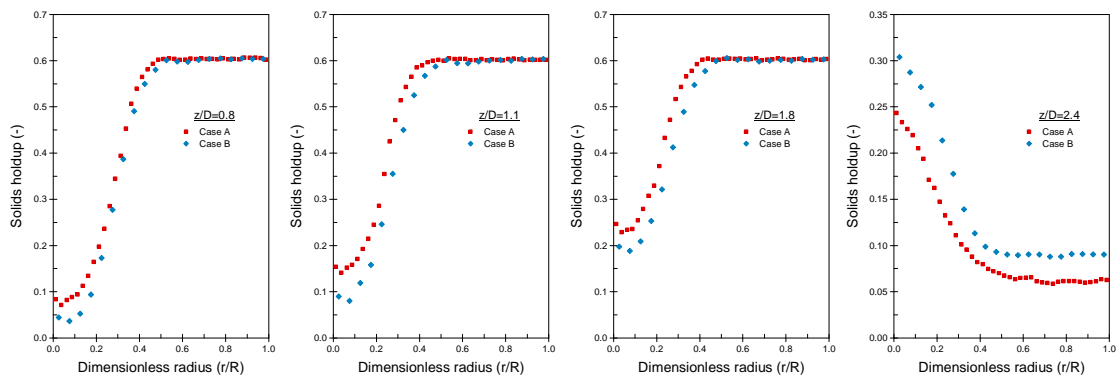


Figure 9. Comparison of radial profiles of solids holdup at z/D levels of 0.8, 1.1, 1.8, and 2.4 for Case A (0.152 m) and Case B (0.076 m) spouted beds.

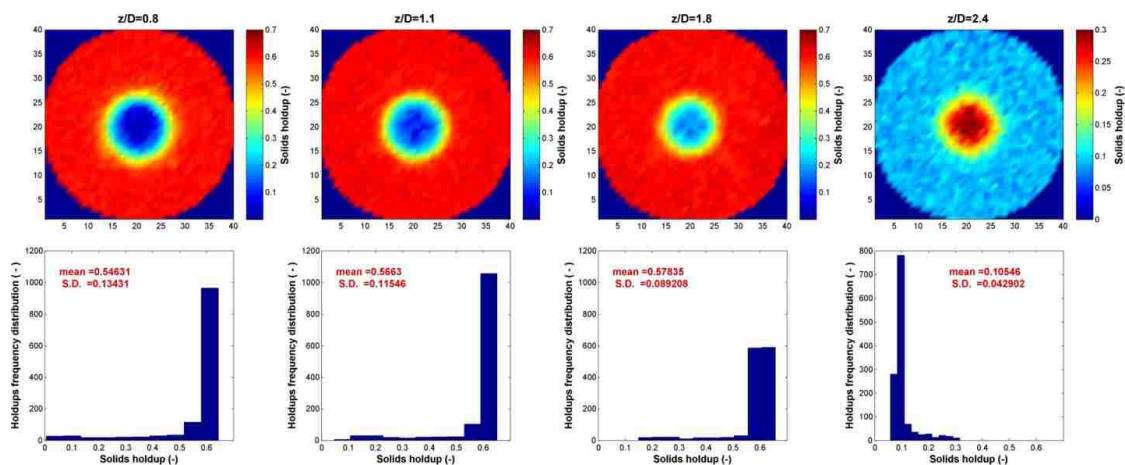


Figure 10. Cross sectional image and corresponding frequency distribution of solids holdup for Case B along the bed height of the 0.076 m spouted bed.

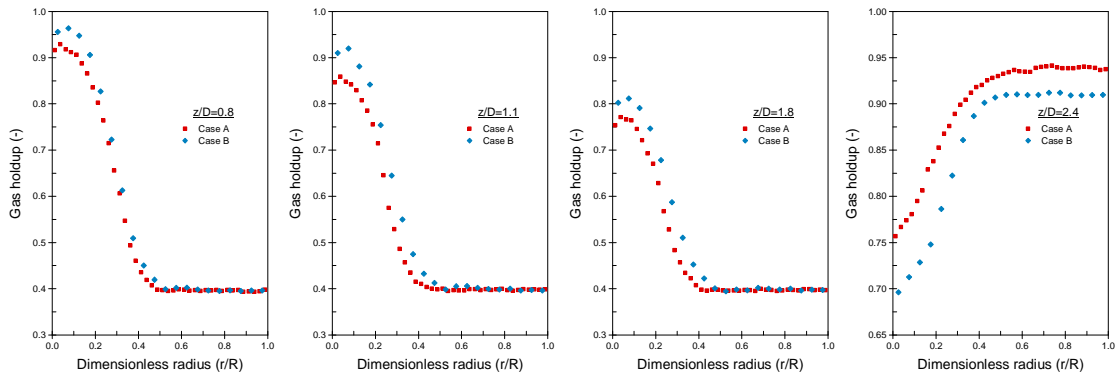


Figure 11. Comparison of radial profiles of gas holdup at z/D levels of 0.8, 1.1, 1.8, and 2.4 for Case A (0.152 m) and Case B (0.076 m) spouted beds.

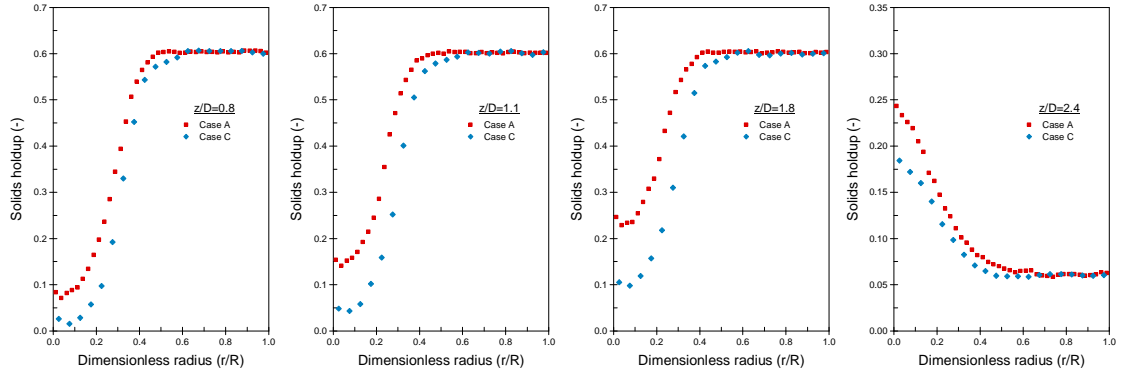


Figure 12. Comparison of radial profiles of solids holdup at z/D levels of 0.8, 1.1, 1.8, and 2.4 for Case A (0.152 m) and Case C (0.076 m) spouted beds.

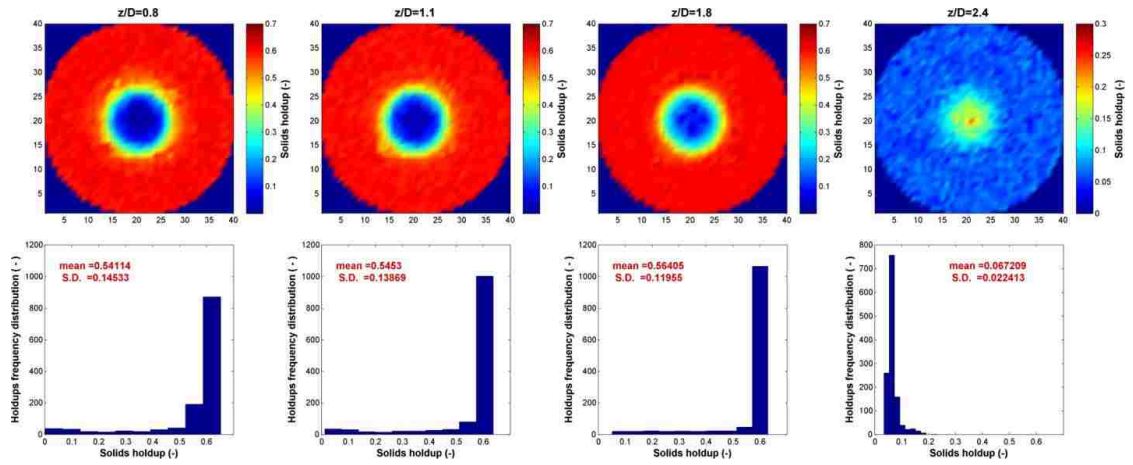


Figure 13. Cross sectional image and corresponding frequency distribution of solids holdup for Case C along the bed height of the 0.076 m spouted bed.

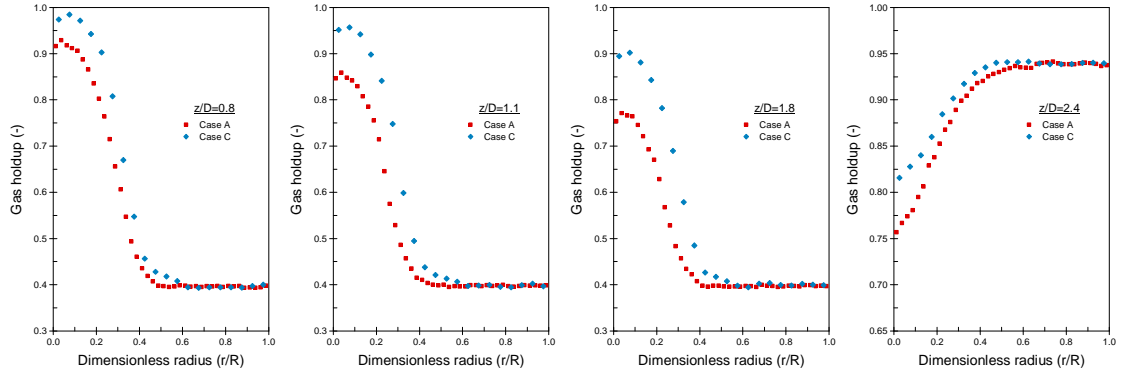


Figure 14. Comparison of radial profiles of gas holdup at z/D levels of 0.8, 1.1, 1.8, and 2.4 for Case A (0.152 m) and Case C (0.076 m) spouted beds.

II. An advanced evaluation of spouted beds scale-up for coating TRISO nuclear fuel particles using radioactive particle tracking (RPT)

Neven Ali^a, Thaar Al-Juwaya^a, Muthanna Al-Dahhan^{ab*}

^aNuclear Engineering,

^bChemical and Biochemical Engineering,

Missouri University of Science and Technology (Missouri S&T) – Rolla

Rolla, MO 65409

Abstract

A set of dimensionless groups has been proposed in the literature by He et al. [He Y. L., Lim C. J., Grace J. R., Scale-up studies of spouted beds, Chemical Engineering Science, 52 (2), 329–339, 1997] to scale-up gas-solid spouted beds while maintaining their hydrodynamics similarity. The literature reported studies do not provide conclusive assessments about this methodology. Therefore, in this work, we have applied an advanced non-invasive radioactive particle tracking (RPT) technique for the first time to evaluate such scale-up methodology by measuring the local solids velocity, normal and shear stresses and the turbulent kinetic energy. The axial and azimuthal averaged radial profiles of solids velocity, normal stresses, shear stresses, and turbulent kinetic energy illustrate that the similarity of the hydrodynamics has not been attained when the proposed set of dimensionless groups has been matched using two sizes of spouted beds of 0.076 m and 0.152 m and sets of operating conditions. The conclusion is consistent with the recent reported findings by measuring cross sectional distribution and radial profiles of solids and gas holdups along the bed height using gamma-ray computed tomography and by the limited point measurements of solids velocity and holdup using optical fiber probe. It is

clear that local measurements of hydrodynamic parameters are essential for detailed assessment of scale-up methodologies. The presented results of our work are also valuable for benchmarking computational fluid dynamics codes and models.

*Corresponding author:

Tel.: +1 573 341 7518; fax: +1 573 341 4377.

E-mail addresses: aldahhanm@mst.edu

Keywords Scale-up, Spouted beds, TRISO, Radioactive Particle Tracking (RPT), 3-D velocity field, turbulence.

1. Introduction

The fossil fuels (oil, coal and natural gas) are becoming increasingly depleted and will not satisfy future needs for energy [1]. Therefore, alternative energy resources have been sought. These alternatives include nuclear energy (particularly the 4th generation nuclear energy), bioenergy (biomass gasification), and other renewable and alternative resources. The Very High-Temperature Reactors (VHTRs) are the most efficient of the fourth generation of nuclear reactors to meet energy demands for the 21st century [2, 3]. Passive safety is one of the most important features that characterize these reactors. The performance and the safety of the VHTRs depend highly on the quality of the TRISO (Tristructural-isotropic) fuel coated particles, and hence the fuel-coating technology and the related processes. In the coating process, the fuel kernel (UO_2 or PU_2) is coated with four layers consisting of a porous buffer pyrolytic carbon layer (buffer PyC), an inner dense pyrolytic carbon layer (IPyC), a silicon carbide layer (SiC) and an outer dense pyrocarbon layer (OPyC) [4]. The technique used for coating the TRISO fuel particles is a gas-solid spouted bed via chemical vapor deposition (CVD) method. The TRISO fuel coating process is very delicate and must meet certain production requirements to be accepted. The

level of defective coated particles is essentially zero, which is a challenge that requires a well understanding of the effects of design and operating variables on the performance of the gas-solid spouted bed coaters. The quality of the TRISO fuel, i.e. whether particles produced are uniformly or non-uniformly coated, is strongly impacted by the hydrodynamics of the gas-solid spouted bed, the solids flow field, and the flow regime characteristics [3, 5-8]. Accordingly, fundamental understanding of the underlying phenomena of the gas-solid spouted bed TRISO fuel particles coater using advanced measurement and diagnostic techniques is essential. This understanding will significantly help in the development of reliable and safe scale-up methodology and design, and ensure desired performance and operation of spouted bed TRISO fuel coaters.

In spouted beds, gas travelling at a high velocity through the inlet nozzle at the conical base of the spouted bed. This high velocity creates a jet in the spout region that picks up particles along the bed and carries them to the top of the bed where the particles create a fountain and disengage from the gas phase to fall down to the annular region. This particle movement follows a pathway of continuous circulation. Hence, the spouted bed usually contains three distinct regions as illustrated in [Fig. 1](#); the central spout, the annulus, and the fountain regions. The particle concentration differs from region to region. In the central spout region, solid particles are pulled from the annulus region, carried through the spout by the gas to the fountain region. In the annulus region, the particles move downward as packed bed. Unsurprisingly, this is also the region with the maximum particles concentration. At the top of the bed, the particles form a fountain, where the particles and the gas phase disengage from each other. With no gas phase to hold them, the particles then fall downwards into the annulus region. Based on the flow structure, spouted beds are great

candidates and well-suited to handle heavy, coarse, sticky, and/or irregularly shaped solids through cyclic flow patterns that are encountered in granulation, coating, gasification, and drying processes [9, 10]. It is clear that such a flow pattern leads to complex hydrodynamics, recirculation flow, and gas–particle interactions. The key hydrodynamics of these contactors are solids flow field, solids circulation, solids velocity and turbulence parameters, gas dispersion, gas holdup radial profiles and cross-sectional distributions, and flow regime characteristics. Unfortunately, there is a lack of engineering and scientific knowledge within literature about spouted beds and their hydrodynamics. Recently, Ali et al. [11] studied the local solids and gas holdup distributions along the bed height using gamma ray computed tomography (CT). Also, Aradhya [12] investigated the local solids holdup and velocity in spouted beds using sophisticated and newly developed optical fiber probes. These studies represent important steps towards increased understandings and ability to evaluate the literature reporting scale-up methodology of matching set of dimensionless groups.

Due to the complex hydrodynamic nature of gas-solid spouted beds, their scale-up, design, and performance have not been well-understood. In the literature, He et al. [13] proposed the following set of dimensionless groups to be matched in order to maintain hydrodynamics similarity of gas-solid spouted beds:

$$\frac{gd_p}{U^2}, \frac{\rho_s d_p U}{\mu}, \frac{\rho_f}{\rho_s}, \frac{H}{d_p}, \frac{D_c}{d_p}, \phi_s, \phi, \varepsilon_o, \text{Dimensionless particle size distribution and}$$

dimensionless bed geometry.

Where, gd_p/U^2 is Froude number, $\rho_s d_p U/\mu$ is Reynolds number, ρ_f/ρ_s is ratio of fluid density to particle density, H/d_p is ratio of bed height to particle diameter, D_c/d_p is ratio of column diameter to particle diameter, ϕ_s is sphericity of particles, ϕ is inertial friction angle

of particle, ϕ , and ε_o is loose packed voidage. He et al. [13] extrapolated upon the scaling of dimensionless groups proposed by Glicksman [14] for gas-solid fluidized beds, so that they could be implemented on gas-solid spouted beds despite their hydrodynamic differences. He et al. [13] measured global parameters in order to claim the validity of such a methodology. Aradhya [12] demonstrated the dissimilarity using limited local point measurements of solids velocity and holdup by implementing an optical fiber probe when the proposed dimensionless groups of [13] were matched. Recently, Ali et al. [11] used gamma ray computed tomography (CT) to assess such [13] scale-up methodology and also found that the similarity of solids and gas holdups cross-sectional distribution and their radial profiles along the bed height was not achieved by matching the proposed dimensionless groups. Following the work of [13], studies have been conducted in the literature to expand upon the dimensionless-group-based scale-up approach of spouted beds by adding the restitution coefficient (e_{ss}) of particles to the set of dimensionless groups proposed by [13], [15, 16]. Also, further expansion was done by adding both the restitution coefficient and friction of the particles [17]. Rojas [18] studied different sizes of shallow spouted beds and different conditions without addressing the scale-up issue. However, [18] developed empirical correlations using various dimensionless groups to estimate various global parameters. Most of these dimensionless groups are represented by the set proposed by [13].

In all the studies mentioned above, the key local hydrodynamic parameters, of solids velocity and turbulent parameters (normal stresses, shear stresses, turbulent kinetics energy) have not yet been measured to assess, in detail, the scale-up methodology based on matching dimensionless groups of [13]. Without performing such evaluations, the

comprehensive assessment of such a scale-up methodology will remain uncertain. As outlined above, the dimensionless groups proposed by [13] represent the foundation and basic groups for the scale-up methodology of gas-solid spouted beds based on matching dimensionless groups. This set of dimensionless groups has not yet been evaluated by measurement of the local solids velocity and turbulent parameters. With these in mind, the dimensionless groups and the work of [13] represent the basis of this work when it comes to assessing the approach for matching dimensionless groups to scale-up gas-solid spouted beds. Accordingly, our study addresses the evaluation of such scale up methodology by implementing the radioactive particle tracking (RPT) technique to locally measure the solids velocity components and the turbulent parameters (including normal stresses, shear stresses, turbulent kinetic energy).

2. Experimental work

2.1 Spouted beds setup

The experimental works were carried out in two conical base spouted bed columns made of Plexiglas. They are of different diameters; one column has a diameter of 0.076 m and the other, 0.152 m. The schematic diagrams of the two spouted beds used are shown in Fig. 2. Both columns were designed to be geometrically similar with a height of 1.14 m and a conical base angle of 60-degrees. The two columns were designed without any ports or connections on their wall in order to eliminate the possibility of any non-symmetric problems, which complicates the RPT reconstructions process. Each unit consists of a one-piece column attached to a conical base. At the bottom of the conical base, there is a gas

distributor made of stainless steel placed to allow the flow of gases to form a jet inside the column. The diameter of the inlet orifice is 9.5 mm for the 0.076 m spouted beds and 19.1 mm for the 0.152 m spouted beds. The gas used was dry compressed air supplied from an industrial compressor with capacity up to 735 CFM and 200 Psig. After the flow passes through the piping components of the compressor, the rate of the flow is regulated using a pressure regulator and rotameter setup consisting of two rotameters connected in parallel to each other. The gas flow rates were measured using the two rotameters and gas flow was introduced into the spouted beds through the inlet orifice (gas distributor). To maintain stable spouting in spouted beds, the conditions of the experiments used in [11] were followed.

2.2 Experimental conditions.

Three different conditions from the study of He et al. [13] for the scale-up of spouted beds with matched and mismatched scaling groups, were selected in this work and are similar to conditions used by Ali et al. [11]. The experimental conditions, including the properties of the particles used and the operating conditions, are listed in [Table 1](#). Case A and Case B were designed to achieve matching dimensionless groups to examine the validity of spouted bed scaling groups. The dimensionless groups of Case B were matched as closely as possible to those of Case A. Then, both Cases were deemed as having matching dimensionless groups. Case A was proposed as the reference Case. Case C (prototype Case) was conducted in order to examine the influence of mismatched scaling groups. The design of Case C was also proposed for the study of common unsuitable scale-up criteria when only the bed dimensions are varied to achieve geometrical similarity;

while others scaling groups were not matched. The initial bed height (H) and the inner column diameter (D_c) in Case C were made to be 0.16 m and 0.076 m, respectively, to achieve similarity with Case A with regards to only bed dimensionless groups. The scaling groups H/D_c , D_c/D_i , and D_c/d_p had values equal to those of Case A. However, two important groups were not matched in Case C—Reynolds number and the Froude number. Reynolds number for Cases A and C were 157 and 54, respectively, and the Froude number for Cases A and C were 54.5 and 51.2, respectively. Dissimilar to Case B, some parameters were not taken into account for Case C, so that we were able to get matching dimensionless groups. For example, the gas in Case C was at atmospheric pressure, while in Case B, the bed pressure was increased to 312 kpa. In addition, the type of particles and their densities were not changed in Case C from those of Case A. Both used glass beads particles ($\rho_s = 2400 \text{ kg/m}^3$). In Case B, steel particles were used to match the scaling groups. Subsequently, Cases A and B will be termed as having matching dimensionless groups and Cases A and C will be termed as having mismatched dimensionless groups.

2.3 The Radioactive Particle Tracking (RPT) Technique.

The Radioactive Particle Tracking (RPT) technique is a non-invasive technique used to track single radioactive particles that match the density and size of those in the bed's solid phase. This is done by measuring emitted gamma ray intensities. The RPT technique has been successfully applied to measure and visualize 3D flow fields and turbulence parameters in different multiphase flow systems [19-33]. In this work, RPT has been implemented to assess in detail, for the first time, the scale-up study of spouted beds based on the matching of dimensionless groups [13]. In addition, implementing the RPT

technique on gas-solid spouted beds will significantly advance the fundamental understanding and knowledge of the complex turbulence patterns of spouted beds and provide reliable data on the turbulent characteristics, regarding the flow, in a non-invasive manner. Increased knowledge on this topic will help to evaluate and validate CFD and related models and closures.

In the RPT experiments, the gamma rays emitted by the tracer particle were collected using twenty-eight high-resolution (5.08 cm x 5.08 cm) NaI (TI) detectors arranged strategically around the spouted bed, as shown in Fig. 3. The 28 detectors are located at 14 axial levels with two detectors in each level facing one another (180-degree angle to each other). The detectors were mounted on movable horizontal aluminum structures that are in turn held by four vertical Unistrut bars equally distanced from the column and separated at 90-degree intervals around the column. Each Unistrut supporter had seven detectors placed at different axial levels. The detectors were positioned vertically with respect to the expected bed dynamic. In addition, each detector was radially arranged 12.7 cm from the symmetrical axis of the column. This location is selected to avoid saturation problem of the detectors when the tracer particle is very close to the wall of the column [34]. The detectors are horizontally level and aligned in both axial and azimuthal directions using a leveling device and twin laser-equipped aluminum fake detectors that faced each other.

The tracer particle for each RPT experiment was made in the case it should be as close as possible to size, density, and shape of the tagged solid phase. The tracer particle is embedded with Co-60 ($d_p = 600 \mu\text{m}$) with an activity of about 500 μCi (microcurie) at the

time of the experiments. The RPT experiment consists of two steps: an RPT calibration process and an RPT actual experimental process.

In order to estimate the position of the tracer particle, calibration was performed before the actual RPT experiment by placing the tracer particle at various known locations. This yielded a calibration map relating counts and particle positions for each detector. In the calibration process, a fully automatic calibration device was used to provide highly accurate RPT measurements. This device can automatically move in all directions to visit hundreds or thousands of known locations inside the spouted bed column. The movement of this device was controlled by a data acquisition system, and locations were detected by a tracer-particle-tipped calibration rod. The generated calibration maps of distance counts for all detectors will be used as part of in-house developed algorithms and programs for reconstructing the positions of the tracer particle during the actual experiment.

The local statistical characteristics were assessed with approximately two million data points obtained from fourteen hours of particle tracking in 0.152 m spouted beds, and one million data points obtained from six hours of particle tracking in 0.076 m spouted beds. For both beds, the counting acquisition frequency was 50 Hz. The 3D instantaneous particle positions were reconstructed from the count rate of the tracer particle using a cross-correlation-based position algorithm coupled with a semi-empirical model in order to provide further calibration points. This method was based on relating tracer particle count rate to the positions of the particle. The cross-correlation-based position method was originally developed and used for the processing of RPT data on gas-solid risers [22]. The method was also used in our laboratory for a pebble bed reactor study [35]. For further

details about the technique and algorithms used to reconstruct the particle positions, the reader can refer to recent works of our group [35, 36].

In order to obtain the time-averaged velocity and turbulence parameters, it is required to identify the initial particle coordinates in the spouted bed column. To accomplish this, cylindrical mesh compartments of equal volume were defined to represent the entire column of the spouted bed. Two important points were considered when determining the sampling compartments: the sufficient occurrences of the particle per compartment, and a good radial profile description for each bed height level. The sampling compartments were evaluated and the column was divided into 1127 and 735 compartments for 0.152 m and 0.076 m spouted beds, respectively. All the while, the eight radial points for the profile description were maintained.

Once the instantaneous positions of the tracer particle and its lagrangian trajectory were defined, the next step was to calculate the instantaneous particle velocity (r , θ , and z) and the turbulence parameters in each compartment. The distance traveled by the particle between two successive positions divided by the time interval needed to travel that distance, yielded its velocity.

$$\begin{pmatrix} u_r \\ u_\theta \\ u_z \end{pmatrix} = \frac{1}{T} \begin{pmatrix} r_{i+1} - r_i \\ r_m (\theta_{i+1} - \theta_i) \\ z_{i+1} - z_i \end{pmatrix} \text{ where } \begin{cases} T = t_{i+1} - t_i \\ r_m = (r_{i+1} + r_i) / 2 \end{cases} \quad (6)$$

Then, based on the ensembled particle total number of occurrences per compartment (N_v), the time-averaged (mean) velocity fields in each compartments (i, j, k) were calculated as follows:

$$\bar{u}_{p(i,j,k)} = \frac{1}{N_v} \sum_{i=1}^{N_v} u_{p(i,j,k)i} \quad p = r, \theta, z \quad (7)$$

For data presentation, the circular azimuthal averaging was performed for each (r,z) level to calculate the azimuthally-averaged velocity ($\bar{u}_{p(i,j,k)}$) for the axial and radial components, where N_θ is the number of compartments in the azimuthal direction. As a result, eight positions of the profile description were obtained along the radial direction for each (z) level:

$$\bar{u}_{(i,k)} = \frac{1}{N_\theta \tilde{N}_{v(i,k)}} = \sum_{j=1}^{N_\theta} \bar{u}_{(i,j,k)} N_{v(i,j,k)} \quad (8)$$

$$\tilde{N}_{v(i,k)} = \frac{1}{N_\theta} \sum_{j=1}^{N_\theta} N_{(i,j,k)} \quad (9)$$

In this equation, $\tilde{N}_{v(i,k)}$ is the average number of velocity occurrences for a given two-dimensional compartment (i, k). Hence, the fluctuation velocity (u') was conventionally calculated by subtracting the mean velocity (\bar{u}) from the instantaneous velocities ensembled (u) as follows:

$$u'_{p(i,j,k)} = u_{p(i,j,k)} - \bar{u}_{p(i,j,k)} \quad (10)$$

Once the fluctuation velocities were obtained, the turbulent stresses, and turbulent kinetic energy per unit mass can be calculated as follows:

$$\tau_{pq} = \overline{u'_{p(i,j,k)} u'_{q(i,j,k)}} \quad p, q = r, \theta, z \quad (11)$$

$$TKE = \frac{1}{2} (\tau_{rr} + \tau_{\theta\theta} + \tau_{zz}) \quad (12)$$

3. Results and discussion

As mentioned earlier, three sets of experimental conditions, in two differently-sized spouted beds, were used to evaluate the dimensionless relationships of [13] so that hydrodynamic similarity is maintained in the spouted beds. The experimental conditions were originally selected to capture matched and mismatched dimensionless groups between the conditions as outlined in [Table 1](#). In this section, Cases A (0.152 m diameter bed) and B (0.076 m diameter bed) were designated to have matching dimensionless groups, and Cases A and C (0.076 m diameter bed) were designated to have mismatched dimensionless groups. Case A represents the reference conditions.

3.1 Radial Profiles of the Averaged Particles Velocity

In this section, the results of the azimuthally and axially averaged axial and radial particle velocities radial profiles are presented and discussed. Due to the insignificance of the averaged azimuthal (angular) particle velocity value, which is smaller than the axial and radial particle velocities, the averaged azimuthal particle velocity is not presented here.

3.1.1 Radial Profiles of the Averaged Axial Particles Velocity

In spouted beds, three distinct regions exist and each one has a specific flow behavior. The solids are carried up by the gas phase in the spout region, which functions

as a gas-solid riser, until it reaches the top of the bed surface. Here, the solids are disengaged from the gas phase and are in the fountain region. The solids fall down freely, due to gravity, onto the annulus region. During such solid circulation, the three known regions of spouted beds are created; they include the spout in the center of the column, the annulus surrounding the spout, and the fountain on the top of the spout-annulus regions. Fig. 4 shows the azimuthally and axially averaged profiles of the averaged axial particle velocity for the reference Case (Case A) and the conditions of matched (Case B) and mismatched (Case C) dimensionless groups in 0.152 m and 0.076 m spouted beds. The results show the magnitude and pattern of the averaged axial velocity of the particles in each region of the spouted beds. In the spout, the particles move upwards (i.e. $U_z > 0$) with a higher axial velocity at the center zone of the spout, where the particles are carried up by the gas phase. The velocity of the solids decrease radially out from the axis (i.e. center of the spout) toward the spout-annulus interface. This is in agreement with the results obtained by the CT technique [11] where weak divergence in the solids holdup profile is observed at the spout-annulus interface. When the particles reach the fountain, the axial velocity is at maximum near the axis but becomes negative (i.e. downward, $U_z < 0$) as particles fall in the outer region of the fountain. For matched (Case B) and mismatched (Case C) conditions, deviations from the averaged axial velocity profile of the reference Case (Case A), are generally apparent in the spout and fountain regions. In the spout region, the average profile deviation percentage from that of the reference Case (Case A) is found to be 18.91% and 45.24% for the conditions of matched (Case B) and mismatched (Case C) dimensionless groups, respectively. In the annulus, the axial particle velocity observed is low and negative for all the Cases. Also, the deviations between the profiles are relatively

small because the particles move downwards slowly in the loosely moving packed bed. This is in agreement with the results obtained using the CT technique [11], where the solids-holdup profiles in this region remain similar and unchanged between the Cases. In the fountain, the average profile deviation percentage from that of Case A, is 47.48% and 46.54% for the conditions of matched (Case B) and mismatched (Case C) dimensionless groups, respectively.

The above results represent the actual velocity values of the solids, which normally differ with increases to the bed size or modifications to operating conditions for similar bed geometries. Therefore, to assess for hydrodynamic similarity, these values should be presented in the form of dimensionless values using a known or measurable parameter. In this case, the minimum spouting velocity (U_{ms}), which can be estimated with an acceptable level of fidelity [37], has been selected to convert the actual velocity values of local solids, into dimensionless values. This can facilitate the attainment of the similarity for scale-up. In this case the actual solids velocities at the scaling-up conditions can be estimated by using the dimensionless local solids velocities of a reference Case—but only if the minimum spouting velocity of those scaling-up conditions can be estimated. Therefore, to assess the comparison between the Cases (Cases A and B and Cases A and C) for matching and mismatching dimensionless group conditions, the profiles of the Cases' axial particle velocities are non-dimensionalized by dividing them by the minimum spouting velocity (U_{ms}). Minimum spouting velocity (U_{ms}) is defined as the minimum superficial gas velocity that is required to obtain the spouting state in spouted beds; below this velocity, solids circulation is absent and all three spouted bed regions are not entirely created. In this work, the minimum spouting velocities (U_{ms}) for the conditions in [Table 1](#) were measured by

increasing the superficial gas velocity slowly from the state of fixed bed to the onset of external spouting. The measured values of minimum spouting velocity (U_{ms}) are listed in [Table 1](#).

Accordingly, the dimensionless axial particle velocity profiles for the conditions of the reference Case (Case A), and cases with matched Case (B) and mismatched Case (C) dimensionless groups are shown in [Fig. 5](#). Deviation is observed between the profiles of these Cases in the spout and the fountain regions. It has been noted that the difference between the profiles have increased when compared to those of the actual axial particle velocities illustrated in [Fig. 4](#). In the spout, the average profile deviation percentage of Cases A and B is 33.97%. Near the axis of the spout, ($r/R=0.0625$) the deviation is 37.15%. Near the spout-annulus interface ($r/R=0.427$), it is 32.36%. In the fountain region, the average profile deviation percentage is also augmented and has a value of 107.41%. The most significant amount of deviation is in the outer region of the fountain where the average value is 169.78%. In the annulus region, the deviation between the profiles remained small and insignificant.

The dimensionless axial particle velocities for the conditions of mismatched (Case C) dimensionless groups are also shown in [Fig. 5](#). The profiles of Case A and Case C spouted beds deviate from each other noticeably in the spout and fountain regions. The deviation is larger near the center of the spout and decreases as the radial distance from the axis increases up to the spout-annulus interface, where the spout is confined by the annulus. Near the axis of the spout ($r/R=0.0625$), the deviation is 49.38%, and at the spout-annulus interface, it is 32.36%. In the fountain region, the deviation increases and has an average

value of 49.04%. The results signify the failure of achieving sufficient hydrodynamics similarity between the cases by matching the dimensionless groups proposed [13].

3.1.2 Radial Profiles of the Averaged Radial Particles Velocity

The horizontal radial component of the particle velocity was measured using RPT for the conditions of matched and mismatched dimensionless groups shown in [Table 1](#). The azimuthally and axially averaged radial profiles of the radial particle velocities for the 0.152 m and the 0.076 m spouted beds are shown in [Fig. 6](#). The magnitudes of the averaged radial particle velocities are small compared to the averaged axial particle velocity. This is because of the symmetrical gas-solids flow within the axes of the spouted beds. The results show the variation in particle movement and depict the behavior of the averaged radial particle velocity in all the three regions (the spout, the annulus, and the fountain). In the spout region, the particle moves towards the axis (i.e. inward, $U_r < 0$) of the spout with the maximum negative value obtained from approximately the middle between the center of the spout and the spout-annulus interface ($r/R=0.2$). After this point from the center, the averaged absolute radial particle velocity decreases until you reach the spout-annulus interface (becomes increasingly less negative in value). For both conditions, the most deviation observed from those of the reference Case (Case A), was in the spout and the fountain regions. In the spout region, the average profile deviation percentage was 45.88% and 54.4%, respectively, for the conditions of matched and mismatched dimensionless groups. In the annulus region, the profiles are nearly flat. The radial particle velocity then changes into positive values (i.e. outward, $U_r > 0$) when the particles reach the fountain region. The profiles show a radial dispersion in the fountain due to scattering of the

particles in the r-direction. The averaged profile deviation percentage is 42.41% and 50.76% for the conditions of matched and mismatched dimensionless groups, respectively.

Similar to the section discussing averaged axial particle velocity, the profiles of the averaged radial particle velocity were non-dimensionalized for both bed sizes by dividing by the minimum spouting velocity (U_{ms}). Fig. 7 shows the deviation of dimensionless radial particle velocities for the conditions of matched and mismatched dimensionless groups. Deviation is witnessed once again between the profiles in the spout and fountain regions for the conditions of matched and mismatched dimensionless groups, from those of the reference Case (Case A). This indicates that matching the dimensionless groups in the scale-up cannot give good predications of radial particle velocities. The averaged profile deviation percentages are 62.84% and 55.31%, respectively, for the conditions of matched and mismatched dimensionless groups. In the fountain, the deviation between dimensionless values of the Cases increased from that of the absolute values, and has an average value of 95.03% and 55.09%, respectively, for the conditions of matched and mismatched dimensionless groups. The results signify that matching dimensionless groups between the two beds correspondingly, gives a large difference between the dimensionless averaged radial particle velocities in the spout region.

3.2 Radial Profiles of the Averaged Particle Normal Stresses

3.2.1 Radial profiles of the Averaged Axial Particle Normal stresses

Fig. 8 illustrates the radial profiles of the azimuthal and axial averaged normal stresses (τ_{zz}) for the reference Case (Case A), the conditions of matched dimensionless groups (Case B), and the conditions of mismatched dimensionless groups (Case C) in 0.152 m and 0.076 m spouted beds, respectively. The results show the magnitude and the pattern of τ_{zz} of the particles in each region of the spouted beds. In the spout, the magnitude of τ_{zz} is much larger than in the other regions. The maximum value is detected in the center zone of the spout region. This is because the axial particle velocities and the related fluctuation velocities are also maximal in the central zone of the spout. Since the axial particle velocities and their fluctuations reduce radially outwards to the annulus zone, the same trend is found for the τ_{zz} . The τ_{zz} for Case A is larger than that of Case B (matched dimensionless groups) and even greater than that of Case C (mismatched dimensionless groups). In the spout region, the absolute relative differences of the profiles, with respect to Case A, are 36.11% and 60.12% for Cases B and C, respectively. The differences in percent among these Cases for τ_{zz} are larger in the center zone of the spout and reduces outwards as you approach the annulus region. At the annulus region, due to the nature of the flow structure, the magnitudes of τ_{zz} are much lower than those of the spout region ($\tau_{zz} < 500-1000$ As compared to τ_{zz} of about 14000 in spout region); also, τ_{zz} magnitudes are similar between cases. This is also due to the velocities of solids and the fact that their fluctuations are small. Remember that solids move downwards as a packed bed as discussed earlier (Fig. 1). At the fountain region, τ_{zz} values are smaller near the bed axis and they increase towards a maxima at the zone of about $r/R=0.4$; and then they decrease towards the bed wall. This trend indicates that the axial particle velocity fluctuations in the

central zone of the bed of the fountain are smaller, despite the fact that particle velocities at the fountain zone are larger. At the zone of about $r/R=0.4$ shown in Fig. 4 the axial particle velocities invert from positive (upward) to negative (downward) values. Therefore, the fluctuations of the axial velocities are larger in this zone of the bed. These fluctuations decrease towards the wall of the bed and hence, τ_{zz} decreases. The same trend is found during the comparison between the Cases. The axial normal stress of Cases A and B deviate from each other by 27.32%; the deviation of Cases A and C is more obvious, at about 65.52%. It is clear that the local radial profiles of τ_{zz} are different when the dimensionless groups are matched. The differences are even more pronounced for the conditions of mismatched dimensionless groups. When the magnitudes of τ_{zz} are converted to dimensionless values with respect to the squared minimum spout velocity, the trend of differences remain the same and the magnitudes of the percentage differences get even larger, as demonstrated in Fig. 8. The average deviation between the profiles for matching dimensionless groups increases to 40.47% and 66.56%, respectively, at the spout and the annulus regions. This further confirms that the list of dimensionless groups provided by [13] for attaining hydrodynamic similarity, is not adequate and that such scale-up methodology is further invalidated.

3.2.2 Radial Profiles of the Averaged Radial particle Normal stresses

Fig. 9 illustrates the magnitudes and radial profiles of the azimuthal and axial radial normal stresses (τ_{rr}) for the reference Case (Case A), the conditions of matched dimensionless groups (Case B), and the conditions of mismatched dimensionless groups (Case C) in 0.152 m and 0.076 m spouted beds. It is obvious that the magnitudes of τ_{rr} are much smaller than those of τ_{zz} in the three studied regions of the spouted beds. In the spout and annulus regions, the τ_{rr} values are comparable to those of τ_{zz} in the annulus region. This is due to negligible velocity and its fluctuations in the radial direction. However, in the fountain region, due to the flow structure of the fountain and the freely falling particles, non-negligible particle radial velocities and their fluctuations exist. Hence, the magnitudes of τ_{rr} are much larger than those in the spout and annulus regions. Similar to τ_{zz} trends and profiles, there are τ_{rr} maxima in the region between $r/R=0.4$ and $r/R=0.6$, which indicates that larger radial particle velocity fluctuations and magnitudes exist in this zone. This is consistent with the trend and profiles of the particle radial velocities shown in Fig. 6. When the magnitudes of τ_{rr} are converted into dimensionless values with respect to the squared minimum spout velocity, the trend of differences remain the same. However, the magnitude percentage difference gets even larger, as demonstrated in Fig. 9. The dimensionless averaged radial normal stresses of Cases A and B deviate from each other by 53.6% and 51.8% at the spout and the annulus regions, respectively. This further confirms the lack of reproducibility regarding the dimensionless groups' approach of [13] for the scale-up of spouted beds for hydrodynamic similarity.

3.2.3 Radial Profiles of the Averaged Azimuthal Particle Normal stresses

The azimuthal and axial averaged azimuthal normal stresses' ($\tau_{\theta\theta}$) radial profiles are illustrated in Fig. 10. Due to the flow nature in the spout and annulus regions, where the particles move downwards in the annulus region and move angularly as they enter into the spout region from the spout-annulus interface, the angular velocity fluctuations are higher than those for radial velocity components. Therefore, the magnitudes of the $\tau_{\theta\theta}$ in the spout and annulus regions are higher than those of the τ_{rr} , but in the spout region, they are smaller than those of the τ_{zz} . In the fountain region, due to the rotational nature of the fountain flow structure, the angular velocity fluctuations are also noticeable. Hence, the magnitudes of $\tau_{\theta\theta}$ are comparable to those in the spout region. However, the trend is different from those of τ_{rr} and τ_{zz} , where maxima do not exist. The maximum values of the $\tau_{\theta\theta}$ are at the center zone of the spout region and they decrease as the annulus region is approached. However, in the fountain region, they decrease towards the wall, where the fluctuations in the angular direction and the magnitude of the angular velocity component get smaller. Also the values at the reference conditions are larger than those at the conditions with matching and mismatching dimensionless groups, which further confirm the non-validity of the proposed set of dimensionless groups [13]. When the magnitudes of $\tau_{\theta\theta}$ are converted into dimensionless values with respect to the minimum spout velocity, the average deviation in the spout between Cases A and B is 41.96%; between Cases A and C, it is 64.93%. This further confirms that the previously mentioned set of dimensionless groups that were proposed to be adequate for scale-up methodology and attaining hydrodynamic similarity, are further invalidated.

3.3 Radial Profiles of the Averaged Particle Shear stresses

Fig. 11 shows the azimuthal and axial averaged shear stresses' radial profiles for the studied conditions mentioned above (Cases A, B, and C). In the spout region, τ_{rz} radial profiles show maxima at the zone between the center of the spout and the spout-annulus interface ($\sim r/R=0.2$). This trend reflects the magnitude of the fluctuations in the axial and radial components of the velocities; their multiplication gives the maximum value at $\sim r/R=0.2$. At about the spout-annulus interface, the τ_{rz} values are negative from about $r/R=0.35$ to about $r/R=0.6$. In the annulus region, the values of τ_{rz} are small compared to those of the spout region due to the nature of the annulus's flow structure. In the fountain region however, the maximum value occurs in the zone of about $r/R=0.7$. At both the center zone and the wall zone, the τ_{rz} values are comparable for all the studied Cases. It is clear that there is a mismatch in the magnitudes of the τ_{rz} between the reference conditions of Case A and the matching dimensionless groups conditions (Case B). The differences get larger between mismatching dimensionless groups (Case A compared with Case C). In addition, when τ_{rz} values are converted into dimensionless values using the minimum spouting gas velocity, the differences in values still exist and get larger, as summarized in [Table 2](#). This confirms that the dimensionless groups proposed by [13] are not adequate for scale-up and for hydrodynamic similarity.

3.4 Radial Profiles of the Averaged particles turbulent kinetic energy

Fig. 13 demonstrates the turbulent kinetic energy in the three regions of the studied spouted beds for the conditions of Cases A, B, and C. The turbulent kinetic energies of the particles are larger in the center zone of the spout region for the Cases and reduces as the spout-annulus interface is approached. This trend is similar to the trends of the τ_{zz} and $\tau_{\theta\theta}$, whose values are significant compared to τ_{rr} . At the annulus region, the turbulent kinetic energy levels off and the magnitudes are smaller than those of the spout region are. In the fountain region, the turbulent kinetic energy magnitudes are comparable to those of the spout region's center zone; the maximum value exists at the region between about $r/R=0.4$ to $r/R=0.5$. This is similar to the trends for τ_{zz} and τ_{rr} , whose values are dominating the estimated values of turbulent kinetic energy. The radial profile values of the turbulent kinetic energies for Case A (reference conditions), noticeably differ from those of Case B, where the dimensionless groups of [13] are matched. When the dimensionless groups are not matched (Case C compared with Case A), the difference in values of the turbulent kinetic energy get larger. This means that more differences in dimensionless groups would lead to more differences in local hydrodynamic parameters. Similar findings related to the differences between Cases A, B, and C were obtained when the turbulent kinetic energy values are converted into dimensionless values. This further confirms the invalidity of the scale-up methodology based on matching dimensionless groups [13]. Additional dimensionless groups would be required in order for hydrodynamic similarity to be attained, which make the methodology even more difficult to implement.

4. Conclusion

The advanced non-invasive radioactive particle tracking (RPT) technique has been implemented to assess, for the first time, the scale-up methodology of gas-solid spouted beds based on matching dimensionless groups proposed by [13]. By measuring the radial profiles of the solids velocity, normal stresses, shear stresses, and turbulent kinetic energy, it has been found that matching the set of dimensionless groups in the studied two sizes of spouted beds did not result in the attainment of hydrodynamic similarity by comparing the values of these parameters and their dimensionless quantities. This finding confirms the findings of [12], who made local point-wise measurements of solids velocity and solids holdup using a sophisticated optical fiber probe. Also, this conclusion is consistent with the findings of [11] based on measuring the time-averaged cross sectional distributions solids and gas holdups and their radial profiles by implementing gamma ray computed tomography (CT) technique. It is noteworthy that adding more dimensionless groups to capture the key phenomena, further complicates the implementation of matching dimensionless groups based scale-up methodology.

Acknowledgment

US Department of Energy - Nuclear Energy Research Initiative (DOE-NERI) grant (NERI DEFC07-07ID14822), the GAANN, chancellor fellowship, and professor Al-Dahhan's lab fund the financial support that made this work possible. The second author would like to thank the Saudi Arabian Cultural Mission (SACM) for sponsoring his PhD studies at MST.

References

- [1] A.V. Herzog, T.E. Lipman, D.M. Kammen, Renewable energy sources, in: Encyclopedia of Life Support Systems (EOLSS). Forerunner Volume-‘Perspectives and Overview of Life Support Systems and Sustainable Development, 2001.
- [2] K. Sawa, S. Ueta, Research and development on HTGR fuel in the HTTR project, Nuclear Engineering and Design, 233 (2004) 163-172.
- [3] C. Tang, Y. Tang, J. Zhu, Y. Zou, J. Li, X. Ni, Design and manufacture of the fuel element for the 10 MW high temperature gas-cooled reactor, Nuclear Engineering and Design, 218 (2002) 91-102.
- [4] K. Verfondern, H. Nabielek, J.M. Kendall, Coated particle fuel for high temperature gas cooled reactors.
- [5] Y.-W. Lee, J.-Y. Park, Y.K. Kim, K.C. Jeong, W.K. Kim, B.G. Kim, Y.M. Kim, M.S. Cho, Development of HTGR-coated particle fuel technology in Korea, Nuclear Engineering and Design, 238 (2008) 2842-2853.
- [6] M. Liu, Y. Shao, B. Liu, Pressure analysis in the fabrication process of TRISO UO₂-coated fuel particle, Nuclear Engineering and Design, 250 (2012) 277-283.
- [7] I.E. Porter, T.W. Knight, M.C. Dulude, E. Roberts, J. Hobbs, Design and fabrication of an advanced TRISO fuel with ZrC coating, Nuclear Engineering and Design, 259 (2013) 180-186.
- [8] G.K. Miller, D.A. Petti, J.T. Maki, D.L. Knudson, An evaluation of the effects of SiC layer thinning on failure of TRISO-coated fuel particles, Journal of Nuclear Materials, 355 (2006) 150-162.
- [9] K.B. Mathur, N. Epstein, 1 - Introduction, in: K.B. Mathur, N. Epstein (Eds.) Spouted Beds, Academic Press, 1974, pp. 1-13.
- [10] W. Shuyan, L. Yongjian, L. Yikun, W. Lixin, D. Qun, W. Chunsheng, Simulations of flow behavior of gas and particles in spouted bed with a porous draft tube, Powder Technology, 199 (2010) 238-247.
- [11] N. Ali, T. Al-Juwaya, M. Al-Dahhana, Assessing the scale-up methodology of gas-solid spouted beds based on matching dimensionless groups using gamma ray computed tomography (CT), Chemical Engineering Research and Design, ## (2016) "Submitted" or "under consideration".

- [12] S.B. Aradhya, Scaleup and hydrodynamics study of gas-solid spouted beds, in: *Chemical and Biochemical Engineering*, Missouri University of Science and Technology, 2013, pp. xxiv, 301 pages.
- [13] Y.L. He, C.J. Lim, J.R. Grace, Scale-up studies of spouted beds, *Chemical Engineering Science*, 52 (1997) 329-339.
- [14] L.R. Glicksman, Scaling relationships for fluidized beds, *Chemical Engineering Science*, 39 (1984) 1373-1379.
- [15] J. Xu, Y. Ji, W. Wei, X. Bao, W. Du, Scale-up relationships of spouted beds, in, 2007.
- [16] W. Du, J. Xu, Y. Ji, W. Wei, X. Bao, Scale-up relationships of spouted beds by solid stress analyses, *Powder Technology*, 192 (2009) 273-278.
- [17] P.A. Shirvanian, J.M. Calo, Hydrodynamic scaling of a rectangular spouted vessel with a draft duct, *Chemical Engineering Journal*, 103 (2004) 29-34.
- [18] L. Rojas, I. Deytia, Investigation of hydrodynamic scaling relationships in shallow spouted beds, in, 2011.
- [19] S. Bhusarapu, M. Cassanello, M.H. Al-Dahhan, M.P. Dudukovic, S. Trujillo, T.J. O'Hern, Dynamical features of the solid motion in gas–solid risers, *International Journal of Multiphase Flow*, 33 (2007) 164-181.
- [20] M.H. Al-Dahhan, Radioisotopes applications in industry: an overview, *Atoms for Peace: an International Journal*, 2 (2009) 324-337.
- [21] S. Bhusarapu, M. Al-Dahhan, M.P. Dudukovic, Quantification of solids flow in a gas–solid riser: single radioactive particle tracking, *Chemical Engineering Science*, 59 (2004) 5381-5386.
- [22] S. Bhusarapu, M.H. Al-Dahhan, M.P. Duduković, Solids flow mapping in a gas–solid riser: Mean holdup and velocity fields, *Powder Technology*, 163 (2006) 98-123.
- [23] M. Cassanello, F. Larachi, A. Kemoun, M.H. Al-Dahhan, M.P. Dudukovic, Inferring liquid chaotic dynamics in bubble columns using CARPT, *Chemical Engineering Science*, 56 (2001) 6125-6134.
- [24] J. Chen, A. Kemoun, M.H. Al-Dahhan, M.P. Duduković, D.J. Lee, L.-S. Fan, Comparative hydrodynamics study in a bubble column using computer-automated radioactive particle tracking (CARPT)/computed tomography (CT) and particle image velocimetry (PIV), *Chemical Engineering Science*, 54 (1999) 2199-2207.

- [25] H.-P. Luo, A. Kemoun, M.H. Al-Dahhan, J.M.F. Sevilla, J.L.G.a. Sánchez, F.G.a. Camacho, E.M. Grima, Analysis of photobioreactors for culturing high-value microalgae and cyanobacteria via an advanced diagnostic technique: CARPT, *Chemical Engineering Science*, 58 (2003) 2519-2527.
- [26] A.R. Rammohan, A. Kemoun, M.H. Al-Dahhan, M.P. Dudukovic, Characterization of Single Phase Flows in Stirred Tanks via Computer Automated Radioactive Particle Tracking (CARPT), *Chemical Engineering Research and Design*, 79 (2001) 831-844.
- [27] A.R. Rammohan, A. Kemoun, M.H. Al-Dahhan, M.P. Dudukovic, A Lagrangian description of flows in stirred tanks via computer-automated radioactive particle tracking (CARPT), *Chemical Engineering Science*, 56 (2001) 2629-2639.
- [28] T. Djeridane, F. Larachi, D. Roy, J. Chaouki, R. Legros, Investigation of the mean and turbulent particle velocity fields in a spouted bed using radioactive particle tracking, *The Canadian Journal of Chemical Engineering*, 76 (1998) 190-195.
- [29] F. Larachi, J. Chaouki, G. Kennedy, M.P. Dudukovic, Chapter 11 - Radioactive particle tracking in multiphase reactors: Principles and applications, in: J.C.L.P. Duduković (Ed.) *Non-Invasive Monitoring of Multiphase Flows*, Elsevier Science B.V., Amsterdam, 1997, pp. 335-406.
- [30] F.ç. Larachi, B.P.A. Grandjean, J. Chaouki, Mixing and circulation of solids in spouted beds: particle tracking and Monte Carlo emulation of the gross flow pattern, *Chemical Engineering Science*, 58 (2003) 1497-1507.
- [31] D. Roy, F. Larachi, R. Legros, J. Chaouki, A study of solid behavior in spouted beds using 3-D particle tracking, *The Canadian Journal of Chemical Engineering*, 72 (1994) 945-952.
- [32] R.K. Upadhyay, S. Roy, Investigation of hydrodynamics of binary fluidized beds via radioactive particle tracking and dual-source densitometry, *The Canadian Journal of Chemical Engineering*, 88 (2010) 601-610.
- [33] M.S. Vesvikar, M. Al-Dahhan, Hydrodynamics investigation of laboratory-scale Internal Gas-lift loop anaerobic digester using non-invasive CAPRT technique, *Biomass and Bioenergy*, 84 (2016) 98-106.
- [34] S. Roy, F. Larachi, M.H. Al-Dahhan, M.P. Duduković, Optimal design of radioactive particle tracking experiments for flow mapping in opaque multiphase reactors, *Applied Radiation and Isotopes*, 56 (2002) 485-503.

[35] V.B. Khane, Experimental and computational investigation of flow of pebbles in a pebble bed nuclear reactor, in, 2014.

[36] M.K.A. Mesfer, Effect of Dense Heat Exchanging Internals on the Hydrodynamics of Bubble Column Reactors Using Non-invasive Measurement Techniques, in: Department of Chemical and Biochemical Engineering, Missouri University of Science and Technology, Rolla, Missouri, 2013.

[37] K.B. Mathur, P.E. Gishler, A technique for contacting gases with coarse solid particles, AIChE Journal, 1 (1955) 157-164.

Notation

d_p	particle diameter, m
D_c	inner column diameter, m
D_i	inlet orifice diameter, m
e_{ss}	restitution coefficient of the particles
Fr	Froude number
g	acceleration of gravity, m s^{-2}
H	static bed height, m
H_F	fountain height, m
H_m	maximum spoutable bed depth, m
L	column length, m
N_v	total number of occurrences per compartment.
\tilde{N}_v	the average number of velocity occurrences for a given two-dimensional compartment (i, k).
N_r	number of radial positions for column discretization.
N_θ	number of azimuthal positions for column discretization.
P	bed pressure, Pa
Re	Reynolds number
R	column radius, cm
T	bed temperature, K
T	time, second
TKE	turbulent kinetic energy (per unit bulk density), $\text{cm}^2 \text{s}^{-2}$
U	superficial gas velocity, m s^{-1}

U_{ms}	minimums pouting velocity, $m\ s^{-1}$
U	axially averaged of the mean particle velocity (\bar{u}), $m\ s^{-1}$
u	instantaneous local particle velocity, cm/s
\bar{u}	averaged particle velocity, cm/s
u'	fluctuating particle velocity, cm/s
z	axial distance form inlet orifice, m

Greek letters

β	fluid-particle interaction coefficient, $kg\ m^3\ s^{-1}$.
ρ_s	particle density, $Kg\ m^{-3}$.
ρ_f	fluid density, $Kg\ m^{-3}$.
μ	fluid viscosity, $Kg\ m^{-1}\ s^{-1}$.
ϕ_s	sphericity of particles.
φ	inertial friction angle of particle, deg .
ε_{mf}	bed voidage at minimum fluidization.
ε_o	voidage at packed bed state
ε_s	solids fraction (or solids holdup).
ε_g	gas fraction (or gas holdup).
τ_{pq}	stress in the pq direction ($p, q = r, \theta, z$), cm^2/s^2 .

Subscripts

'	Dimensionless parameter.
---	--------------------------

List of Tables

Table 1. Experimental conditions (Dimensions, particle properties, and scaling parameters) for matched and mismatched dimensionless groups; used for the scale-up of spouted beds [13].

Table 2. Percentage differences in shear stresses among the studied conditions of Cases A, B, and C.

List of figures

Fig. 1. Schematic diagram of spouted beds.

Fig. 2. Schematic diagram of the 0.076 m and 0.152 m spouted beds.

Fig. 3. Schematic diagram showing the positions of 14-detectors arranged around the 0.152 m spouted bed.

Fig. 4. Azimuthally and axially averaged radial profiles of the axial particle velocity for the conditions of the reference Case (Case A), the case with matched dimensionless groups (Case B), and the case with mismatched dimensionless groups (Case C) for 0.152 m and 0.076 m spouted beds in the spout/annulus and the fountain regions.

Fig. 5. Azimuthally and axially averaged radial profiles of the dimensionless axial particle velocity for the conditions of matched and mismatched dimensionless groups for 0.152 m and 0.076 m spouted beds in the spout/annulus and the fountain regions ($U_{ms} = 89, 61, 68$ cm/s, respectively for Cases A, B, and C).

Fig. 6. Azimuthally and axially averaged radial profiles of the radial particle velocity for the conditions of matched and mismatched dimensionless groups for 0.152 m and 0.076 m spouted beds in the spout/annulus and the fountain regions.

Fig. 7. Azimuthally and axially averaged radial profiles of the dimensionless radial particle velocity for the conditions of matched and mismatched dimensionless groups for 0.152 m and 0.076 m spouted beds in the spout/annulus and the fountain regions ($U_{ms} = 89, 61, 68$ cm/s, respectively for Cases A, B, and C).

Fig. 8. Azimuthally and axially averaged radial profiles of (a) the axial normal stresses and (b) the dimensionless axial normal stresses with respect to the squared minimum spouting velocity, in the spout/annulus and the fountain regions for the conditions of matched and

mismatched dimensionless groups for 0.152 m and 0.076 m spouted beds ($U_{ms} = 89, 61,$ and 68 cm/s, respectively for Case A, B, and C).

Fig. 9. Azimuthally and axially averaged radial profiles of the radial normal stresses in (a) and (b) the dimensionless radial normal stress, in the spout/annulus and (d) the fountain regions for the conditions of matched and mismatched dimensionless groups for 0.152 m and 0.076 m spouted beds ($U_{ms} = 89, 61,$ and 68 cm/s, respectively for Case A, B, and C).

Fig. 10. Azimuthally and axially averaged radial profiles of (a) the azimuthal normal stresses, and (b) the dimensionless azimuthal normal stresses, in the spout/annulus and the fountain regions for the conditions of matched and mismatched dimensionless groups for 0.152 m and 0.076 m spouted beds ($U_{ms} = 89, 61,$ and 68 cm/s, respectively for Case A, B, and C).

Fig. 11 Azimuthally and axially averaged radial profiles of the shear stresses for the conditions of matched and mismatched dimensionless groups for 0.152 m and 0.076 m spouted beds in the spout/annulus and the fountain regions.

Fig. 12. Azimuthally and axially averaged radial profiles of the dimensionless shear stresses in the spout/annulus and the fountain regions for the conditions of matched and mismatched dimensionless groups for 0.152 m and 0.076 m spouted beds ($U_{ms} = 89, 61,$ and 68 cm/s, respectively for Case A, B, and C).

Fig. 13. Azimuthally and axially averaged radial profiles of turbulent kinetic energy (per unit bulk density), And (b) the dimensionless turbulent kinetic energy, in the spout/annulus and the fountain regions for the conditions of matched and mismatched dimensionless groups for 0.152 m and 0.076 m spouted beds ($U_{ms} = 89, 61,$ and 68 cm/s, respectively for Case A, B, and C).

Table 1. Experimental conditions (Dimensions, particle properties, and scaling parameters) for matched and mismatched dimensionless groups; used for the scale-up of spouted beds [13].

Condition/Case	A	B	C
D_c (m)	0.152	0.076	0.076
D_i (mm)	19.1	9.5	9.5
L (m)	1.14	1.14	1.14
H (m)	0.323	0.16	0.16
T (K)	298	298	298
P (kPa)	101	312	101
Particles	Glass	Steel	Glass
d_p (mm)	2.18	1.09	1.09
ρ_s (kg/m ³)	2400	7400	2450
ρ_f (kg/m ³)	1.21	3.71	1.21
μ ($\times 10^5$)(Pa.s)	1.81	1.81	1.81
U (m/s)	1.08	0.75	0.74
U_{ms} (measured, m/s)	0.89	0.61	0.68
Scaling groups			
ϕ_s	1	1	1
φ (°)	26	28	27
ε_{mf}	0.41	0.42	0.42
H/D_c	2.1	2.1	2.1
D_c/D_i	8	8	8
D_c/d_p	70	70	70
ρ_s/ρ_f	1994	1995	2029
$Re = \rho_f d_p U / \mu$	157	168	54
$Fr = U^2 / g d_p$	54.5	52.6	51.2
$\rho_s d_p U / \mu$ ($\times 10^{-3}$)	313	334	109
$U^2 / g D_c$	0.78	0.75	0.73

Table 2. Percentage differences in shear stresses among the studied conditions of Cases A, B, and C.

Dimensionless shear stress	τ_{rz}'	$\tau_{z\theta}'$	$\tau_{r\theta}'$	τ_{rz}'	$\tau_{z\theta}'$	$\tau_{r\theta}'$
	Deviation (%) in spout			Deviation (%) in fountain		
Case A	-	-	-	-	-	-
Case B	62.03	54.71	47.56	52.96	40.2	57.76
Case C	69.98	58.02	58.31	40.17	48.74	41.19

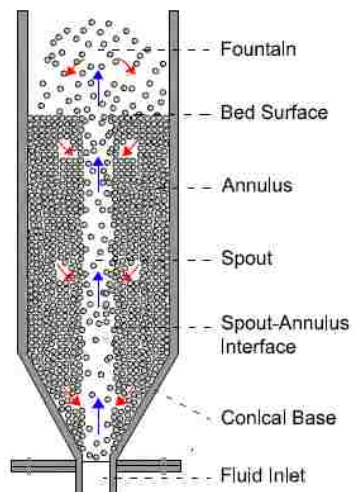


Fig. 1. Schematic diagram of spouted beds.

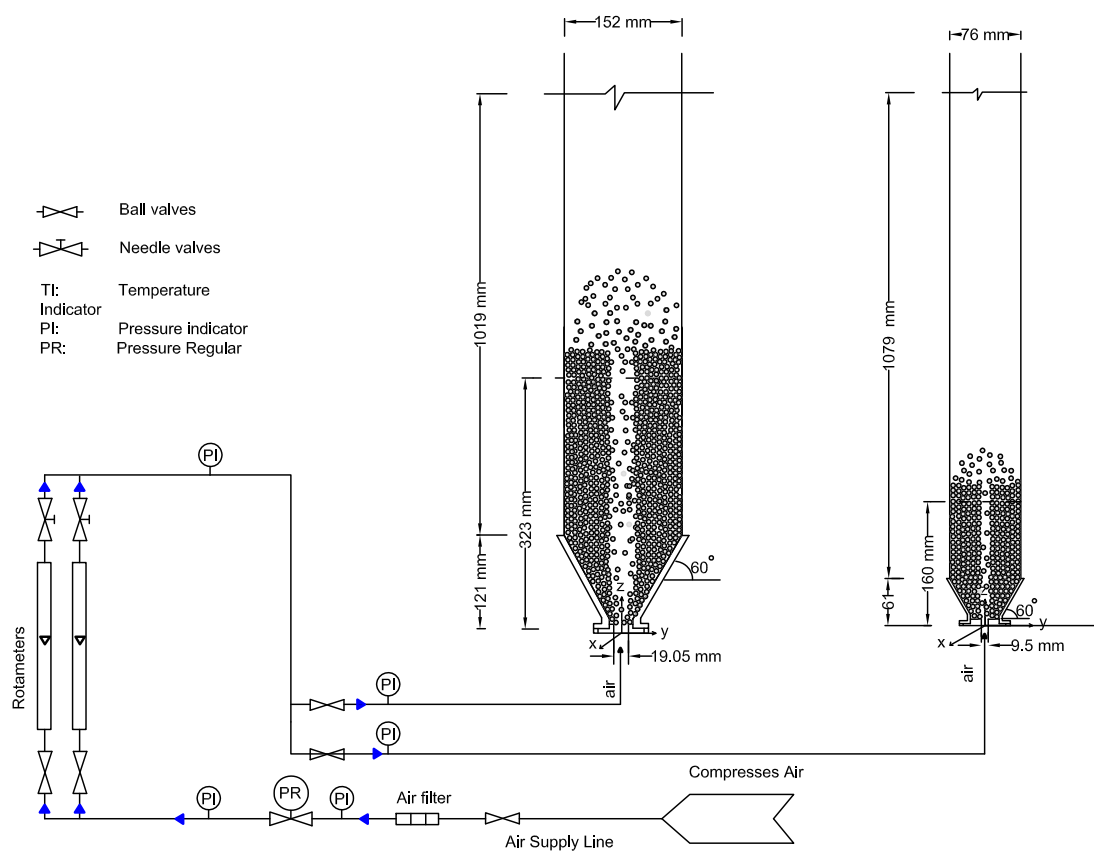


Fig. 2. Schematic diagram of the 0.076 m and 0.152 m spouted beds.

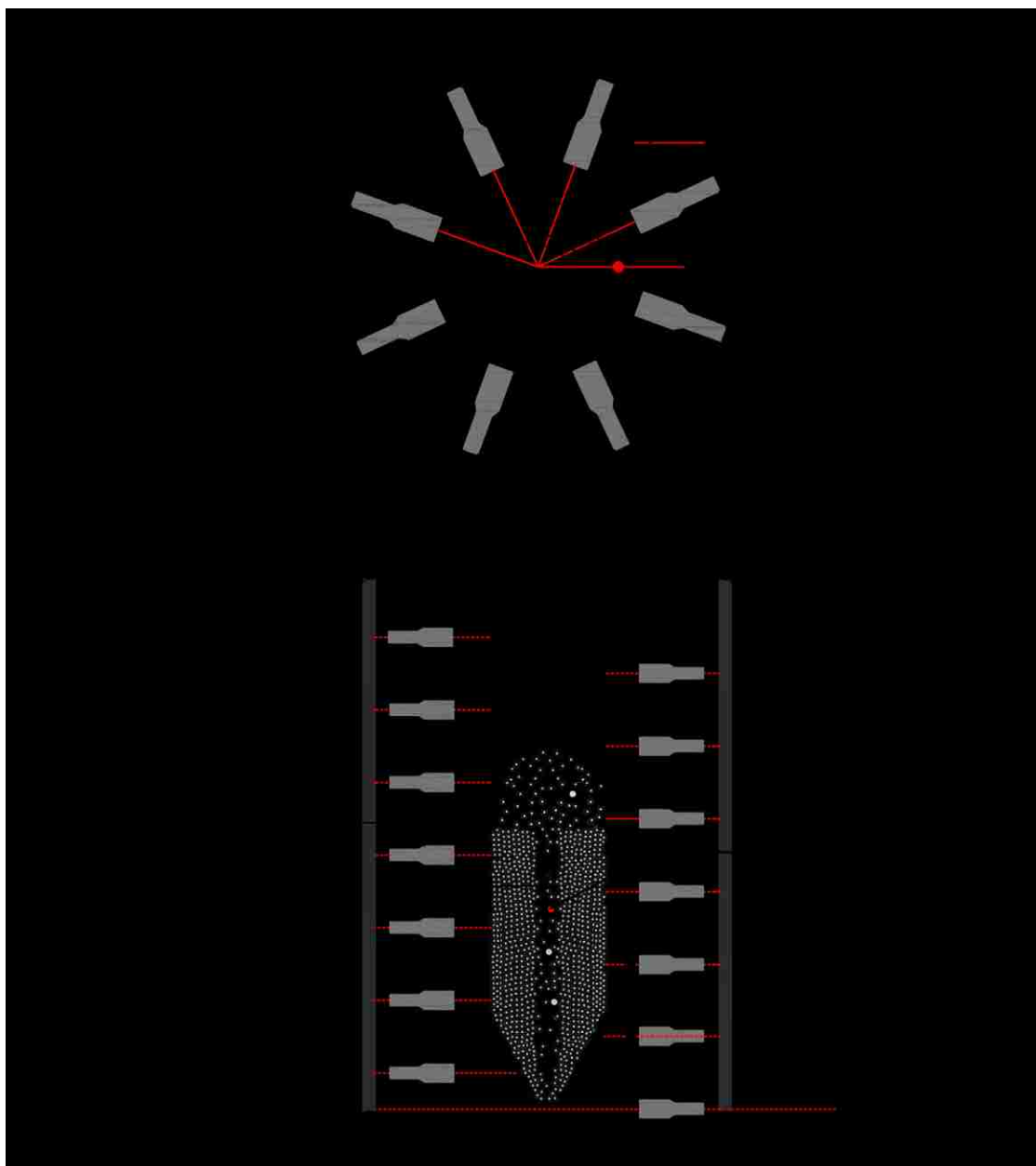


Fig. 3. Schematic diagram showing the positions of 14-detectors arranged around the 0.152 m spouted bed.

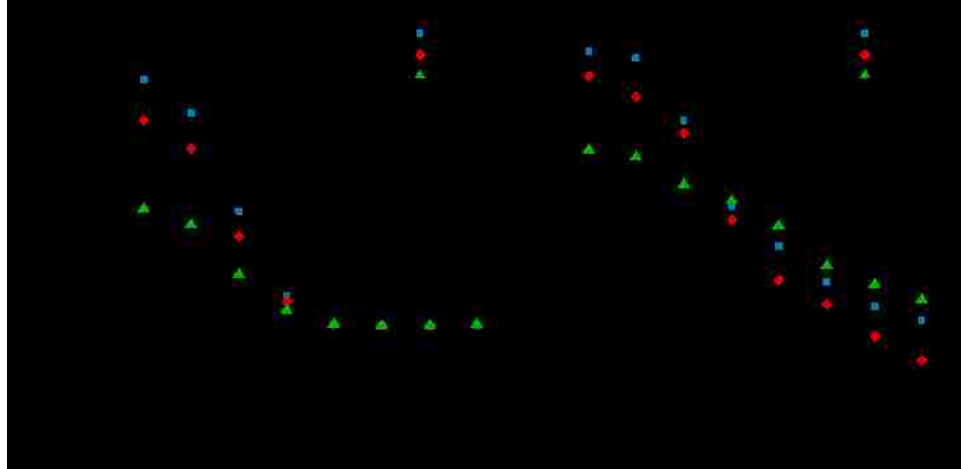


Fig. 4. Azimuthally and axially averaged radial profiles of the axial particle velocity for the conditions of the reference Case (Case A), the case with matched dimensionless groups (Case B), and the case with mismatched dimensionless groups (Case C) for 0.152 m and 0.076 m spouted beds in the spout/annulus and the fountain regions.

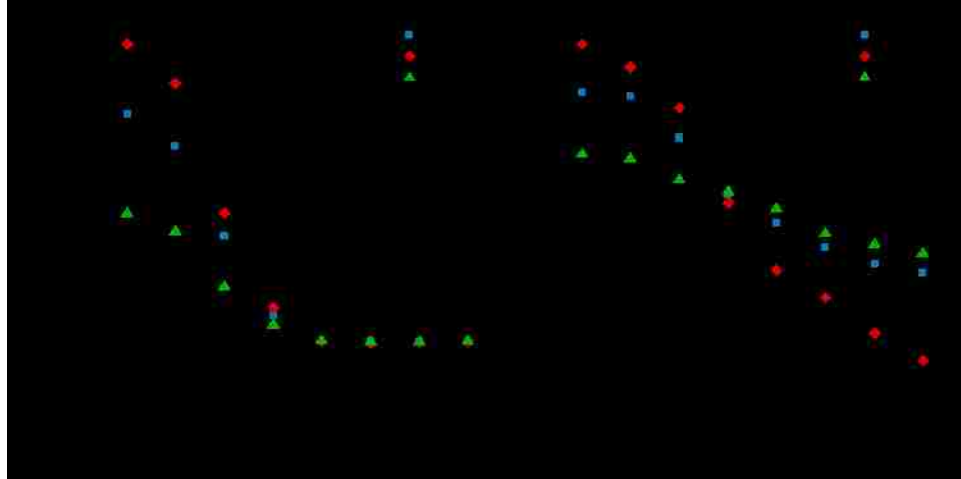


Fig. 5. Azimuthally and axially averaged radial profiles of the dimensionless axial particle velocity for the conditions of matched and mismatched dimensionless groups for 0.152 m and 0.076 m spouted beds in the spout/annulus and the fountain regions ($U_{ms} = 89, 61, 68$ cm/s, respectively for Cases A, B, and C).

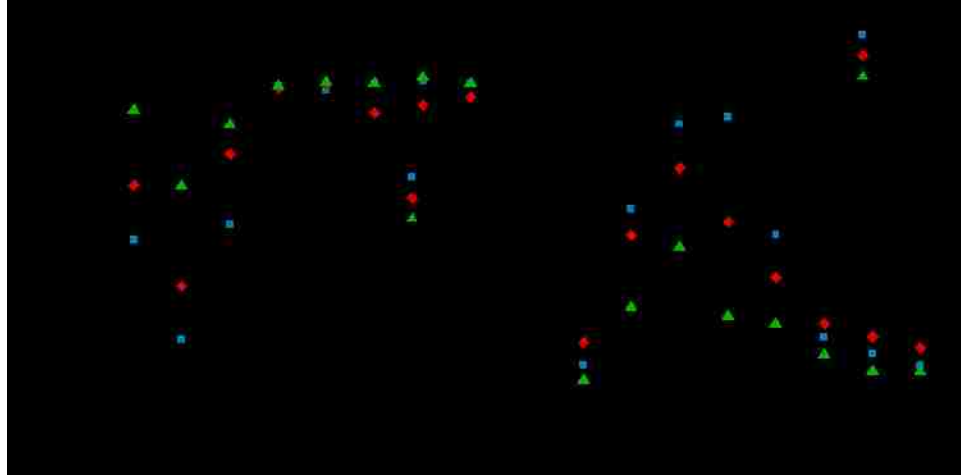


Fig. 6. Azimuthally and axially averaged radial profiles of the radial particle velocity for the conditions of matched and mismatched dimensionless groups for 0.152 m and 0.076 m spouted beds in the spout/annulus and the fountain regions.

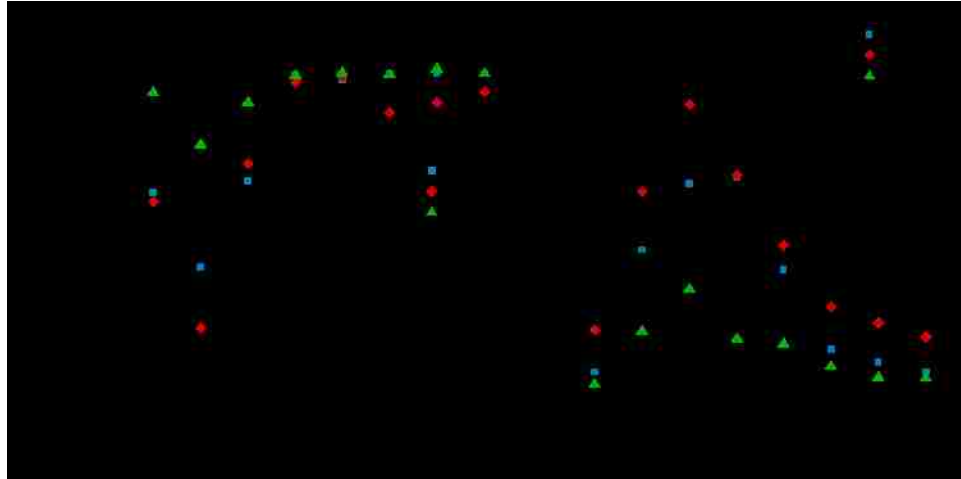


Fig. 7. Azimuthally and axially averaged radial profiles of the dimensionless radial particle velocity for the conditions of matched and mismatched dimensionless groups for 0.152 m and 0.076 m spouted beds in the spout/annulus and the fountain regions ($U_{ms} = 89, 61, 68$ cm/s, respectively for Cases A, B, and C).

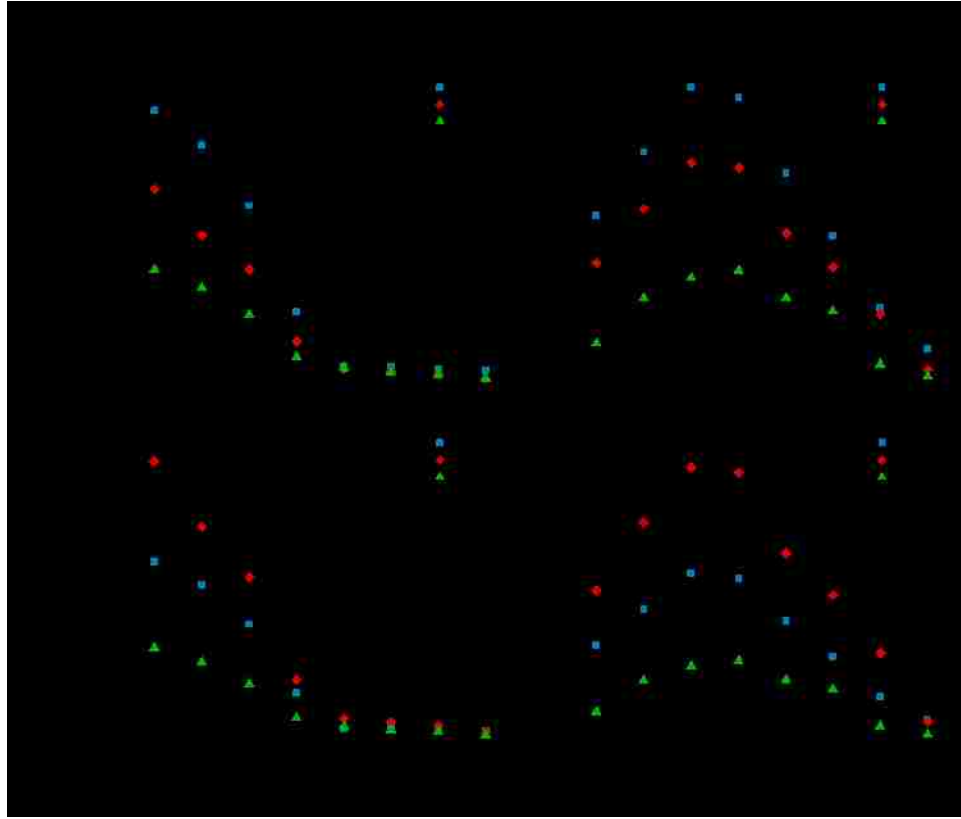


Fig. 8. Azimuthally and axially averaged radial profiles of (a) the axial normal stresses and (b) the dimensionless axial normal stresses with respect to the squared minimum spouting velocity, in the spout/annulus and the fountain regions for the conditions of matched and mismatched dimensionless groups for 0.152 m and 0.076 m spouted beds ($U_{ms} = 89, 61, \text{ and } 68 \text{ cm/s}$, respectively for Case A, B, and C).

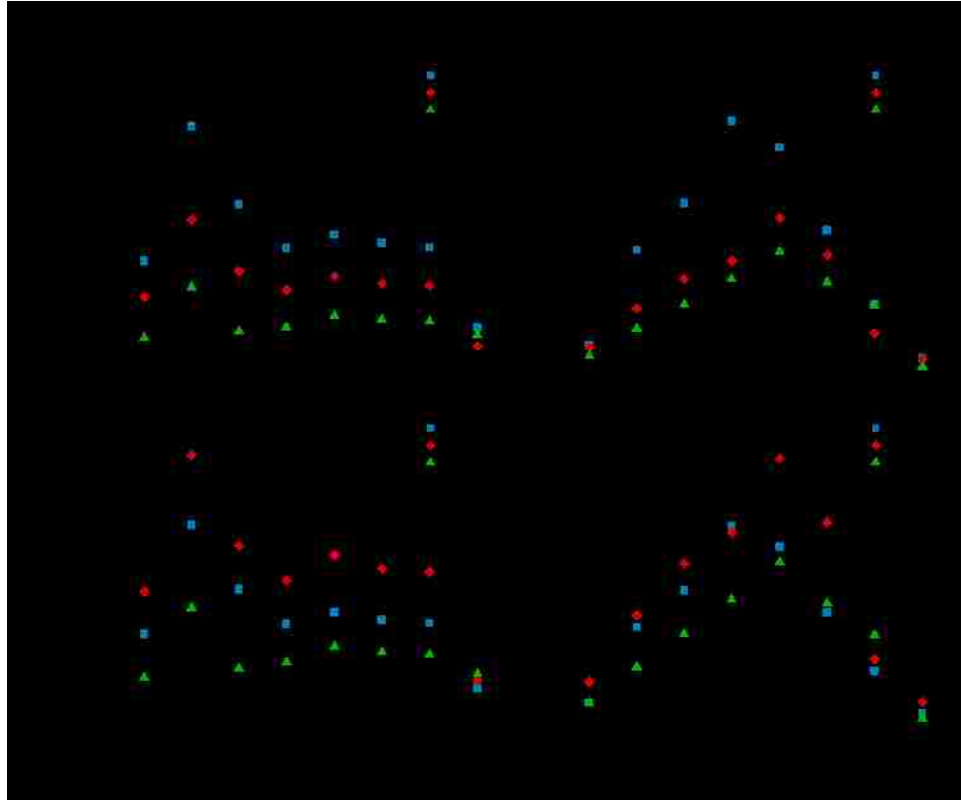


Fig. 9. Azimuthally and axially averaged radial profiles of the radial normal stresses in (a) and (b) the dimensionless radial normal stress, in the spout/annulus and (d) the fountain regions for the conditions of matched and mismatched dimensionless groups for 0.152 m and 0.076 spouted beds ($U_{ms} = 89, 61, \text{ and } 68 \text{ cm/s}$, respectively for Case A, B, and C).

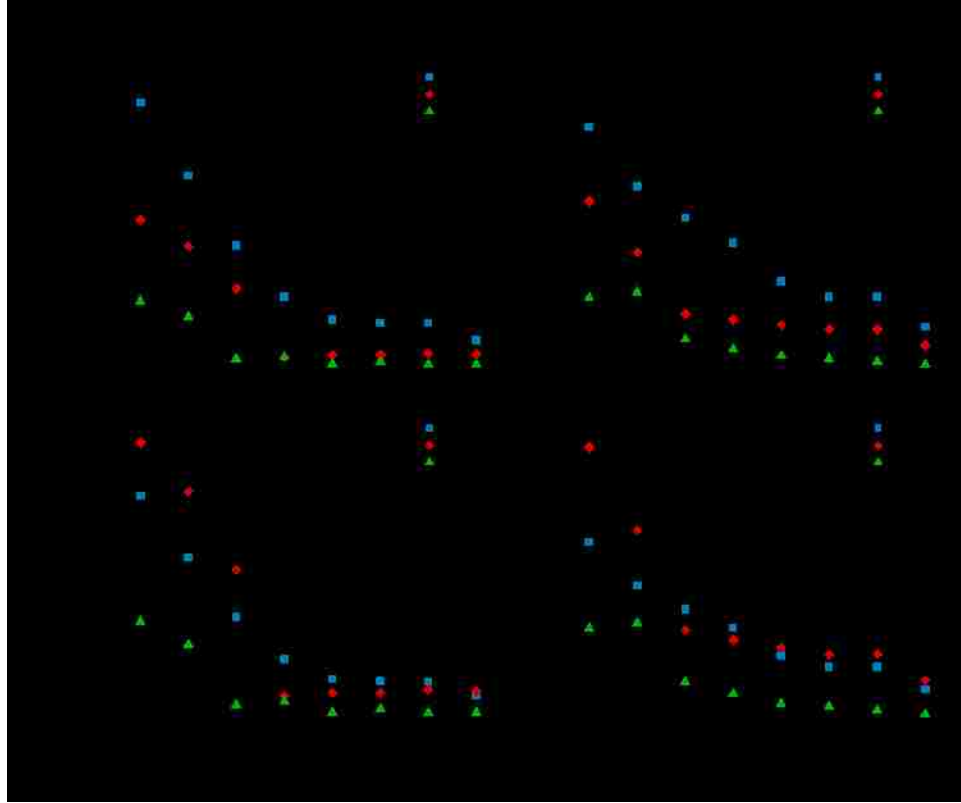


Fig. 10. Azimuthally and axially averaged radial profiles of (a) the azimuthal normal stresses, and (b) the dimensionless azimuthal normal stresses, in the spout/annulus and the fountain regions for the conditions of matched and mismatched dimensionless groups for 0.152 m and 0.076 m spouted beds ($U_{ms} = 89, 61, \text{ and } 68 \text{ cm/s}$, respectively for Case A, B, and C).

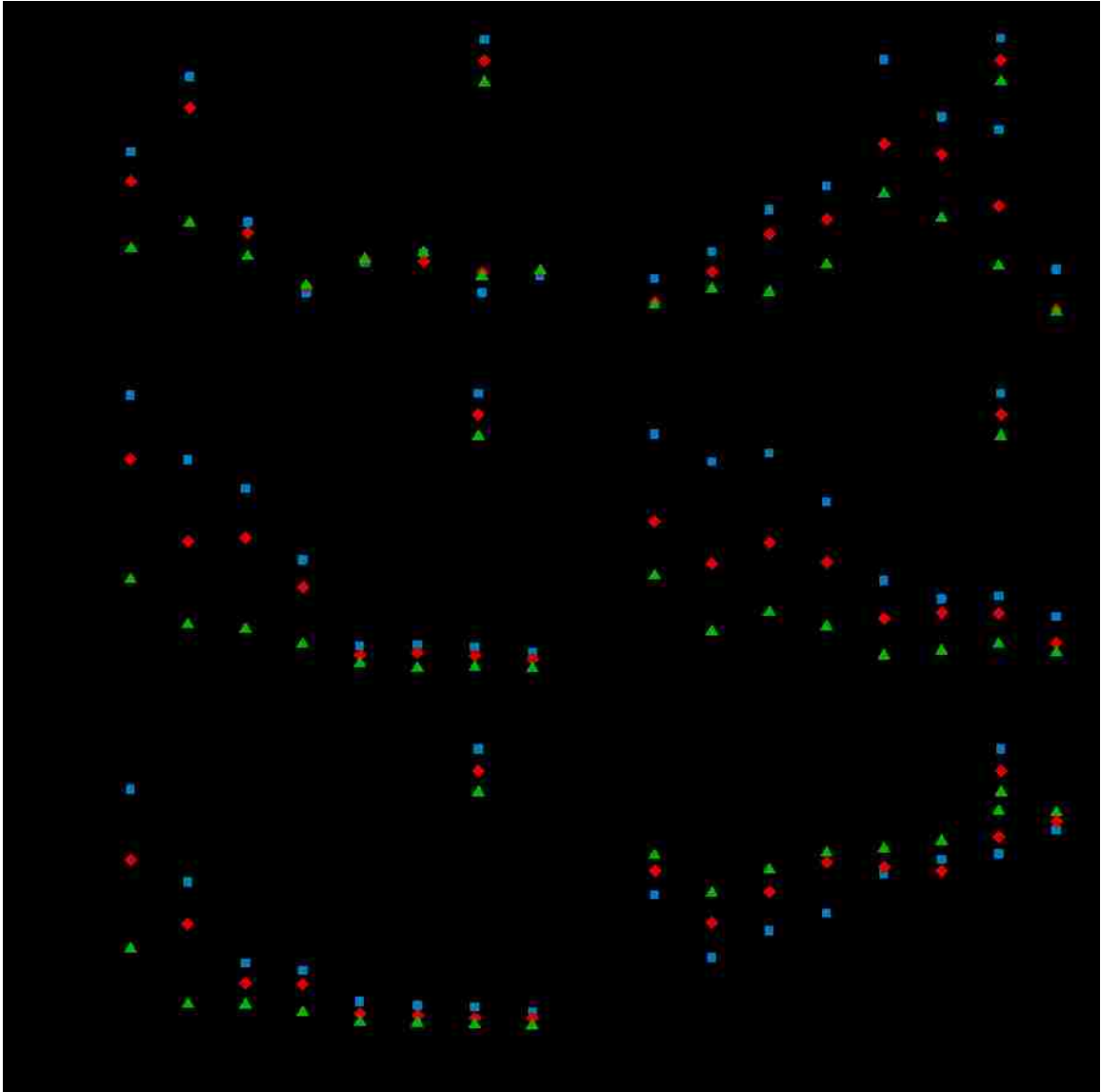


Fig. 11. Azimuthally and axially averaged radial profiles of the shear stresses for the conditions of matched and mismatched dimensionless groups for 0.152 m and 0.076 m spouted beds in the spout/annulus and the fountain regions.

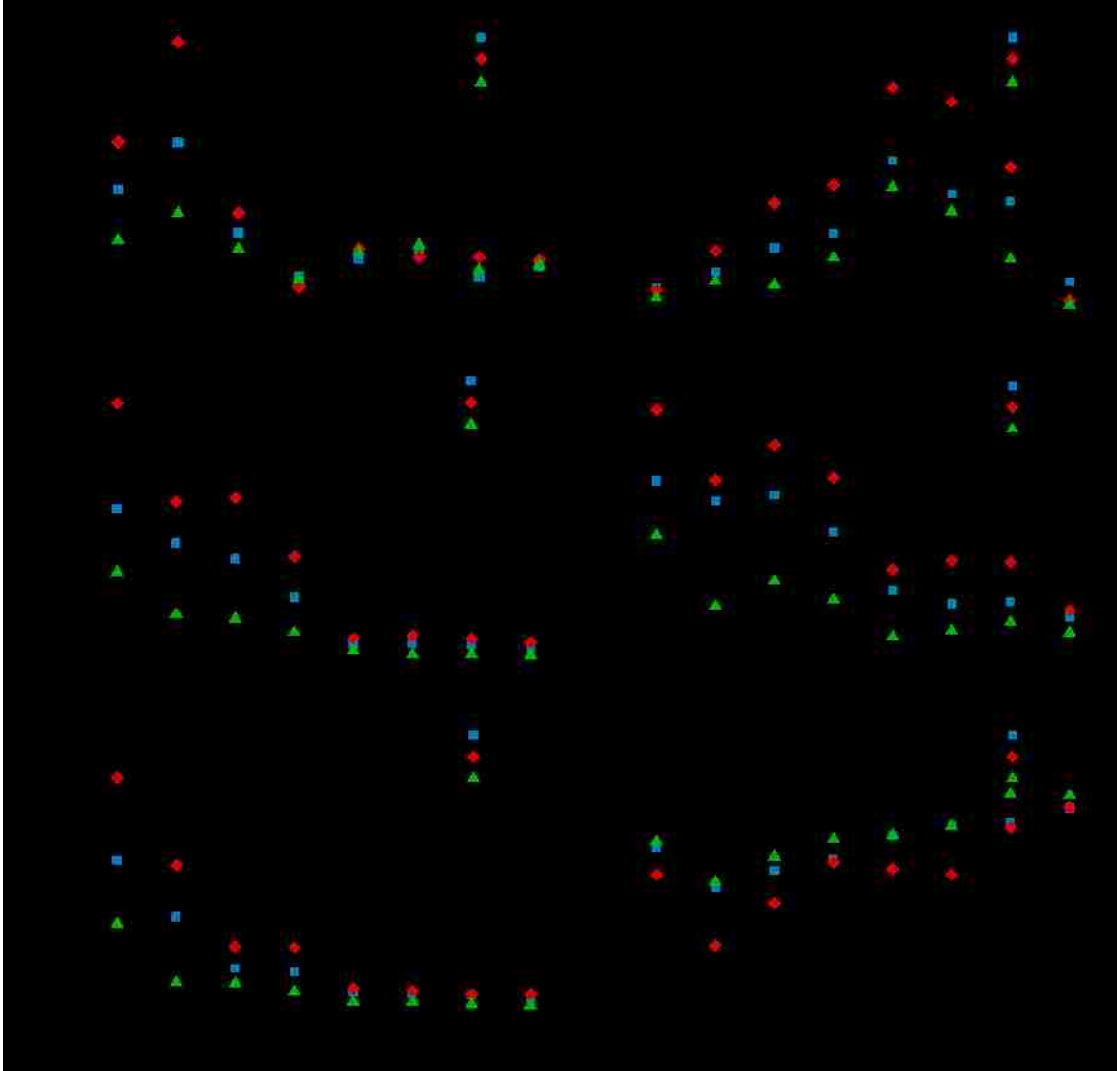


Fig. 12. Azimuthally and axially averaged radial profiles of the dimensionless shear stresses in the spout/annulus and the fountain regions for the conditions of matched and mismatched dimensionless groups for 0.152 m and 0.076 m spouted beds ($U_{ms} = 89, 61,$ and 68 cm/s, respectively for Case A, B, and C).

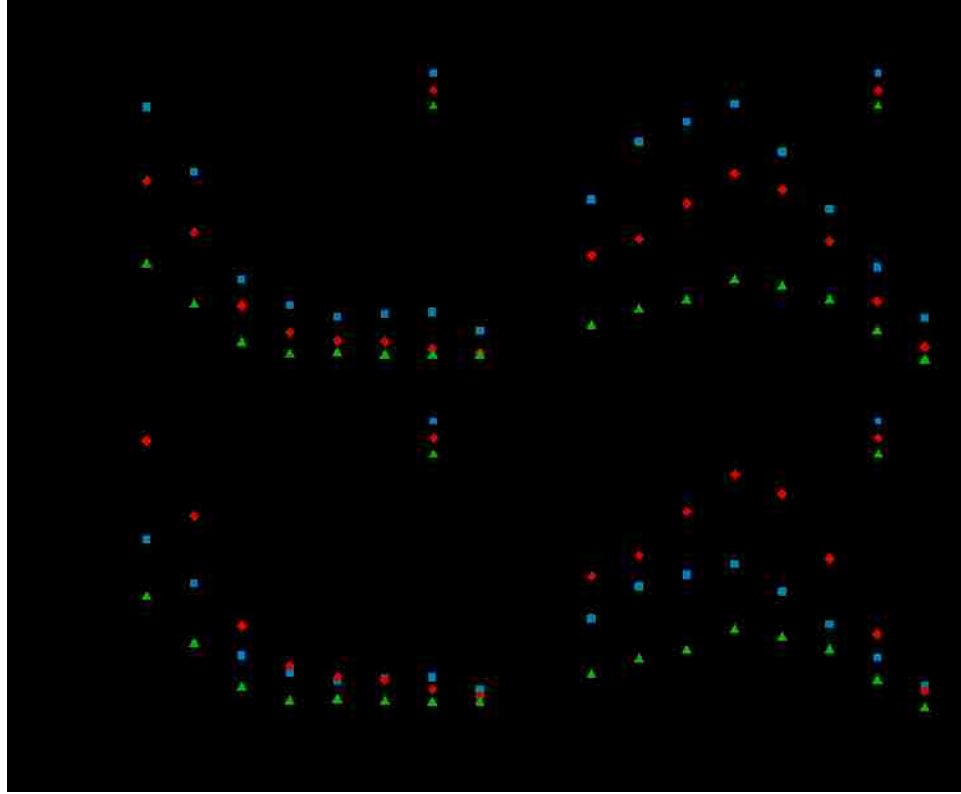


Fig. 13. Azimuthally and axially averaged radial profiles of turbulent kinetic energy (per unit bulk density), And (b) the dimensionless turbulent kinetic energy, in the spout/annulus and the fountain regions for the conditions of matched and mismatched dimensionless groups for 0.152 m and 0.076 m spouted beds ($U_{ms} = 89, 61, \text{ and } 68 \text{ cm/s}$, respectively for Case A, B, and C).

III. Evaluating the new mechanistic scale-up methodology of gas-solid spouted beds using gamma ray computed tomography (CT).

Neven Ali^a, Thaar Al-Juwaya^a, Muthanna Al-Dahhan^{ab*}

^aNuclear Engineering,

^bChemical and Biochemical Engineering,

Missouri University of Science and Technology (Missouri S&T) – Rolla

Rolla, MO 65409

Abstract

In this work, we implemented the gamma ray computed tomography (CT) technique to evaluate the new mechanistic scale-up methodology of gas-solid spouted beds by locally measuring the time-averaged cross-sectional distribution of solids and gas holdups, as well as their radial profiles along the bed height. The new scale-up methodology is based on maintaining a similar radial profile of the gas holdup at a height within the bed, to achieve local and global hydrodynamic similarity. The global hydrodynamic similarity will be determined through comparisons of dimensionless quantities regarding hydrodynamics since the gas dynamic dictates the hydrodynamics of the gas-solid spouted bed. Two sizes of spouted beds (with diameters of 0.076 m and 0.152 m) were used with conditions that provided close magnitudes and trends of radial profiles of gas holdup; and with conditions that provide mismatches in magnitudes of the gas holdup radial profiles. The results clearly show the validity of the new method for scale-up, where the solids and gas holdup profiles are close to each other at all the heights and in the three regions (spout, annulus and fountain) of spouted beds, when the radial profiles of the gas holdup are close at one height between the two studied beds. In addition, the CT results clearly identified three regions

mentioned above (spout, annulus, and fountain regions). In the spout region, the solids holdup increases along the spout height. When the radial profiles of gas holdups are different in two spouted beds, the differences are noticeable in local solids and gas holdups, which further endorse the new mechanistic scale-up methodology.

*Corresponding author:

Tel.: +1 573 341 7518; fax: +1 573 341 4377.

E-mail addresses: aldahhanm@mst.edu

Keywords Scale-up, Spouted beds, TRISO, Radioactive Particle Tracking (RPT), 3-D velocity field, turbulence.

1. Introduction

The conventional energy sources such as oil, coal, and natural gas have effectively led to global economic prosperity. On the other hand, these fossil fuels have also led to major environmental damage and negative human health afflictions. Furthermore, fossil fuel supplies are being depleted, and will not satisfy the energy needs of the future [1]. Therefore, alternative energy and power resources have been sought out in forms such as nuclear energy, biomass conversion, and renewable energy. One of the significant uses of nuclear energy is to generate electricity [2]. For example, the United States generates 20 percent of its electricity from nuclear energy. In general, clean, reliable and affordable electricity is generated from nuclear power plants. Nuclear reactor technology passes through various developmental stages and generations in order to advance its performance, safety and efficiency. In today's world, three generations of nuclear power systems are in use. To address future energy needs and challenges, ten countries have agreed on a framework for international cooperation on research for an advanced generation of nuclear

energy systems, known as Generation IV. Among the Gen IV reactors is the Very High Temperature Reactor (VHTR) that is designed to provide high-temperature heat ($\sim 1000^{\circ}\text{C}$) for hydrogen production, and process heat besides electricity. The VHTR comes in two forms of gas cooled modular type reactors: Pebble Bed Reactor (up to 200 MWe) and Prismatic Block Reactor (up to 600 MWe) [3]. For both of these reactors, the nuclear fuels are made of TRISO nuclear fuel particles. Since these two reactors are promising modular reactors, scaling-up the process of manufacturing TRISO nuclear fuel particles with robustness becomes a critical step for the commercialization of these reactors. Spouted beds have been used to coat, with four layers, these TRISO nuclear fuel particles using a chemical vapor deposition process [4-6]. In addition, spouted beds have found reliable and efficient applications in the gasification of biomass to produce energy, power and chemicals in addition to other important industrial applications such drying and granulation, where heavy, coarse, sticky and irregular particles are used [7-11]. Therefore, proper scale-up of the gas-solid spouted beds becomes essential for such future commercialization and for reliably fulfilling the future demands for energy.

In gas-solid spouted beds, the gas phase is introduced as a jet into a bed of particles through the conical base; this conical base is attached to a cylindrical column or through a conical bed where three distinct regions are created (the spout, fountain and annular regions as shown in Fig. 1. Hence, the flow pattern of gases and solids flow as well as their interactions in spouted beds are complex. As such, the scale-up and the design of these contactors/reactors are challenging. He et al. [12] suggested a set of dimensionless groups for scaling up and for the hydrodynamic similarity of gas-solid spouted beds. Aradhya [13], Ali et al. [14] and Ali et al. [15] evaluated dimensionless groups for spouted bed

hydrodynamics similarity using local measurements of both gas and solids holdups; solids velocity and turbulent parameters by optical fiber probe; gamma ray computed tomography (CT); and by radioactive particle tracking (RPT). They found that such methodology is not valid and the proposed dimensionless groups are not adequate when one wants to scale-up and maintain the hydrodynamics similarity in spouted beds. Since the gas dynamic dictates the hydrodynamics of the gas-solid spouted bed accordingly, a new mechanistic methodology for hydrodynamics similarity of spouted beds—by matching the radial profile of gas holdup in a height within the bed of the spouted bed—was proposed [13, 16]. The methodology stated that “when two flow fields of spouted beds are geometrically similar and have matched gas phase holdup profiles at a similar dimensionless height of the beds, the two flow fields attain hydrodynamics similarity in terms of the dimensionless quantities of the hydrodynamic.” By trial-and-error and by guidance of computational fluid dynamics (CFD), [13] found the design and operating conditions that provide more accurate magnitudes and trends of the gas holdup profiles at heights within the bed. [13] and [16] validated this methodology using limited local measurements at one angular location of the optical fiber probe. Such evaluation lacked details, and was therefore insufficient. In order to perform a more elaborate and useful evaluation of the proposed new methods, detailed local measurements of the hydrodynamics within the bed and along the bed height in all the three regions are needed. Accordingly, this work focuses on using the gamma ray computed tomography (CT) technique to: 1) examine whether the conditions used by [13] truly provide gas holdup profile magnitudes and trends that are close and similar to the original scale; 2) to evaluate further the attainment of the similarity in the local solids and

gas holdup distributions and their radial profiles at various levels and regions of the spouted beds.

2. Experimental Work

2.1 Experimental Set-up of the Spouted Beds

We carried out the experimental work in two conically-based spouted bed columns made of Plexiglas; inner diameters are 0.076 m and 0.152 m, which is similar to those used and discussed by [14]. The schematic diagrams of these two spouted beds are shown in Fig. 2. Both columns were without ports to avoid additional attenuation for CT experimentation; additional attenuation would complicate data processing. These conical bases had a cylindrical section 1.14 m in height and a 60-degree conical base angle. The gas phase entered the bed from the bottom through a stainless steel gas distributor mounted on an orifice (9.5 mm and 19.1 mm diameters for the 0.076 m and 0.152 m beds, respectively) with a high open area to create the needed jet for spouting conditions. Dry compressed air was used as the gas phase and its flow was regulated using a pressure regulator and rotameter setup consisting of two rotameters connected in parallel. To sustain stable spouting conditions, the ratio between the column diameter and the particle diameter (D_c/d_p) was maintained to be less than 25~30 [17]; $D_c/D_i > 3\sim 12$ [10]; and $H < H_m$ [18]. D_i is the diameter of the gas inlet, d_p is the diameter of the particle, D_c is the diameter of the column, H is the height of the static bed, and H_m is the height of the maximum spoutable bed.

2.2 Experimental conditions

[13] used computational fluid dynamics (CFD) and trial-and-error to identify three different sets of conditions, which consist of reference conditions based on those of [12]. A set of conditions provided matching (closer in magnitudes and trend) radial profiles of the gas holdup, and another set of conditions provided mismatching (different magnitudes) radial profiles of gas holdup. These conditions are summarized in Table 1. [13] used an optical fiber probe at three levels ($z/D=1.1, 1.8, 2.5$) but also one angular location of the probe for each level to measure the radial profiles of solids and gas holdups; the angular location of the probe at each level allowed confirmation regarding matching and mismatching of these profiles for the conditions listed in Table . Hence, there is a need to assess such matching and mismatching across the cross-sectional area by using CT; furthermore, there is a need to evaluate the newly-developed mechanistic scale-up methodology by comparing the cross-sectional distributions and radial profiles of solids and gas holdups at various levels along the bed height of the studied spouted beds. Accordingly, the sets of conditions in Table have been used in this work.

2.3 Dual Source Gamma Ray Computed Tomography (DSCT).

DSCT consists of two sealed sources (Cs-137 and Co-60) and two sets of 15 NaI detectors located in front on each sealed source, as shown in .Since only two phases—flow of gas and solid—exist in gas-solid spouted beds, only one sealed source of Cs-137 and its corresponding NaI detectors have been used. The technique has been described in literature authored by [14]. Furthermore, a detailed discussion of the CT technique, related mechanical assembly, electronics data acquisition, the operation, and the Alternative

Minimization (AM) algorithm used for image reconstruction can be found elsewhere [14, 19, 20].

3. Results and Discussion

3.1 Assessing [13] sets of conditions for matching and mismatching radial profiles of gas holdups using CT

As mentioned earlier, [13] identified a set of conditions for matching radial profiles of gas holdups and used these conditions to assess the newly-developed mechanistic scale-up methodology using limited local measurements in one angular location by optical fiber probe at $z/D = 1.1, 1.8$ and 2.4 . These conditions have been assessed and verified in this section using CT by measuring the cross-sectional distribution of the gas holdup at $z/D = 1.8$ for both beds (0.076 m and 0.152 m diameter). Fig. 4 demonstrates the cross-sectional distributions of gas holdup and the related frequency distributions. It is obvious that these selected sets of conditions provide similarity in the gas holdup distribution. By azimuthally averaging the gas holdup cross-sectional distribution, the gas holdup radial profile of the set of conditions was obtained. Fig. 5 visualizes the comparison between the gas holdup radial profiles at $z/D=1.8$ of the conditions identified by [13], which give matching magnitudes and trends of the gas holdups. Our results using CT confirm the conditions of [13] for matching radial profiles of gas holdup. According to the newly-developed scale-up methodology, the solids and the gas holdup distributions and their radial profiles at various heights of the bed, particularly in the spout and in the fountain, should be close to each other or similar. These findings and validation of the new scale-up method are

discussed in the following section. This validation has been achieved by performing CT measurements and analyzing the data at various heights of the spouted bed.

3.2 Assessing the new mechanistic scale-up methodology using CT technique

Fig. 6 and Fig. 7 show the measured time-averaged cross-sectional distribution and the corresponding frequency distribution of the solids holdup for the 0.152 m and 0.076 m spouted beds at a z/D of 0.8, 1.1, 1.8, and 2.4, respectively. The scale bar right of the images indicates the fraction of the solids holdup. Red represents a higher solids holdup, and blue represents a lower solids holdup. The color distributions of the images clearly highlight the spout and the annulus regions. The cross-sectional images illustrate the unchanged value of the solids holdup in the annulus region along the bed height. As mentioned above, this is because the particles in this region move downward in a moving packed bed mode while feeding solids to the spout region. The frequency distribution is higher at the limit of the solids holdup of the annulus region ($\epsilon_s \sim 0.6$), and skewed to the right where the frequency distributions are small in the spout region. A skewed (non-symmetric) distribution is expected for all levels due to smaller and higher solids holdup values in the spout and annulus regions, respectively. From a statistical perspective, the skewed distributions indicate the hydrodynamic complexities that exist in spouted beds and further confirm the divergence between the three regions (the spout, the annulus, and the fountain). The cross-sectional distribution and the corresponding frequency distribution of solids holdup at the fountain region show the smaller solids holdup in the outer region of the fountain where particles fall back into the bed surface, and confirm the divergence between this region and the other regions of the spout and the annulus. The frequency distributions in the fountain

region, unlike other regions, have left-skewing and are narrower. This indicates that solids holdup values are closer in the outer region of the fountain and have a small deviation among each other. The mean and standard deviation of the holdup values were calculated. The pixels outside the column diameter (pixels with solids holdup equals zero), were excluded from the statistical analysis. Table 2 summarizes the absolute percentage differences of the mean and the standard deviation of the frequency distributions for the conditions of the reference case and of the similar gas holdup profiles. The results signify the very similar solids holdup distributions in term of mean and standard deviation between the conditions of the reference case and the conditions of the similar gas holdup profile.

The solids holdup radial profiles of the spouted beds are compared for the conditions of the reference case (0.152) and of the similar gas holdup profile (0.076 m) to further assess the new scale-up methodology. Matching solids holdup profiles between the conditions can be observed in Fig. 8 for all z/D levels. The profiles show that the solids holdup in the spout is minimal at the bottom section of the bed, and increases with increasing bed height. The solids holdup is also minimal near the axis of the spout and increases radially toward the spout-annulus interface. In the annulus, the solids holdup profiles are similar for all the levels of the two beds. The absolute percentage deviations between the profiles were calculated for all the levels. The average percentage difference between the profiles in the spout region for similar gas holdup conditions is 4.8%, 1.75%, and 1.21%, at z/D levels of 0.8, 1.1, and 1.8, respectively. The average percentage difference between the profiles in the fountain region is 8.11%. From the results above, one further concludes that matching solids holdup profiles in all regions and bed heights were achieved.

Fig. 9 and Fig. 10 show the measured time-averaged cross-sectional distribution and the corresponding frequency distribution of the gas holdup for the 60.152 m and 0.076 m spouted beds, respectively. Since two phases—gas and solids—have been used and $\varepsilon_g = 1 - \varepsilon_s$, the trends and the findings resulting from analyzing the gas holdup cross-sectional distributions and radial profiles should be similar to those presented in the previous section of solids holdups. For convenient comparison between the images, the maximum and minimum of the scale bars were maintained to be same for both beds with respect to the z/D levels. The color distributions of the images clearly highlight the spout and the annulus regions; the annulus is the dense region with lower gas holdup located in the column's annular and surrounding the dilute region; the spout is located in the middle of the column. With a close look at the images for z/D levels of 0.8, 1.1, and 1.8, one can find out and further confirm the unchanged value of the gas holdup in the annulus region along the bed height. As mentioned earlier, the particles in this region move downward and slowly, resulting in the creation of small voids for the gas phase to pass through. The frequency distributions of the images are higher at the limit of the gas holdup of the annulus region ($\varepsilon_g \sim 0.3$), and skewed to the left where the frequency distributions are small in the spout; similar to the solids holdup mentioned earlier, a skewed (non-symmetric) distribution is expected for all levels due to smaller and higher gas holdup values in the spout and annulus regions. In the fountain region, the images show the higher gas holdup values which, as expected, exist in the outer region of the fountain where less particles exist upon the freefall back into the bed surface due to gravity. Further confirmation can be concluded from the image of the fountain regarding the divergence between the three regions; the spout, the annulus, and the fountain. Non-similar to the other regions, the frequency distributions in

the fountain region have right-skewing, and are narrower. This indicates that the gas holdup values were closer in the outer region of the fountain and had small differences among each other.

Table 3 summarizes the absolute percentage differences of the mean and the standard deviation of the frequency distributions for the conditions of the reference case and of the conditions of the similar gas holdup profiles. Like those of the solids holdup discussion earlier, the results demonstrate the very similar gas holdup distributions in terms of the mean and the standard deviation between the conditions of the reference case and the conditions of the similar gas holdup profile.

As shown in Fig. 11, matching gas holdup profiles were observed for the two beds at all z/D levels including that of the fountain region. At the cone section ($z/D=0.8$), the average percentage difference of gas holdup in the spout region is 0.95 %. Near the center of the spout ($r/R=0.025$), the difference is 0.56 %; at $r/R=0.125$, it is 1.16 %; at $r/R=0.225$, it is 1.71%; at $r/R=0.325$, it is 2.27 %; and at $r/R=0.425$, it is 0.32 %. In the annulus region, the gas holdup profiles of the two beds are matched and unchanged along the bed height. This is mainly because the solids move gradually and slowly downward in the annulus. At $z/D=1.1$, the average percentage difference in the spout region is 0.99 %; at $r/R=0.025$, the difference is 0.32%; at $r/R=0.125$, it is 0.71%; at $r/R=0.225$, it is 1.52%; at $r/R=0.325$, it is 1.31%; and at $r/R=0.425$, the difference is 0.06 %. At $z/D=1.8$, the average percentage difference in the spout region is 0.71%. Near the center of the spout, the difference is 0.48 %; at $r/R=0.125$, it is 1.14 %; at $r/R=0.225$, it is 1.27%; at $r/R=0.325$, it is 0.72%; and at $r/R=0.425$, it is 0.32%. In the fountain region, the gas holdup profile was found to be well matched with that of the reference case. The average percentage difference of the gas

holdup between the two beds in the fountain region is 1.22%. From the above remarks, a conclusion can be drawn saying that very good agreement was achieved between the gas holdup profiles at all the heights—including the fountain region—of the conditions of the reference case (Case A) and the conditions identified by for similar gas holdup profile (called similar ε_g).

3.3 Solids and gas holdups along the bed height using CT technique at the conditions when the radial profiles of the gas holdup are not similar

The examination of the conditions that provide non-similar gas holdup radial profiles with respect to reference Case A was necessary to further evaluate and validate the new methodology of scale-up using CT. Evaluation of the conditions of non-similar gas holdup radial profiles was conducted in the 0.076 m spouted bed. Fig. 12 shows the measured time-averaged cross-sectional distributions and the corresponding frequency distributions of the solids holdup for the conditions of non-similar gas holdup profiles (0.076 m) at z/D levels of 0.8, 1.1, 1.8, and 2.4.

These results are compared with the results of Case A, presented in Fig. 6. It is obvious that there are noticeable differences in solids holdup cross-sectional distributions at all the studied heights along the bed, including the fountain region.

Fig. 13 shows the comparison between the solids holdup profiles for Case A (0.152 m) and for the conditions of non-similar gas holdup profile with respect to Case A at z/D levels of 0.8, 1.1, 1.8, and 2.4. The absolute percentage deviations between the profiles were evaluated for all z/D levels. The average percentage deviation for all the individual values of solids holdup in the spout region is 46.26%, 44.29%, and 38.12%, at z/D levels of 0.8, 1.1, and 1.8, respectively. The average percentage difference between the profiles

in the fountain region is 26.43%. The results above display the clear differences in the solids holdup profiles between the two beds for the reference case and for the conditions of non-similar gas holdup profiles. Such findings further support the new scale-up methodology that is validated as per the discussion and results presented in the previous section.

Fig. 14 shows the measured time-averaged cross-sectional distribution and the corresponding frequency distributions of the gas holdup for the conditions of non-similar gas holdup profiles (0.076 m) at z/D levels of 0.8, 1.1, 1.8, and 2.4, respectively. The color distributions of the images clearly highlight the spout and the annulus regions for the 0.076 m spouted bed. The cross-sectional images confirm the unchanged value of the gas holdup in the annulus region for 0.076 m spouted bed along the bed height, which further confirms the similarity of the gas holdup profiles in this region. However, deviation can be observed between the images in the spout region of the two beds. This deviation becomes more obvious if we consider the frequency distributions of the local gas holdup values in terms of mean, standard deviation, and the distribution curve shape for both conditions. At $z/D=0.8$, the mean of the gas holdups frequency distribution is 0.438 and 0.459, respectively, for Case A and the conditions of non-similar gas holdup profiles. At $z/D=1.1$, the mean of the gas holdups frequency distribution is 0.429 and 0.455, respectively, for Case A and the conditions of non-similar gas holdup profiles. At $z/D=1.8$, the mean of the gas holdups frequency distribution is 0.417 and 0.436, respectively, for Case A and the conditions of non-similar gas holdup profiles. Deviation is also found between the two cases in the fountain region where the mean of the gas holdup distribution was 0.927 and 0.933, respectively, for Case A and the conditions of non-similar gas holdup profiles. From

the results above, it is clear that matching the dimensionless groups between the two beds is not sufficient to achieve good hydrodynamic similarity. These results can be compared with those of Case A. The difference between these two sets of results are clear.

Fig. 15 shows the comparison between the gas holdup radial profiles for the conditions of the reference case (0.152 m) and for non-similar gas holdup profile (0.076 m) at z/D levels of 0.8, 1.1, 1.8, and 2.4. The results show that the gas holdup profiles of the two beds deviate from each other substantially in the spout and fountain regions, and have similar values in the annulus region due to the downward flow nature of solids in the moving bed, as mentioned earlier. At $z/D=0.8$, the average percentage difference between the two profiles in the spout region is 11.47%. Near the center of the spout ($r/R=0.025$), the difference is 5.54%; at $r/R=0.125$, it is 8.3%; at $r/R=0.225$, it is 15.21%; at $r/R=0.325$, it is 16.22%; and at $r/R=0.425$, it is 6.81%. At $z/D=1.1$, the average difference in the spout region between the profiles is 18.53%. The deviation near the center of the spout ($r/R=0.025$) is 11.65%; at $r/R=0.125$, it is 15.12%; at $r/R=0.225$, it is 23.76%; at $r/R=0.325$, it is 26.95%; and at $r/R=0.425$, it is 7.54%. At $z/D=1.8$, the average difference between the profiles in the spout region is 22.25%. The difference in the spout is 17.37% at $r/R=0.025$; at $r/R=0.125$, it is 20.15%; at $r/R=0.225$, it is 30.79%; at $r/R=0.325$, it is 29.79%; and at $r/R=0.425$, it is 7.44%. The average percentage difference between the profiles in the fountain region is 8.36%. From the results above, the gas holdup profiles were not matched between the two beds at all the measured levels when the conditions of the non-similar gas holdup profiles are used. As mentioned earlier, these findings further confirm the validity of the new scale-up methodology for the local measurements made in this study using CT technique.

3.4 Comparison between the measurements of CT technique of this work and the optical fiber probe technique of [13]

[13] used an optical fiber probes technique to measure solids and gas holdup radial profiles. With the guidance of CFD, he identified the conditions that provided a similar gas holdup profile to that of the reference case (Case A). The optical probe is an invasive point measurement technique used to measure the velocity of the moving particles, and/or the local solids holdup in gas-solid systems. The operation of this technique relies on the transmitted and received lights from the optical fibers equipped on the probe. The transmitter fibers send the light rays by using an optical fiber. The light rays reflect off particles in motion and return to the same fiber, where they travel to a receiver. The signal obtained depends on the local concentration of the particles and their structure. A reliable calibration method ensures that the optical phase signal has been accurately converted to solids holdup [13]. Advanced optical probes developed by The Institute of Process Engineering of the Chinese Academy of Science were used for gas-solids spouted bed experiments [13]. Detailed explanations of the optical probe measurements are provided elsewhere [13]. The optical probe was manually mounted through different axial measurement ports on the wall of the spouted beds at all sides of the column (90-degree separation). The z/D levels used for the measurements were 1.1, 1.8, and 2.4 for 0.152 m and 0.076 m spouted beds. The probe was then introduced at different radial positions in the bed to take the measurements. As discussed above, these conditions have been confirmed using CT. In order to further confirm the obtained results by both [13] and this work, comparison between the results of the optical fiber probe and the CT techniques have been conducted here. Fig. 16 illustrates this comparison. The agreement between the

profiles is excellent. However, the most noticeable difference between the profiles, was near the spout-annulus interface. This is expected, as the interface between the spout and the annulus does not stay steady, which made it possible for the probe to provide subpar measurements in this region. Whereas the optical probe applies based on a point measurement, the non-invasive CT technique can provide a more reliable means for assessment by visualizing the entire cross-section of the bed.

4. Conclusion

We demonstrated, in this work, the evaluation and validation of the new scale-up mechanistic methodology using the non-invasive gamma ray computed tomography (CT) technique to measure the local distributions and radial profiles of solids and gas holdups. It has been confirmed that when the radial profiles of gas holdup are matched or are close to each other for two beds of different sizes and conditions, the similarity in local solids and gas holdups is attained in all three regions of the spouted bed; the spout, the annulus and the fountain. However, when there are differences in the gas holdup radial profile between two sets of conditions and sizes, the similarity in local holdups is not achieved. This finding further endorses the new scale-up methodology of the gas-solids spouted beds. The CT technique was able to distinguish the three regions of the spouted beds mentioned above. It also demonstrated that the cross-sectional solids holdup of the spout region increases along the height of the spout where the particles are fed to the spout from the annulus region. To assess further the new scale-up methodology, it is recommended to employ other types of non-invasive techniques capable of measuring the local solids

velocity field and the turbulent parameters, which are the key to determining the solids mixing and the interactions between the solid and gas phases.

Acknowledgments

US Department of Energy - Nuclear Energy Research Initiative (DOE-NERI) grant (NERI DEFC07-07ID14822), the GAANN, chancellor fellowship, and professor Al-Dahhan's Lab Fund are acknowledged for the financial support that made this work possible.

References

- [1] A.V. Herzog, T.E. Lipman, D.M. Kammen, Renewable energy sources, Encyclopedia of Life Support Systems (EOLSS). Forerunner Volume-‘Perspectives and Overview of Life Support Systems and Sustainable Development, 2001.
- [2] U.S.D.o. Energy, S.a.T. Office of Nuclear Energy, D.C. Washington, The History of Nuclear Energy, (1994).
- [3] Y.-W. Lee, J.-Y. Park, Y.K. Kim, K.C. Jeong, W.K. Kim, B.G. Kim, Y.M. Kim, M.S. Cho, Development of HTGR-coated particle fuel technology in Korea, Nuclear Engineering and Design, 238 (2008) 2842-2853.
- [4] K. Sawa, 3.06 - TRISO Fuel Production, in: R.J.M. Konings (Ed.) Comprehensive Nuclear Materials, Elsevier, Oxford, 2012, pp. 143-149.
- [5] M. Liu, Y. Shao, B. Liu, Pressure analysis in the fabrication process of TRISO UO₂-coated fuel particle, Nuclear Engineering and Design, 250 (2012) 277-283.
- [6] I.E. Porter, T.W. Knight, M.C. Dulude, E. Roberts, J. Hobbs, Design and fabrication of an advanced TRISO fuel with ZrC coating, Nuclear Engineering and Design, 259 (2013) 180-186.
- [7] M. Olazar, S. Alvarez, R. Aguado, M.J. San José, Spouted Bed Reactors, Chemical Engineering & Technology, 26 (2003) 845-852.
- [8] M.a.J. San José, S. Alvarez, A.O. de Salazar, M.n. Olazar, J. Bilbao, Influence of the particle diameter and density in the gas velocity in jet spouted beds, Chemical Engineering and Processing: Process Intensification, 44 (2005) 153-157.
- [9] C.R. Duarte, M. Olazar, V.V. Murata, M.A.S. Barrozo, Numerical simulation and experimental study of fluid–particle flows in a spouted bed, Powder Technology, 188 (2009) 195-205.
- [10] K.B. Mathur, N. Epstein, 1 - Introduction, in: K.B. Mathur, N. Epstein (Eds.) Spouted Beds, Academic Press 1974, pp. 1-13.

- [11] W. Shuyan, L. Yongjian, L. Yikun, W. Lixin, D. Qun, W. Chunsheng, Simulations of flow behavior of gas and particles in spouted bed with a porous draft tube, *Powder Technology*, 199 (2010) 238-247.
- [12] Y.L. He, C.J. Lim, J.R. Grace, Scale-up studies of spouted beds, *Chemical Engineering Science*, 52 (1997) 329-339.
- [13] S.B. Aradhya, Scaleup and hydrodynamics study of gas-solid spouted beds, *Chemical and Biochemical Engineering*, Missouri University of Science and Technology, 2013, pp. xxiv, 301 pages.
- [14] N. Ali, T. Al-Juwaya, M. Al-Dahhana, Demonstrating the non-similarity in local holdups of gas-solid spouted beds obtained by CT with scale-up methodology based on dimensionless groups., *Chemical Engineering Research and Design*, ## (2016) "*Submitted*" or "*under consideration*".
- [15] N. Ali, T. Al-Juwaya, M. Al-Dahhana, An advanced evaluation of spouted beds scale-up for coating TRISO nuclear fuel particles using radioactive particle tracking (RPT), *Experimental Thermal and Fluid Science*, ## (2016) "*Submitted*" or "*under consideration*".
- [16] M. Al-Dahhan, S. Aradhya, F. Zaid, N. Ali, T. Aljuwaya, Scale-up and On-line Monitoring of Gas-solid Systems Using Advanced and Non-invasive Measurement Techniques, *Procedia Engineering*, 83 (2014) 469-476.
- [17] P.P. Chandnani, N. Epstein, Spoutability and spout detabilization of fine particles with a gas, *Engineering Foundation*, United States, 1986.
- [18] Y.L. He, C.J. Lim, J.R. Grace, Spouted bed and spout-fluid bed behaviour in a column of diameter 0.91 m, *The Canadian Journal of Chemical Engineering*, 70 (1992) 848-857.
- [19] R. Varma, S. Bhusarapu, J.A.O. Sullivan, M.H. Al-Dahhan, A comparison of alternating minimization and expectation maximization algorithms for single source gamma ray tomography, *Measurement Science and Technology*, 19 (2008) 015506.

[20] M.K.A. Mesfer, Effect of Dense Heat Exchanging Internals on the Hydrodynamics of Bubble Column Reactors Using Non-invasive Measurement Techniques, Department of Chemical and Biochemical Engineering, Missouri University of Science and Technology, Rolla, Missouri, 2013.

Notation

d_p	particle diameter, m
D	inner column diameter, m
D_c	inner column diameter, m
D_i	inlet orifice diameter, m
e_{ss}	restitution coefficient of the particles
Fr	Froude number
g	acceleration of gravity, m s^{-2}
H	static bed height, m
H_0	initial height, m
H_l	particle rebounding height, m
H_F	fountain height, m
H_m	maximum spoutable bed depth, m
L	column length, m
l	the chord length of each pixel
P	bed pressure, Pa
Re	Reynolds number
R	column radius, cm
r	radial position, cm
T	bed temperature, K
U	superficial gas velocity, m s^{-1}
U_{mf}	minimum fluidization velocity, m s^{-1}
U_{ms}	minimum spouting velocity, m s^{-1}

x	index for pixel in image domain
y	index for projection or source detector pair
z	axial distance from inlet orifice, m

Greek letters

β	fluid-particle interaction coefficient, $\text{kg m}^3 \text{s}^{-1}$
ρ_s	particle density, Kg m^{-3}
ρ_f	fluid density, Kg m^{-3}
μ	fluid viscosity, $\text{Kg m}^{-1} \text{s}^{-1}$
ϕ_s	sphericity of particles
φ	inertial friction angle of particle, deg
ε_{mf}	bed voidage at minimum fluidization
ε_o	voidage at packed bed state
ε_s	solids phase fraction (or solids holdup)
ε_g	gas holdup fraction (or gas holdup)

Table 1. Experimental Conditions for similar and non-similar gas holdup radial profiles for the hydrodynamics similarity of spouted beds identified by [Aradhya \(2013\)](#).

Conditions/Case	A (Reference case)	Similar gas-holdup profiles (ϵ_g) _r	Non-similar gas-holdup profiles (ϵ_g) _r
D_c (m)	0.152	0.076	0.076
D_i (mm)	19.1	9.5	9.5
L (m)	1.14	1.14	1.14
H (m)	0.323	0.16	0.16
T (K)	298	298	298
P (kPa)	101	364	101
Particles	Glass	Steel	Glass
d_p (mm)	2.18	1.09	1.09
ρ_s (kg/m ³)	2400	7400	2450
ρ_f (kg/m ³)	1.21	3.71	1.21
μ (x 10 ⁵) (Pa.s)	1.81	1.81	1.81
U (m/s)	1.08	0.64	0.74

Table 2. Mean and standard deviation of the solids holdup distribution for the conditions of the reference case and similar gas holdup profiles listed in Table 1.

z/D	solids holdup distributions	Case A (Reference case)	Similar gas-holdup profiles (ϵ_g) _r	Absolut deviation %
		0.152 m spouted bed	0.076 m spouted bed	
0.8	mean	0.562	0.560	0.27%
	STD	0.112	0.122	9.10%
1.1	mean	0.571	0.570	0.28%
	STD	0.103	0.091	11.60%
1.8	mean	0.583	0.580	0.53%
	STD	0.076	0.077	0.94%
2.4	mean	0.073	0.074	0.72%
	STD	0.035	0.031	11.81%

Table 3. Mean and standard deviation of the gas holdup distribution for the conditions of the reference case and similar gas holdup profiles listed in Table 1.

z/D	Gas holdup distributions	Case A (Reference case)	Similar gas-holdup profiles (ϵ_g) _r	Absolut deviation %
		0.152 m spouted bed	0.076 m spouted bed	
0.8	mean	0.43846	0.43998	0.35%
	STD	0.11206	0.12226	9.10%
1.1	mean	0.4288	0.4305	0.40%
	STD	0.10327	0.09129	11.60%
1.8	mean	0.41694	0.42003	0.74%
	STD	0.07599	0.07671	0.94%
2.4	mean	0.9267	0.92622	0.05%
	STD	0.03494	0.03081	11.81%

Table 4. Mean and standard deviation of the gas holdup distribution for the conditions of the reference case and Non-similar gas holdup profiles listed in Table 1.

z/D	Gas holdup distributions	Case A (Reference case)	Non-similar gas-holdup profiles (ϵ_g) _r	Absolute deviation %
		0.152 m spouted bed	0.076 m spouted bed	
0.8	mean	0.43846	0.45886	4.65%
	STD	0.11206	0.14533	29.69%
1.1	mean	0.4288	0.4547	6.04%
	STD	0.10327	0.13869	34.30%
1.8	mean	0.41694	0.43595	4.56%
	STD	0.07599	0.11955	57.31%
2.4	mean	0.9267	0.93279	0.66%
	STD	0.03494	0.02241	35.85%

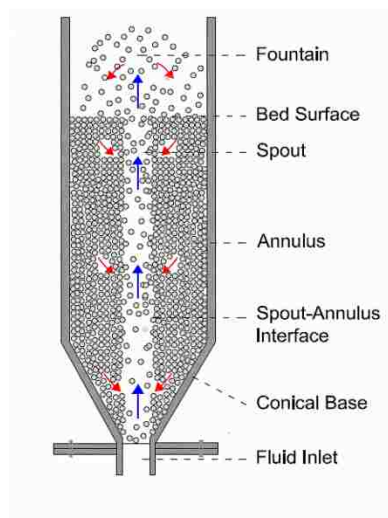


Fig. 1. Schematic diagram of spouted beds.

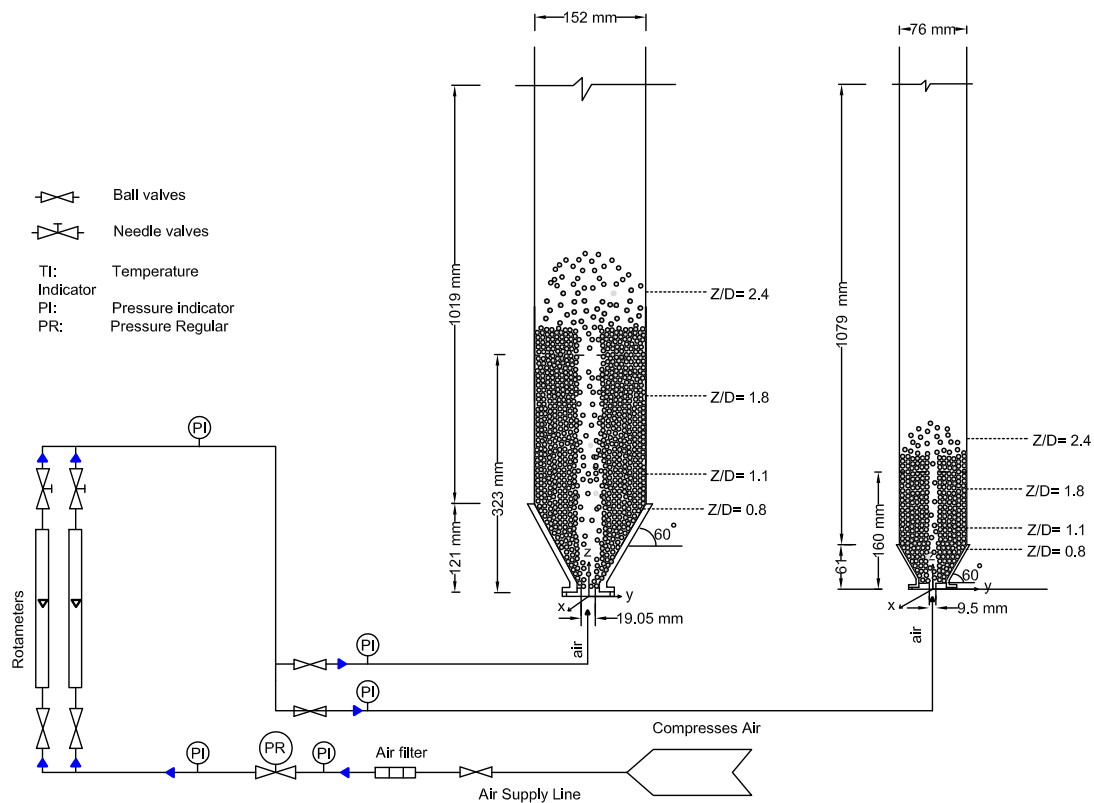


Fig. 2. Schematic diagram of 0.076 m and 0.152 m spouted beds.



Fig. 3. Photograph of the DSCT technique, and 6-inch spouted bed inside the setup for scan.

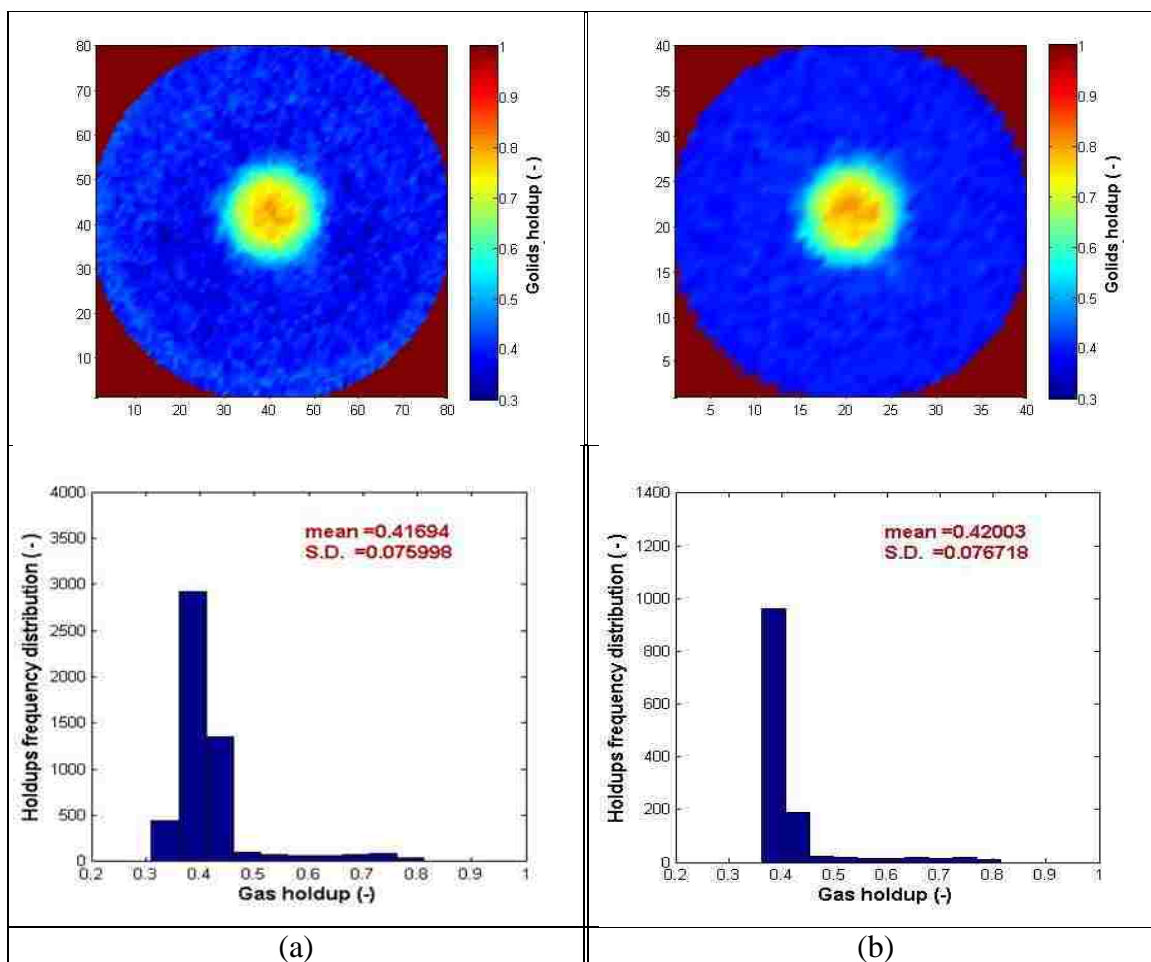


Fig. 4. Cross-sectional distribution and corresponding frequency distribution of gas holdup for the conditions of (a) the reference case of 0.152 m spouted beds at $z/D=1.8$ and (b) similar radial profile of 0.076 m spouted beds at $z/D=1.8$

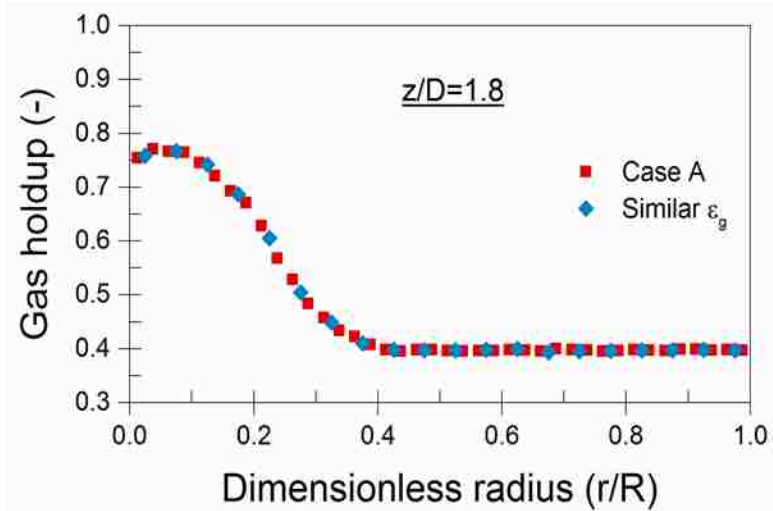


Fig. 5. Comparison of gas holdup radial profiles at $z/D = 1.8$, for the conditions of reference case (Case A) in 0.152 m spouted bed, and for the conditions that give similar radial profile of gas holdup (called similar ϵ_g) in 0.076 m spouted beds (Table 2.1)

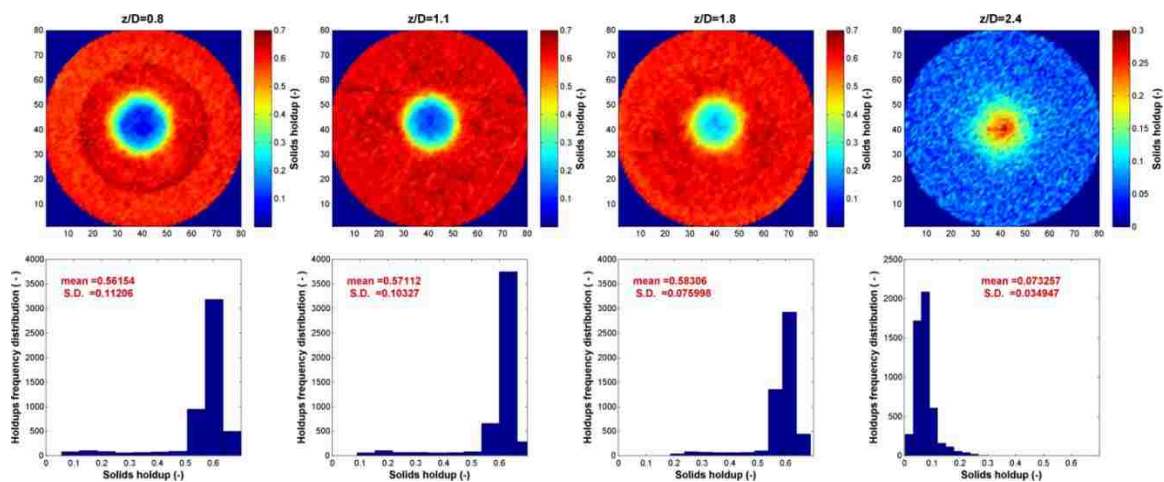


Fig. 6. Cross-sectional distribution and corresponding frequency distribution of solids holdup for Case A along the bed height of the 0.152 m spouted beds.

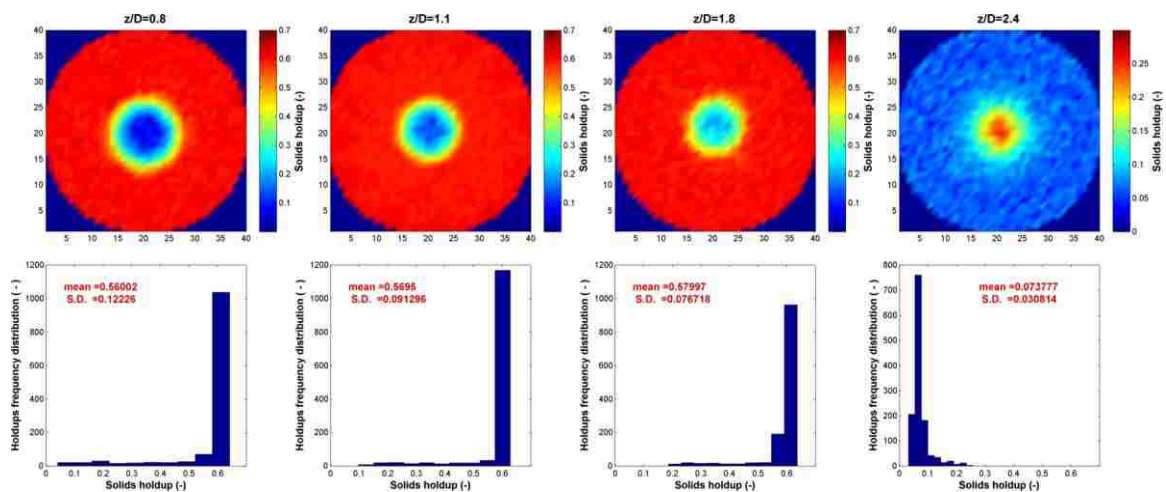


Fig. 7. Cross-sectional distribution and corresponding frequency distribution of the solids holdup for the conditions of similar gas holdup profiles along the bed height of the 0.076 m spouted bed.

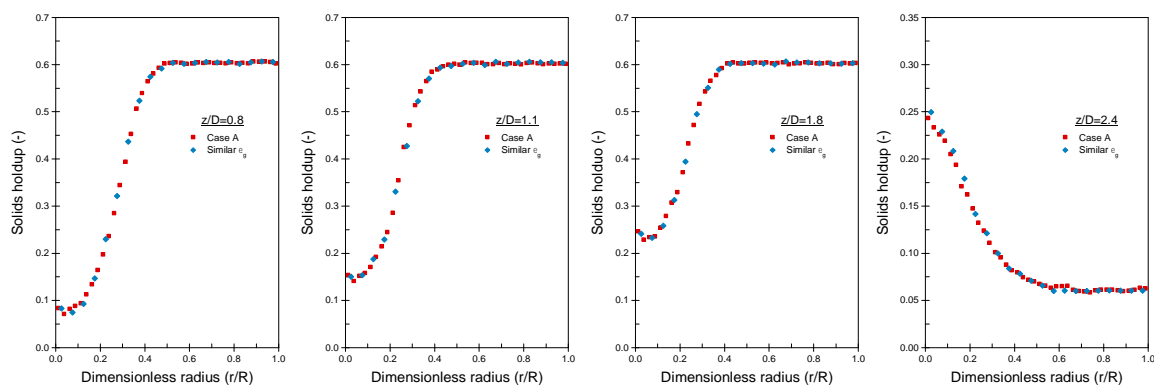


Fig. 8. Comparison of solids holdup radial profiles at z/D levels of 0.8, 1.1, 1.8, and 2.4 for the conditions of reference case (Case A), and similar radial profile of gas holdup (called similar ε_q) in 0.152 m and 0.076 m spouted beds.

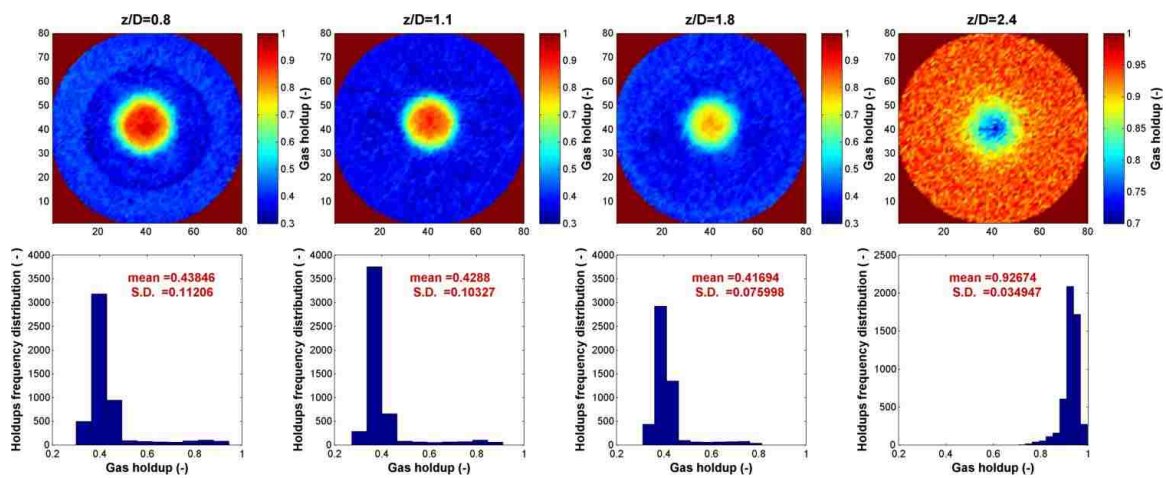


Fig. 9. Cross-sectional distribution and corresponding frequency distribution of gas holdup for Case A along the bed height of the 0.152 m spouted bed.

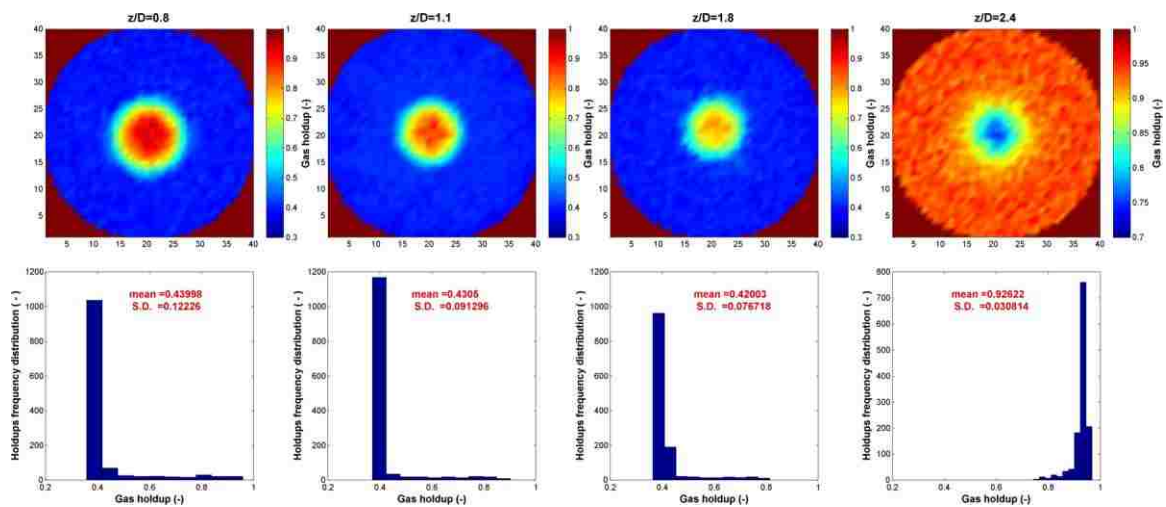


Fig. 10. Cross-sectional distribution and corresponding frequency distribution of gas holdup for the conditions of similar gas holdup profiles along the bed height of the 0.076 m spouted bed.

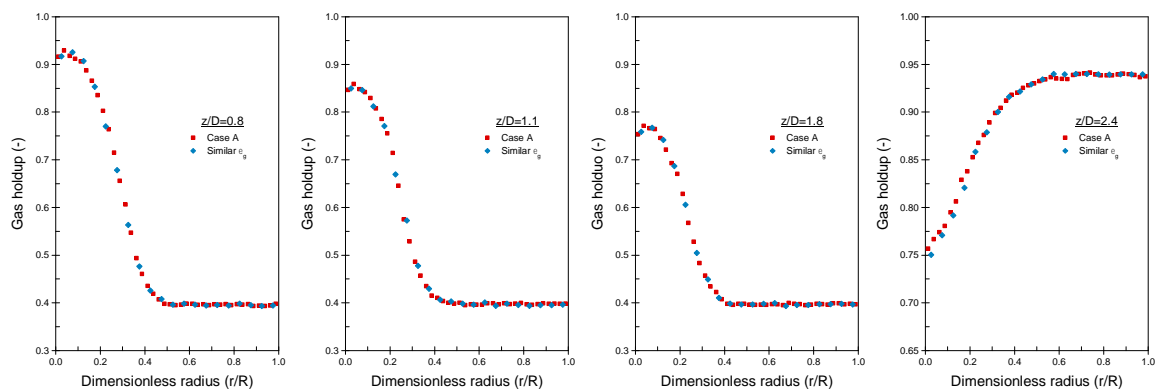


Fig. 11. Comparison of gas holdup radial profiles at z/D levels of 0.8, 1.1, 1.8, and 2.4 for the conditions of reference case (Case A), and similar radial profile of gas holdup (called similar ϵ_g) in 0.152 m and 0.076 m spouted beds.

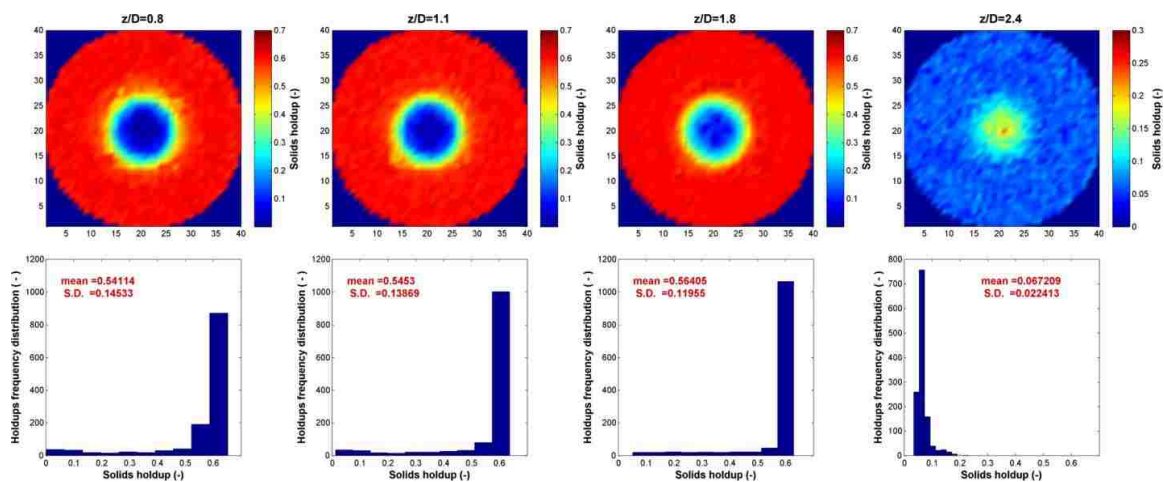


Fig. 12. Cross-sectional image and corresponding frequency distribution of solids holdup for Case C along the bed height of 0.076 m spouted bed.

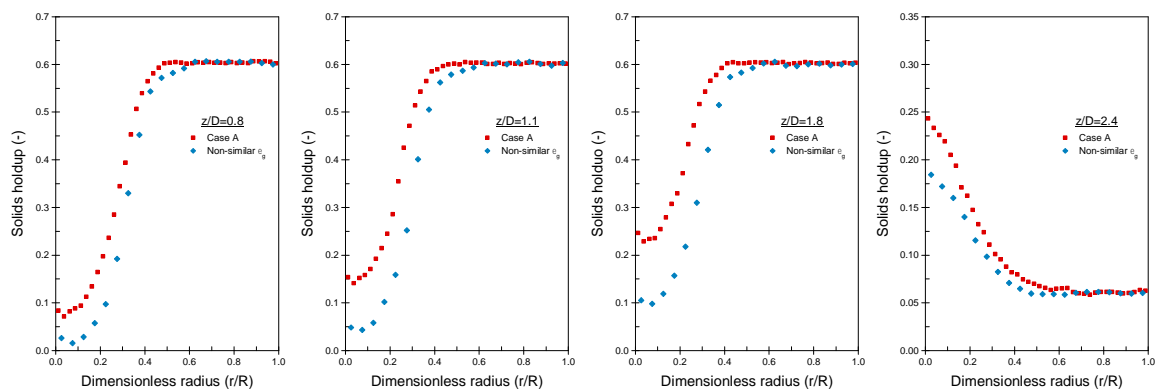


Fig. 13. Comparison of solids holdup radial profiles at z/D levels of 0.8, 1.1, 1.8, and 2.4 for the conditions of reference case (Case A), and Non-similar radial profile of gas holdup (called non-similar ϵ_g) in 0.152 m and 0.076 m spouted beds.

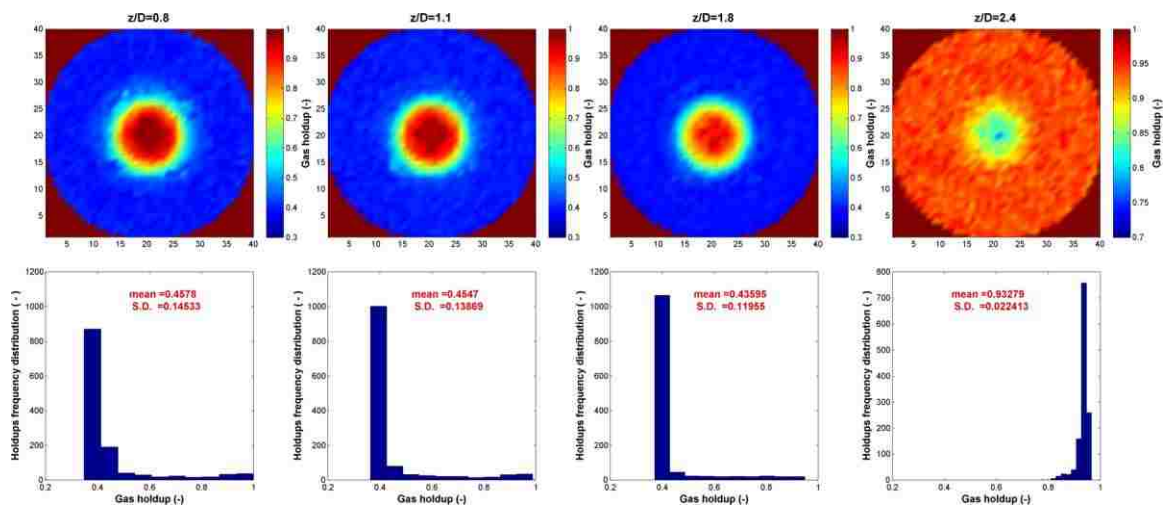


Fig. 14. Cross-sectional distribution and corresponding frequency distribution of the conditions of similar gas holdup profiles along the bed height of the 0.076 m spouted bed.

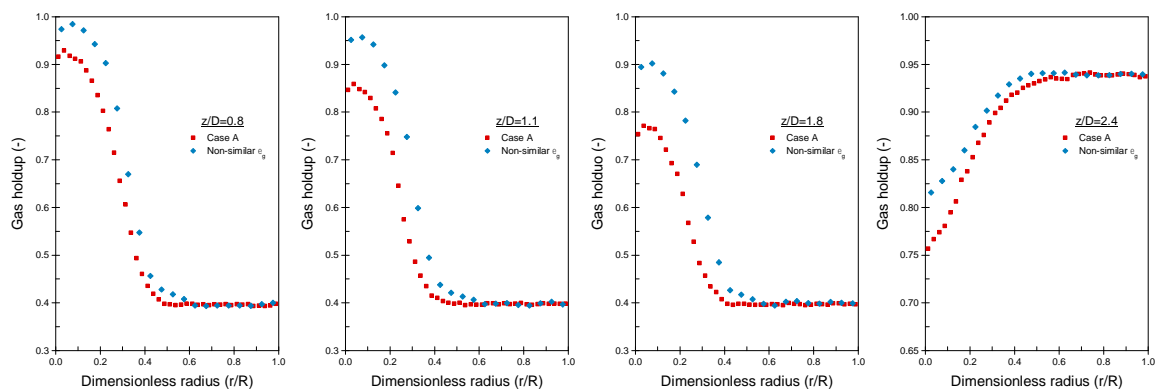


Fig. 15. Comparison of gas holdup radial profiles at z/D levels of 0.8, 1.1, 1.8, and 2.4 for the conditions of reference case (Case A), and Non-similar radial profile of gas holdup (called non-similar ϵ_g) in 0.152 m and 0.076 m spouted beds.

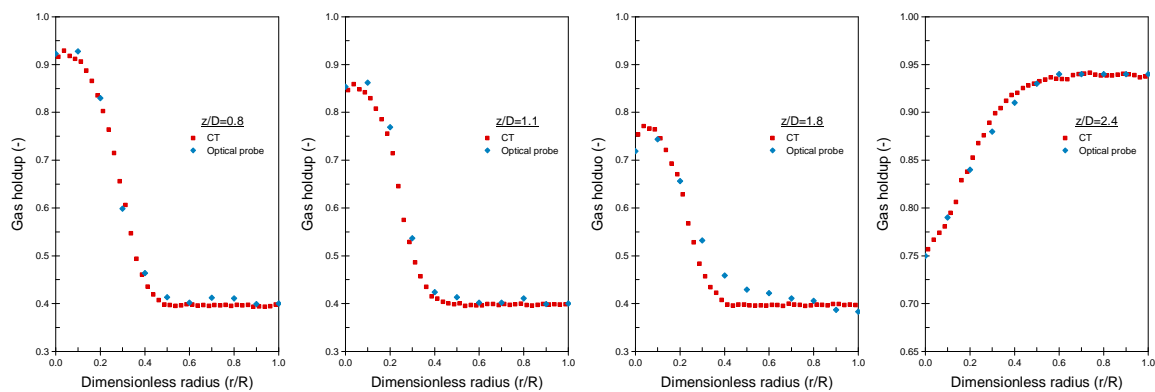


Fig. 16. Comparison of gas holdup profiles measured using CT and Optical probe by [13].

IV. An advanced evaluation the new mechanistic scale-up methodology of gas-solid spouted using radioactive particle tracking (RPT)

Neven Ali^a, Thaar Al-Juwaya^a, Muthanna Al-Dahhan^{ab*}

^aNuclear Engineering,

^bChemical and Biochemical Engineering,

Missouri University of Science and Technology (Missouri S&T) – Rolla

Rolla, MO 65409

Abstract

We implemented for the first time our radioactive particle tracking (RPT) as advanced noninvasive technique to further evaluate and validate in details our newly developed mechanistic scale up methodology based on matching radial profile of gas-holdup. Two spouted bed diameters of 0.076 m and 0.152 m were used. Three sets of conditions were implemented which consist of the conditions of the reference case, conditions that provided similar gas holdup radial profile to that of the reference case and conditions that provided non-similar gas holdup radial. The results confirm the validation of the scale up methodology in terms of obtaining closers dimensionless values and radial profiles of the components of the particles velocities, normal stresses, shear stresses and turbulent kinetic energy. The results further advance the knowledge and understanding of the gas-solids spouted beds provide deeper insight on their solids dynamics and presenting important benchmarking data for validating computational fluid dynamics codes and models.

*Corresponding author:

Tel.: +1 573 341 7518; fax: +1 573 341 4377.

E-mail addresses: aldahhanm@mst.edu

Keywords Scale-up, Spouted beds, TRISO, Radioactive Particle Tracking (RPT), 3-D velocity field, turbulence.

1. Introduction

The performance of the Very High Temperature Reactors (VHTRs) depend highly on the quality of the TRISO nuclear fuel coated particles. Such quality needs proper and reliable coating technology as well as its associated processes (López-Honorato, Tan, Meadows, Marsh, & Xiao, 2009). Four layers are used to carry out the coating of nuclear fuel particles, which are comprised of Buffer PyC (Pyrolytic Carbon) layer, SiC (Silicon Carbide) layer; OPyC (Outer Dense Pyrocarbon) layer and IPyC (Inner Dense Pyrolytic Carbon) layer. The coating of the TRISO fuel particles has been carried out in “Gas-Solid Spouted Beds” using Chemical Vapor Deposition (CVD) process. The spouted bed refers to the gas-particle contactors that have been used to handle coarser particles (Kishan B. Mathur & Epstein, 1974; K. B. Mathur & Gishler, 1955; M. Olazar, Alvarez, Aguado, & San José, 2003). In these gas-solid spouted bed coaters which can handle coarser particles, the gas is introduced through a single nozzle at the center of flat or a conical base creating a central gas jet (Duarte, Olazar, Murata, & Barrozo, 2009). The jet entrains the solid particles near the bottom of the bed and then transport them upward via a central zone called spout region towards the top. During such transport, the upward-moving solids exit at the top of the bed and consequently disengaged from the gas in the Fountain region. The solids fall back to the bed surface and then move slowly downward by gravity in the outer annular zone called annular region as shown in Figure 1. Thus, spouted beds typically have three different regions each with specific flow behavior: the spout, the annulus, and the

fountain regions. The spout is a dilute region shaped in the core of the bed, and confined by the annulus region. The annulus is a dense region surrounding the spout and extends radially toward the bed wall. The fountain is on the top of the spout-annulus regions. Hence, the mechanism of solids movements in each region varies which complicate the hydrodynamics, design scale up and performance of gas-solid spouted beds. Importantly, the net effect of the movement of the solids in two opposing solid flows is to provide a toroidal-like circulation cell, which is the explicit definition of the overall circulation of the solids in spouted beds (Rojas & Deytia, 2011). Moreover, there is an interface that is created between the downward-moving solids (annular region) and the upward-moving solids (spout region), which varies in time and space (Rojas & Deytia, 2011). Also, the overall circulation rate can be enhanced by the separation between the downward and the upward flow zones. Such flow behavior of gas-solid spouted beds benefits various industrial applications including coating and production of TRISO nuclear fuel particles (Duarte, et al., 2009; Kishan B. Mathur & Epstein, 1974; M. Olazar, et al., 2003; Martin Olazar, San José, Alvarez, Morales, & Bilbao, 1998; San José, Olazar, Alvarez, Izquierdo, & Bilbao, 1998).

It has been demonstrated that the fuel coating process of TRISO is extremely critical and it is required to satisfy several production specifications (Kim, et al., 2008; Miller, Maki, Knudson, & Petti, 2010; Miller, Petti, & Maki, 2004; Miller, Petti, Maki, & Knudson, 2006; van der Walt, Nel, Crouse, Jansen, & Kekana, 2011). One of these key specifications or requirements is that the particles must attain proper and sufficient coating layers with zero percent deficits. The hydrodynamics associated of the gas solid spouted beds affect the quality and effectiveness of such coating processes of the nuclear fuel

particles (Liu, Shao, & Liu, 2012; Miller, et al., 2010). Effective contact needs to be attained between the active vapor (gas) and particles for obtaining proper and sufficient layers of coating. Such effective contacts between gas and solid particles vary when the size of the spouted beds change. Therefore, hydrodynamics similarity must be sought during the scale up of spouted beds from small and/or cold flow conditions to large and/or industrial conditions. Such hydrodynamics similarity means attaining similarity in trends and in values or in dimensionless values of the hydrodynamic parameters. For commercialization of the VHTRs point of view and for other industrial applications such drying, granulation, coating, gasification, and chemical reactions, large scales of spouted beds are needed.

Despite the several studies that have been conducted on the gas-solid spouted beds, their hydrodynamics and scale up are not well understood due to complex interactions among the phases (Al-Dahhan, Aradhya, Zaid, Ali, & Aljuwaya, 2014; Djeridane, Larachi, Roy, Chaovki, & Legros, 1998; Du, Xu, Ji, Wei, & Bao, 2009; He, Lim, & Grace, 1997). Hence, the scale-up of gas-solid spouted beds to achieve hydrodynamics similarity is a challenging task. Therefore, a comprehensive knowledge of the solids flow pattern and their turbulent parameters in spouted beds are of major interest which aid in advancing their design, scale up and operation. Such knowledge has not yet been acquired due to the lack of utilization of proper advanced non-invasive measurement techniques (Djeridane, et al., 1998).

Many attempts have been made in the literature proposing and validating various scale-up methodologies. For example, (He, et al., 1997) proposed a scale up methodology based on matching selected dimensionless groups and they validated it by measuring

global hydrodynamic parameters. However, (Aradhya, 2013) and (Ali, Al-Juwaya, & Al-Dahhana, 2016a, 2016b) demonstrated that (He, et al., 1997) approach of matching dimensionless groups for scale up of spouted beds is not sufficient for achieving hydrodynamics similarity based on measuring local hydrodynamics parameters using optical fiber probe (Aradhya, 2013), gamma ray computed tomography (CT) and radioactive particle tracking (RPT) techniques (Ali, et al., 2016a, 2016b). Recently, (Al-Dahhan, et al., 2014) and (Aradhya, 2013) proposed a new mechanistic methodology based on the fact that the gas phase dictates the dynamics of the system which is stated as follows: “when two flow fields of spouted beds (with different sizes and/or conditions) are geometrically similar and have closer (which is called matched) gas phase holdup radial profiles at a bed height within the developed flow region, the local values or local dimensionless values of the hydrodynamic parameters and their trends attain similarity or they get close to each other at corresponding locations in the two flow fields”. Hence, by matching the gas holdup radial profile the scale up can be properly achieved. In such approach for scale up of spouted beds, the goal is to predict the actual solids local dynamics (solids velocities and turbulent parameters) in a larger size spouted bed and/or in a bed with industrial conditions by using the similarity in the dimensionless parameters of the solids dynamics (solids velocities and turbulent parameters) which are obtained in a smaller size and/or in cold flow conditions. It is worth to mention that the local actual values of the solids velocity and turbulent parameters will not be the same when the size and the conditions of the spouted beds are changed due to the variation in the conditions. However, the question arises whether there is a possibility to maintain similar dimensionless parameters if the scale up method captures the key phenomena in the spouted beds which

can be facilitated to estimate the actual solids dynamics in the other spouted beds. (Aradhya, 2013) validated this new methodology using optical fiber probe at selected and limited point measurements at various dimensionless height using optical fiber probe that measured local solids holdup and solids axial velocity. (Ali, Al-Juwaya, & Al-Dahhana, 2016c) validated this new methodology using gamma ray computed tomography (CT) that measured cross sectional distribution of solids and gas holdups at selected dimensionless height and their radial profiles. Unfortunately, there are no detailed measurements of the 3D solids velocity and their turbulent parameters that evaluate in details this new scale up methodology. Therefore, the focus of this work is to implement advanced non-invasive radioactive particle tracking (RPT) technique that can measure solids velocity and the turbulent parameters in 3D to further evaluate in detail the newly developed mechanistic scale up methodology.

2. Experimental work

2.1 Spouted beds setup

The experimental works were carried out in two conical base spouted bed columns made of Plexiglas with inner diameter of 0.076 m (3 inch) and a 0.152 m (6 inch) similar to those used and discussed by (Ali, et al., 2016c). The schematic diagrams of these two spouted beds are shown Figure 2. Both columns were without ports to avoid additional attenuation for RPT experiments that would complicate its data processing and they have cylindrical section of 1.14 m height and conical base of 60-degree angle. The gas phase enters the bed from the bottom through a stainless steel gas distributor mounted on an

orifice (9.5 mm, and 19.1 mm diameter for 3-inch and 6-inch bed, respectively) with high open area to create the needed jet for spouting conditions. Dry compressed air was used as the gas phase which its flow was regulated using a pressure regulator and two flowmeters connected in parallel. Stable spouting conditions were maintained in all experiments according to the criteria reported by (Ali, et al., 2016b; Aradhya, 2013; Chandnani & Epstein, 1986; He, et al., 1997; Kishan B. Mathur & Epstein, 1974).

2.2 Experimental conditions.

(Aradhya, 2013) used computational fluid dynamics (CFD) and trial and error to identify three different sets of conditions which consist of the reference conditions based on the reference conditions of (He, et al., 1997) and one set of conditions that provided matching (closer in magnitude and profile) radial profile of the gas holdup and the third set of conditions provided mismatching (different magnitude and profile) radial profile of gas holdup. These conditions are summarized in Table 1. (Aradhya, 2013) used optical fiber probe at three levels ($z/D=1.1, 1.8, 2.5$) but one angular location of the probe for each level to measure solids and gas holdups radial profile and to confirm the matching and mismatching of these profiles for the conditions listed in Table 1. (Ali, et al., 2016c) confirmed these conditions for matching radial profile of gas holdup using gamma ray computed tomography (CT) and furthermore validated the newly developed mechanistic scale up methodology by comparing the cross sectional distribution and radial profiles of solids and gas holdups at various levels along the bed height of the studied spouted beds. Accordingly, the sets of conditions of Table 1 have been used in this work.

2.3 The Radioactive Particle Tracking (RPT) Technique.

The Radioactive Particle Tracking (RPT) technique is a non-invasive technique used to track a single radioactive particle by detecting the intensity of emitted gamma rays and it is used to visualize the flow fields of multiphase flow systems. The RPT has been successfully applied using a single radioactive tracer particle to measure the 3D flow field and turbulent parameters in different multiphase flow systems (Bhusarapu, Al-Dahhan, & Dudukovic, 2004; Chen, et al., 1999; Larachi, Grandjean, & Chaouki, 2003; Rados, Shaikh, & Al-Dahhan, 2005; Rammohan, Kemoun, Al-Dahhan, & Dudukovic, 2001; Roy, Larachi, Legros, & Chaouki, 1994). The details of applying the RPT technique to the investigation the solids flow fields in the present spouted bed setup will not be repeated here and was thoroughly discussed in our recent work (Ali, et al., 2016a). Thus, the RPT has been implemented to assess in detail, for the first time, the newly scale-up methodology of spouted beds based on matching the gas holdup profile. The experimental results of the time-averaged 3-D solids velocity field and turbulence parameters (normal stress, shear stress, kinetic energy) in the three regions of the spouted bed are presented and discussed.

3. Results and Discussion

As mentioned earlier, three sets of experimental conditions in two different sizes of spouted beds were used to further evaluate and validate the newly developed scale up methodology for hydrodynamics similarity of spouted beds. The experimental conditions were originally selected to capture the matched and mismatched radial profiles of gas holdup as listed in Table 1 above. In this section, Cases A (6-inch diameter bed) and B (3-inch diameter bed) are designated as similar gas holdup radial profiles, and cases A and C

(3-inch diameter bed) are designated as non-similar gas holdup radial profiles. The results below demonstrate the evaluation of the hydrodynamics similarity of the new mechanistic methodology for scale-up of spouted beds when gas-holdup radial profiles are similar and the hydrodynamics non-similarity when non-similar gas holdup radial profiles are encountered. In the discussed results we call the conditions that reflect the sets of conditions above as Case A (reference conditions), Similar gas-holdup ϵ_g and Non-similar gas-holdup ϵ_g .

3.1 Solids Velocity Field

3.1.1 Azimuthally and axially averaged radial profiles of axial particles velocity.

Figure 3 shows the particles flow structure in terms of time averaged radial profiles of axial particles velocity which is averaged azimuthally and axially over the cylindrical part of the measured section of the bed. In all the studied cases, the particles move upward (i.e., upward, $U_z > 0$) with higher axial velocity in the spout region as the particles are carried up by the gas in this region. Maximum particle velocity is observed near the center of the spout region. The particles velocity decreases radially from the center of the spout zone toward the interface between the spout and annulus regions. (Ali, et al., 2016c) showed using CT technique that solids holdup is a minimum at the center and increases toward the annulus region where the solids particles are fed into the spout region from the spout and annulus interface z . It is clear here that as the solids holdup is low their axial velocity is high. This is because more energy of the gas is dissipated to carry the solids when more solids presence to be carried. In the annulus region the particles move downward ($U_z < 0$) at small velocity as they are moving by gravity in a granular flow

structure (or a moving bed). When reaching the fountain, the axial velocity is maximum near the axis and turns to negative values (i.e., downward, $U_z < 0$) in the outer region of the fountain due to the free fall of the particles as illustrated in Figure 3.

The results show the difference between the values of the axial particle velocity profile of Case A and those of similar and non-similar gas holdup profiles with lesser differences for similar gas holdup profile. For both conditions, the difference between the profiles was large in the spout and the fountain regions from those of the reference case in the annulus region. It is expected of such differences in the values of particles velocities due to the wide variation in the conditions of both studied spouted beds including different bed sizes. To understand this deviation, the impact of the operating and design variables in each set of conditions need to be studied. However, this is not the purpose of the present study, as it requires many RPT experiments to investigate the effect of each variable such as column diameter, cone angle, bed height, spouting velocity, size and density of particles, and many others. In the spout region, the absolute percentage deviation between the profiles was found to be 41.67% and 53.46% for the conditions of similar and non-similar gas holdup profile, respectively. In the fountain, the absolute percentage deviation in the profiles was found to be 43.48% and 46.34% for the conditions of similar and non-similar gas holdup profiles, respectively. In the annulus, the observed axial particle velocity is low and negative for all the cases, and the difference between the profiles is relatively small. This is because the particles move slowly and downwards in this region, more like as in moving bed as mentioned earlier. This is in agreement with the results obtained using CT technique of (Ali, et al., 2016c) where the solid-holdup profiles in this region were similar and unchanged. However, even though the two beds are geometrically similar, in order to

examine the similarity between the two beds the actual axial particles velocity should be converted to non-dimensional values to assess for the similarity needed for scale up.

Therefore, the profiles of the axial particle velocity in the two beds are non-dimensionalized by dividing them by the minimum spouting velocity. The minimum spouting velocity (U_{ms}) is defined as the minimum superficial gas velocity required to obtain the onset external spouting state in spouted beds, and below this velocity, solids circulation is absent, and all the three regions in spouted beds are not fully created. Indeed, such critical velocity is an important hydrodynamic parameter for the design and operation of spouted beds processes. The minimum spouting velocity can be obtained experimentally or estimated by correlations. It is a function of the physical properties of particles (density, size, and shape), bed geometry (column diameter, inlet diameter, and cone angle), static bed height, and gas properties (density, viscosity). In this work, the minimum spouting velocity (U_{ms}) was measured experimentally for the 6-inch and the 3-inch spouted beds for all the sets of operating conditions of Table 1. The height of the static bed particles (i.e. H_o , bed height) was fixed at a fixed bed position using a length scale attached on the wall of the column. We increased the gas flow rate slowly with small increment while we monitored the bed. The velocity at which the spouting initiated was measured and identified as the minimum spouting velocity. We repeated the measurement 5 times and the average value was used. The average measurement values of U_{ms} for each set of conditions were compared with the predictions of the correlation of (Kishan B. Mathur & Epstein, 1974) for deep spouted beds ($H_o/D_c > 1$). H_o refers to the initial static beds height, and D_c refers to the column diameter. The estimated values by the correlation are found

close to the measured ones (give average % difference). The minimum spouting velocity for the 6-inch and the 3-inch spouted beds are listed in Table 2.

Figure 4 shows the dimensionless axial particles velocity for the conditions of similar and non-similar gas holdup profiles with respect to the reference case (Case A). It is clear that when gas holdup profiles are similar or close, similarity in the dimensionless axial particle velocity of the cylindrical part of the bed was attained (Figure 3a). The average deviation between the profiles of these two cases in the spout region is 5.12%. In the annulus region the similarity is very close where the particles move slowly and by gravity. In the fountain region, the similarity in the dimensionless particles velocity was also achieved between the reference case (Case A) and the case of similar gas holdup profile as shown in Figure 4 with the average percentage deviation was 13.93%. It is relatively high due to some variation at some local dimensionless radial positions.

For the conditions of non-similar gas holdup profiles, Figure 4 clearly show non-similar dimensionless radial profile of averaged axial particles velocity in both spout and fountain regions where the deviation with respect to the reference case A is significant. The dimensionless axial particles velocities of 6-inch and 3-inch spouted beds deviates from each other and are more pronounced in the spout region with an average difference of 44.7%. The deviation is larger near the center of the spout and decrease as the radial distance from the axis increases until the spout-annulus interface where the spout is confined by the annulus. Also, large deviation is obtained in the fountain region, where the average percentage deviation between the profiles was 49.04%.

Indeed, these results confirm that the gas dictates the dynamics of the gas-solid spouted beds and the radial profile of the gas holdup can properly represent the key role of

dynamics of the gas phase on the solids flow field of the spouted beds. Same trends of the results and findings have been obtained for the other components of the particles velocities (radial and azimuthal velocities). In the following sections, we will discuss only the radial particles velocity, as the findings are similar for the azimuthal particles velocity in addition the latter is smaller compared to the other components.

3.1.2 Azimuthally and axially averaged radial profiles of radial particles velocity.

The radial component of the particles velocity has been measured using the RPT technique for the conditions of Case A and similar and non-similar gas holdup profiles. The radial profiles of the radial particles velocity for the 6-inch and 3-inch spouted beds are shown in Figure 5. The results show the radial particles velocity in all the three regions (spout, annulus, and fountain). In the spout region, the particle moves towards the axis ($U_r < 0$) of the spout, and has a parabolic profile with maximum value obtained at the middle distance ($r/R=0.2$) between the center of the spout and the spout-annulus interface, and minimum value when the particle reach the spout-annulus interface. The results show the difference between the profiles for the conditions of Case A and similar and non-similar gas holdup profiles. For the two sets of conditions (Case A and similar gas holdup profile and Case A and non-similar gas holdup profile), the difference in the values of the particles velocities was large in both the spout and the fountain regions.. This is expected as explained earlier for the axial particles velocities. In the spout region, the average percentage deviation between the profiles was found to be 52.04% and 70.26%, respectively, for the conditions of similar and non-similar gas holdup profiles with respect to Case A. However, the magnitudes of the radial particle velocities are small and insignificant comparing to the axial particle velocity. This is because in the spout region

the flow is dictated by the axial flowing of the particles (gas-solid riser form of flow). In the fountain region, radial velocity turns to positive values (i.e., outward, $U_r > 0$). The profiles show a radial dispersion in the fountain due to the radial scatter of the particles in such region. Maximum velocity was observed at ($r/R=0.44$), and then the velocity was decelerated in the outer region of the fountain. Notice that these results are coherent and in good agreement with the results concerning the behavior of the axial particles velocity. The absolute percentage deviation between the profiles was found to be 35.79% and 50.76% for the conditions of similar and non-similar gas holdup profiles, respectively with respect to Case A. In the annulus region, the radial velocity is small and the particles move toward the spout region (i.e., inward, $U_r < 0$), and the deviation between the profiles was small.

In order to have a basis of comparison between the two beds for hydrodynamics similarity, the profiles of the radial particle velocity was non-dimensionalized for both beds and for the studied conditions by dividing them by the minimum spouting velocity (U_{ms}).

Figure 6 shows the profiles of the dimensionless averaged radial particles velocity for the conditions of similar and non-similar gas holdup profiles in the cylindrical and fountain parts of the bed. Less deviation is observed for the condition of similar gas holdup profiles from those of the reference case (Case A), indicating that matching gas holdup profiles can lead hydrodynamics similarity between the two beds. In the spout, the average percentage deviation between the profiles is 5.12%, at ($r/R=0.0625$) is 9.27%, at ($r/R=0.187$) is 8.46%, and at ($r/R=0.312$) is 8.92%. In the fountain region, the average percentage deviation is 36.4% which is larger than that in the spout region. In the annulus region, the radial particles velocity remains small and insignificant.

The profiles of the dimensionless radial particles velocity for the conditions of non-similar gas-holdup profiles are shown also in Figure 6. Clearly large deviation is observed between the profiles from those of the reference case (Case A) in the spout and the fountain regions. The average percentage deviation between the profiles in the spout is 55.31%. In the fountain region, the average percentage deviation between the profiles is 62.67%. To conclude, the gas holdup profiles were not close from those of the reference case (case A), resulting in significant deviation in the dimensionless radial particles velocity.

Consequently, these findings provide further confirmation of the relevant role of the gas holdup in the scale-up of spouted beds and how properly can be used to represent the gas dynamics influence in gas-solid spouted beds.

3.2 Azimuthally and axially averaged radial profiles of the particles normal stresses.

Figure 7, Figure 8, and Figure 9 illustrate the averaged radial profiles of the particles axial, radial and azimuthal normal stresses, respectively for both values in cm^2/s^2 and dimensionless values of these normal stresses where they are converted to dimensionless values by dividing them by the square of the minimum spouting velocity (U_{ms}^2) (cm^2/s^2). The figures demonstrate same trend as obtained for the particles velocity discussed above. For the dimensional values of the particles normal stresses the deviations were noticeable between those of the reference case (Case A) and those of the conditions for similar and non-similar gas holdup profiles. However, when the particles normal stresses were non-dimensionalized with respect to the square of the minimum spouting velocity, the similarity was attained between the reference case (Case A) and the case with similar gas holdup radial profiles. When the gas holdup radial profiles are not similar the

non-similarity in the dimensionless normal stresses was obtained. Table 3 summarizes the average percentage differences in dimensional values and dimensionless values of the particles normal stresses between the studied conditions.

It is obvious that the magnitudes of τ_{rr} (Figure 8) are much smaller than those of τ_{zz} (Figure 7) in all the three regions of the studied spouted beds. In the regions of spout and the annulus the τ_{rr} values are comparable to those of τ_{zz} in the annulus region. This is due to negligible velocity and its fluctuations in the radial direction. However, in fountain region due to the flow structure of the fountain and the freely fallen particles, non-negligible radial velocity and its fluctuations exist. Hence, the magnitudes of τ_{rr} are much larger than those in the spout and annulus region. Similar to τ_{zz} trends and profiles, there are maxima of the τ_{rr} in the region between $r/R = 0.4$ to 0.6 which indicate that larger fluctuations and magnitudes of the radial particles velocity at this zone. This is consistent with the trend and profiles of the particles radial velocity shown in

Figure 5. When the magnitudes of τ_{rr} are converted to dimensionless values with respect to the square of the minimum spout velocity, the trend of differences remain the same and the magnitudes of the percentage differences get even larger as demonstrated in Figure 8.

The azimuthal normal stresses ($\tau_{\theta\theta}$) are illustrated in Figure 9. Due to the nature of the flow in spout and annulus regions where the particles while they move downward in the annulus region they move angularly and they enter into the spout region tangentially and hence the angular velocity fluctuations are higher than those for the radial velocity components. Therefore, the magnitudes of the $\tau_{\theta\theta}$ in the spout and annulus regions are higher than those of the τ_{rr} but in the spout region they are smaller than those of the τ_{zz} . In

the fountain region, due to the rotation nature of the fountain flow structure, the fluctuations of the angular velocity is also noticeable and hence the magnitudes of $\tau_{\theta\theta}$ are comparable to those in the spout region. However, the trend is different from those of τ_{rr} and τ_{zz} where maxima do not exist. The maximum values of the $\tau_{\theta\theta}$ are at the center zone of the spout region and they decrease toward the annulus region. However in the fountain region they decrease toward the wall where the fluctuations in the angular direction and the magnitude of the angular component of the velocity get smaller.

3.3 Azimuthally and axially averaged radial profiles of particles shear stresses

Figure 10 and Figure 11 show the averaged radial profiles of shear stress for the studied conditions mentioned above (Cases A, case of similar gas holdup profile and case of non-similar gas holdup profile) for both dimensional values (magnitude) in cm^2/s^2 (Figure 10) and for dimensionless values with respect to the square of the minimum spouting velocity (Figure 11). Also the figures demonstrate same trend as obtained for the averaged normal stresses and for particles velocity discussed above. For the dimensional values of the particles shear stresses the deviations were noticeable between those of the reference case (Case A) and those of the conditions for similar and non-similar gas holdup profiles. However, when the particles shear stresses were non-dimensionalized with respect to the square of the minimum spouting velocity, the similarity was attained between the reference case (Case A) and the case with similar gas holdup radial profiles. When the gas holdup radial profiles are not similar the non-similarity in the dimensionless particles shear stresses was obtained. Table 4 summarizes the average percentage differences in the actual and dimensionless particles shear stresses between the studied conditions.

In the spout region τ_{rz} radial profiles show maxima at the zone between the center of the spout and the spout annulus interface ($\sim r/R=0.2$). This trend reflects the magnitude of the fluctuations in the axial and radial components of the velocities where their multiplication gives the maximum value at $\sim r/R=0.2$. At about the spout/annulus interface the τ_{rz} values get negative at the zone of about $r/R=0.35$ to about $r/R=0.6$. In the annulus region, the values of τ_{rz} are small compared to those of the spout region due to the nature of the flow structure of the annulus region described above. In the fountain region however the maxima occur in the zone of about $r/R=0.7$. At both the center zone and the wall zone the τ_{rz} values are comparable for all the studied cases. It is clear that there is mismatch in the dimensional magnitudes of the τ_{rz} between the reference conditions of Case A and the case of similar gas holdup radial profile. The differences get larger between Case A and the case of non-similar gas holdup profile. When τ_{rz} values are converted to dimensionless values using the squared minimum spouting gas velocity, the differences in values get smaller (Attainment of similarity) for the Case A and the case of similar gas holdup. However, the differences still exist and are larger between the case A and the case of non-similar gas holdup profile (Table 4).

This confirms further the validation of the newly developed scale up methodology for hydrodynamics similarity of spouted beds and the key role of the gas holdup profiles in dictating the hydrodynamics.

3.4 Azimuthally and axially averaged radial profiles of the particles turbulent kinetic energy

Figure 12 demonstrates the turbulent kinetic energy in the three regions of the studied spouted beds for the conditions of Case A, the case of similar gas holdup radial profile and the case of non-similar gas holdup radial profile. The figures demonstrate the same trend as obtained for the averaged shear stresses, normal stresses and for particles velocity discussed earlier. For the dimensional values of the particles turbulent kinetic energy the differences were obvious between those of the reference case (Case A) and those of the conditions for similar and non-similar gas holdup profiles. However, when the values of the particles turbulent kinetic energy were non-dimensionalized with respect to the square of the minimum spouting velocity, the similarity was attained between the reference case (Case A) and the case with similar gas holdup radial profiles. When the gas holdup radial profiles are not similar the non-similarity in the dimensionless particles turbulent kinetic energy was obtained. Table 5 summarizes the average percentage differences in the dimensional values and dimensionless values of the particles turbulent kinetic energy between the studied conditions.

Figure 12 illustrates that the turbulent kinetic energy of the particles are larger in the center zone of the spout region for all the sets of the studied conditions and get reduced toward the spout/annulus interface. This trend is similar to the trends of the τ_{zz} and $\tau_{\theta\theta}$ which their values are significant compared to τ_{rr} . At the annulus region the turbulent kinetic energy leveled off and the magnitudes are smaller compared to those of the spout region. In the fountain region the turbulent kinetic energy magnitudes are comparable to those in the center zone of the spout region and show maxima at about $r/R = 0.4 - 0.5$. This is similar to the trend of τ_{zz} and τ_{rr} which their values are dominating the estimated values

of the turbulent kinetic energy. The dimensionless values of the radial profiles of the turbulent kinetic energy for the Case A (reference conditions) are closer when gas holdup radial profile is similar as compared to those when the radial gas holdup profiles are non-similar. In the spout region, the average percentage deviations between the profiles of the reference case (Case A) and the conditions of similar and non-similar gas holdup profiles are, respectively, 56.43% and 72.02%. In the fountain, the average percentage deviations between the profiles of the Case A and the conditions of similar and non-similar gas holdup profiles are, respectively, 60.8% and 71.47%.

However, for the dimensionless values in the spout region, the average percentage deviations between the profiles of the reference case and the conditions of similar and non-similar gas holdup profiles are 17.05% and 52.07%, respectively. In the fountain, the average percentage deviations between the profiles of the reference case and the conditions of similar and non-similar gas holdup profiles are 15.47% and 51.12%, respectively. This further confirms the validity of the newly developed scale –up methodology based on matching gas holdup radial profiles.

4. Concluding Remarks

The advanced non non-invasive radioactive particle tracking technique has been implemented for the first time to evaluate and further validate our newly developed scale up methodology based on matching the radial profile of the gas holdup at the developed flow region of the bed. The results confirm that when the radial profiles of the gas holdup are matched or get closer to each other hydrodynamics similarity has been obtained in

terms of the dimensionless values and radial profiles of the components of the particles velocities, normal stresses, shear stresses and turbulent kinetic energy. However, when there were mismatching in the radial profiles of the gas holdups between set of conditions, non-similarity in these parameters were obtained and as the differences between the holdup profiles increases, the non-similarity in these parameters further enhanced. These findings further confirm the findings of (Al-Dahhan, et al., 2014; Ali, et al., 2016c; Aradhya, 2013). In addition, the findings confirm that the gas phase dictate the dynamics of gas-solid spouted beds and the radial profile of the gas holdup can represent the role of the gas phase on the solids dynamics of the bed. The knowledge and the data obtained provide valuable inside on the solids dynamics of spouted bed and presenting benchmarking data to validate computational fluid dynamics codes and models.

It is recommended that this new methodology can be enabled and applied in practice by implementing computational fluid dynamics after it is validated to search for the conditions that can provide similar gas holdup profiles measured at the desired conditions of either lab scales or cold flow conditions. Gamma ray densitometry which is used in industry as nuclear gauge densitometry for liquid or slurry level monitoring and control can be used on site to evaluate and to refine the operating conditions for enabling the industrial implementation of our newly developed scale up methodology for gas-solid spouted beds.

References

- Al-Dahhan, M., Aradhya, S., Zaid, F., Ali, N., & Aljuwaya, T. (2014). Scale-up and On-line Monitoring of Gas-solid Systems Using Advanced and Non-invasive Measurement Techniques. *Procedia Engineering*, 83, 469-476.
- Ali, N., Al-Juwaya, T., & Al-Dahhana, M. (2016a). An advanced evaluation of spouted beds scale-up for coating TRISO nuclear fuel particles using radioactive particle tracking (RPT). *Experimental Thermal and Fluid Science*, ##, "Submitted" or "under consideration".
- Ali, N., Al-Juwaya, T., & Al-Dahhana, M. (2016b). Assessing the scale-up methodology of gas-solid spouted beds based on matching dimensionless groups using gamma ray computed tomography (CT). *Chemical Engineering Research and Design*, ##, "Submitted" or "under consideration".
- Ali, N., Al-Juwaya, T., & Al-Dahhana, M. (2016c). Evaluating the new mechanistic scale-up methodology of gas-solid spouted beds using gamma ray computed tomography (CT). *Powder Technology*, ##, "Submitted" or "under consideration".
- Aradhya, S. B. (2013). *Scaleup and hydrodynamics study of gas-solid spouted beds*. Unpublished Doctoral Dissertations, Missouri University of Science and Technology.
- Bhusarapu, S., Al-Dahhan, M., & Dudukovic, M. P. (2004). Quantification of solids flow in a gas–solid riser: single radioactive particle tracking. *Chemical Engineering Science*, 59, 5381-5386.
- Chandnani, P. P., & Epstein, N. (1986). *Spoutability and spout detabilization of fine particles with a gas*. United States: Engineering Foundation.
- Chen, J., Kemoun, A., Al-Dahhan, M. H., Duduković, M. P., Lee, D. J., & Fan, L.-S. (1999). Comparative hydrodynamics study in a bubble column using computer-automated radioactive particle tracking (CARPT)/computed tomography (CT) and particle image velocimetry (PIV). *Chemical Engineering Science*, 54, 2199-2207.

- Djeridane, T., Larachi, F., Roy, D., Chaovki, J., & Legros, R. (1998). Investigation of the mean and turbulent particle velocity fields in a spouted bed using radioactive particle tracking. *The Canadian Journal of Chemical Engineering*, 76, 190-195.
- Du, W., Xu, J., Ji, Y., Wei, W., & Bao, X. (2009). Scale-up relationships of spouted beds by solid stress analyses. *Powder Technology*, 192, 273-278.
- Duarte, C. R., Olazar, M., Murata, V. V., & Barrozo, M. A. S. (2009). Numerical simulation and experimental study of fluid-particle flows in a spouted bed. *Powder Technology*, 188, 195-205.
- He, Y. L., Lim, C. J., & Grace, J. R. (1997). Scale-up studies of spouted beds. *Chemical Engineering Science*, 52, 329-339.
- Kim, W. K., Lee, Y. W., Cho, M. S., Park, J. Y., Ra, S. W., & Park, J. B. (2008). Nondestructive measurement of the coating thickness for simulated TRISO-coated fuel particles by using phase contrast X-ray radiography. *Nuclear Engineering and Design*, 238, 3285-3291.
- Larachi, F. ç., Grandjean, B. P. A., & Chaouki, J. (2003). Mixing and circulation of solids in spouted beds: particle tracking and Monte Carlo emulation of the gross flow pattern. *Chemical Engineering Science*, 58, 1497-1507.
- Liu, M., Shao, Y., & Liu, B. (2012). Pressure analysis in the fabrication process of TRISO UO₂-coated fuel particle. *Nuclear Engineering and Design*, 250, 277-283.
- López-Honorato, E., Tan, J., Meadows, P. J., Marsh, G., & Xiao, P. (2009). TRISO coated fuel particles with enhanced SiC properties. *Journal of Nuclear Materials*, 392, 219-224.
- Mathur, K. B., & Epstein, N. (1974). 1 - Introduction. In K. B. Mathur & N. Epstein (Eds.), *Spouted Beds* (pp. 1-13): Academic Press.
- Mathur, K. B., & Gishler, P. E. (1955). A technique for contacting gases with coarse solid particles. *AIChE Journal*, 1, 157-164.

- Miller, G. K., Maki, J. T., Knudson, D. L., & Petti, D. A. (2010). Calculating failure probabilities for TRISO-coated fuel particles using an integral formulation. *Journal of Nuclear Materials*, 399, 154-161.
- Miller, G. K., Petti, D. A., & Maki, J. T. (2004). Consideration of the effects of partial debonding of the IPyC and particle asphericity on TRISO-coated fuel behavior. *Journal of Nuclear Materials*, 334, 79-89.
- Miller, G. K., Petti, D. A., Maki, J. T., & Knudson, D. L. (2006). An evaluation of the effects of SiC layer thinning on failure of TRISO-coated fuel particles. *Journal of Nuclear Materials*, 355, 150-162.
- Olazar, M., Alvarez, S., Aguado, R., & San José, M. J. (2003). Spouted Bed Reactors. *Chemical Engineering & Technology*, 26, 845-852.
- Olazar, M., San José, M. J., Alvarez, S., Morales, A., & Bilbao, J. (1998). Measurement of particle velocities in conical spouted beds using an optical fiber probe. *Industrial & Engineering Chemistry Research*, 37, 4520-4527.
- Rados, N., Shaikh, A., & Al-Dahhan, M. H. (2005). Solids flow mapping in a high pressure slurry bubble column. *Chemical Engineering Science*, 60, 6067-6072.
- Rammohan, A. R., Kemoun, A., Al-Dahhan, M. H., & Dudukovic, M. P. (2001). Characterization of Single Phase Flows in Stirred Tanks via Computer Automated Radioactive Particle Tracking (CARPT). *Chemical Engineering Research and Design*, 79, 831-844.
- Rojas, L., & Deytia, I. (2011). *Investigation of hydrodynamic scaling relationships in shallow spouted beds*.
- Roy, D., Larachi, F., Legros, R., & Chaouki, J. (1994). A study of solid behavior in spouted beds using 3-D particle tracking. *The Canadian Journal of Chemical Engineering*, 72, 945-952.

San José, M. a. J., Olazar, M., Alvarez, S., Izquierdo, M. A., & Bilbao, J. (1998). Solid cross-flow into the spout and particle trajectories in conical spouted beds. *Chemical Engineering Science*, 53, 3561-3570.

van der Walt, I. J., Nel, J. T., Crouse, P. L., Jansen, A. A., & Kekana, S. J. (2011). The treatment of TRISO coated particles with CF₄ in a low temperature plasma. *Journal of Nuclear Materials*, 413, 156-161.

Notation

d_p	particle diameter, m
D_c	inner column diameter, m
D_i	inlet orifice diameter, m
e_{ss}	restitution coefficient of the particles
Fr	Froude number
g	acceleration of gravity, m s^{-2}
H	static bed height, m
H_F	fountain height, m
H_m	maximum spoutable bed depth, m
L	column length, m
P	bed pressure, Pa
Re	Reynolds number
R	column radius, cm
T	bed temperature, K
T	time, second
TKE	turbulent kinetic energy (per unit bulk density), $\text{cm}^2 \text{s}^{-2}$
U	superficial gas velocity, m s^{-1}
U_{mf}	minimum fluidization velocity, m s^{-1}
U_{ms}	minimum spouting velocity, m s^{-1}
U	axially averaged of the mean particle velocity (\bar{u}), m s^{-1}
u	instantaneous local particle velocity, cm/s
\bar{u}	averaged particle velocity, cm/s

u'	fluctuating particle velocity, cm/s
z	axial distance from inlet orifice, m

Greek letters

β	fluid-particle interaction coefficient, $\text{kg m}^3 \text{s}^{-1}$.
ρ_s	particle density, Kg m^{-3} .
ρ_f	fluid density, Kg m^{-3} .
μ	fluid viscosity, $\text{Kg m}^{-1} \text{s}^{-1}$.
ϕ_s	sphericity of particles.
φ	inertial friction angle of particle, deg.
ε_{mf}	bed voidage at minimum fluidization.
ε_o	voidage at packed bed state
ε_s	solids fraction (or solids holdup).
ε_g	gas fraction (or gas holdup).
τ	stress in the pq direction (p, q = r, θ , z), cm^2/s^2 .

Subscripts

'	Dimensionless parameter.
---	--------------------------

Table 1. Experimental Conditions for similar and non-similar gas holdup radial profiles for the hydrodynamics similarity of spouted beds identified by (Aradhya, 2013).

Condition/Case	A (Reference case)	Similar gas-holdup profiles (ϵ_g) _r	Non-similar gas-holdup profiles (ϵ_g) _r
D_c (m)	0.152	0.076	0.076
D_i (mm)	19.1	9.5	9.5
L (m)	1.14	1.14	1.14
H (m)	0.323	0.16	0.16
T (K)	298	298	298
P (kPa)	101	364	101
Particles	Glass	Steel	Glass
d_p (mm)	2.18	1.09	1.09
ρ_s (kg/m ³)	2400	7400	2450
ρ_f (kg/m ³)	1.21	3.71	1.21
μ (x 10 ⁵) (Pa.s)	1.81	1.81	1.81
U (m/s)	1.08	0.64	0.74

Table 2. Comparison between the measured and the correlation predictions of the minimum spouting velocity.

Bed Geometry	A (Reference case)	Similar gas-holdup profiles (ϵ_g)r	Non-similar gas-holdup profiles (ϵ_g)r
D_c (mm)	152	76	76
D_i (mm)	19.1	9.5	9.5
H (mm)	323	160	160
γ ($^\circ$) cone angle	60	60	60
Experimental Values	0.89 m/s	0.58 m/s	0.68
Correlation prediction of Mathur and Gishler, 1995	0.85 m/s	0.59 m/s	0.68

Table 3. Percentage differences in normal stresses among the studied sets of conditions of the Case A and similar and non-similar gas holdup profiles.

Normal stress	τ_{zz}	τ_{rr}	$\tau_{\theta\theta}$	τ_{zz}	τ_{rr}	$\tau_{\theta\theta}$
	Average deviation (%) in spout			Average deviation (%) in fountain		
Case A	-	-	-	-	-	-
Similar gas holdup	<u>51.06</u>	<u>54.86</u>	<u>70.3</u>	<u>43.05</u>	<u>58.07</u>	<u>63.95</u>
Non-similar gas holdup	<u>60.12</u>	<u>69.25</u>	<u>78.79</u>	<u>65.52</u>	<u>48.74</u>	<u>78.86</u>
Dimensionless normal stress	τ'_{zz}	τ'_{rr}	$\tau'_{\theta\theta}$	τ'_{zz}	τ'_{rr}	$\tau'_{\theta\theta}$
	Deviation (%) in spout			Deviation (%) in fountain		
Case A	-	-	-	-	-	-
Similar gas holdup	<u>12.88</u>	<u>10.56</u>	<u>30.08</u>	<u>25.58</u>	<u>16.85</u>	<u>27.83</u>
Non-similar gas holdup	<u>50.64</u>	<u>47.33</u>	<u>63.98</u>	<u>57.33</u>	<u>35.57</u>	<u>63.78</u>

Table 4. Percentage differences in shear stresses among the studied conditions of the reference case, similar and non-similar gas holdup profiles.

Dimensionless shear stress	τ_{rz}	$\tau_{z\theta}$	$\tau_{r\theta}$	τ_{rz}	$\tau_{z\theta}$	$\tau_{r\theta}$
	Deviation (%) in spout			Deviation (%) in fountain		
Case A	-	-	-	-	-	-
similar	<u>52.47</u>	<u>52.7</u>	<u>47.71</u>	<u>53.34</u>	<u>55.98</u>	<u>51.64</u>
Non-similar	<u>65.79</u>	<u>73.56</u>	<u>71.14</u>	<u>65.08</u>	<u>70.08</u>	<u>65.67</u>
Dimensionless shear stress	τ_{rz}'	$\tau_{z\theta}'$	$\tau_{r\theta}'$	τ_{rz}'	$\tau_{z\theta}'$	$\tau_{r\theta}'$
	Deviation (%) in spout			Deviation (%) in fountain		
Case A	-	-	-	-	-	-
Similar	<u>22.65</u>	<u>12.6</u>	<u>23.13</u>	<u>37.69</u>	<u>18.03</u>	<u>26.82</u>
Non-similar	<u>69.98</u>	<u>58.02</u>	<u>58.31</u>	<u>40.17</u>	<u>48.74</u>	<u>41.19</u>

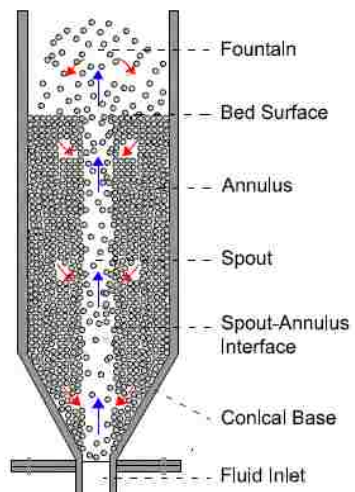


Figure 1. Schematic diagram of spouted beds.

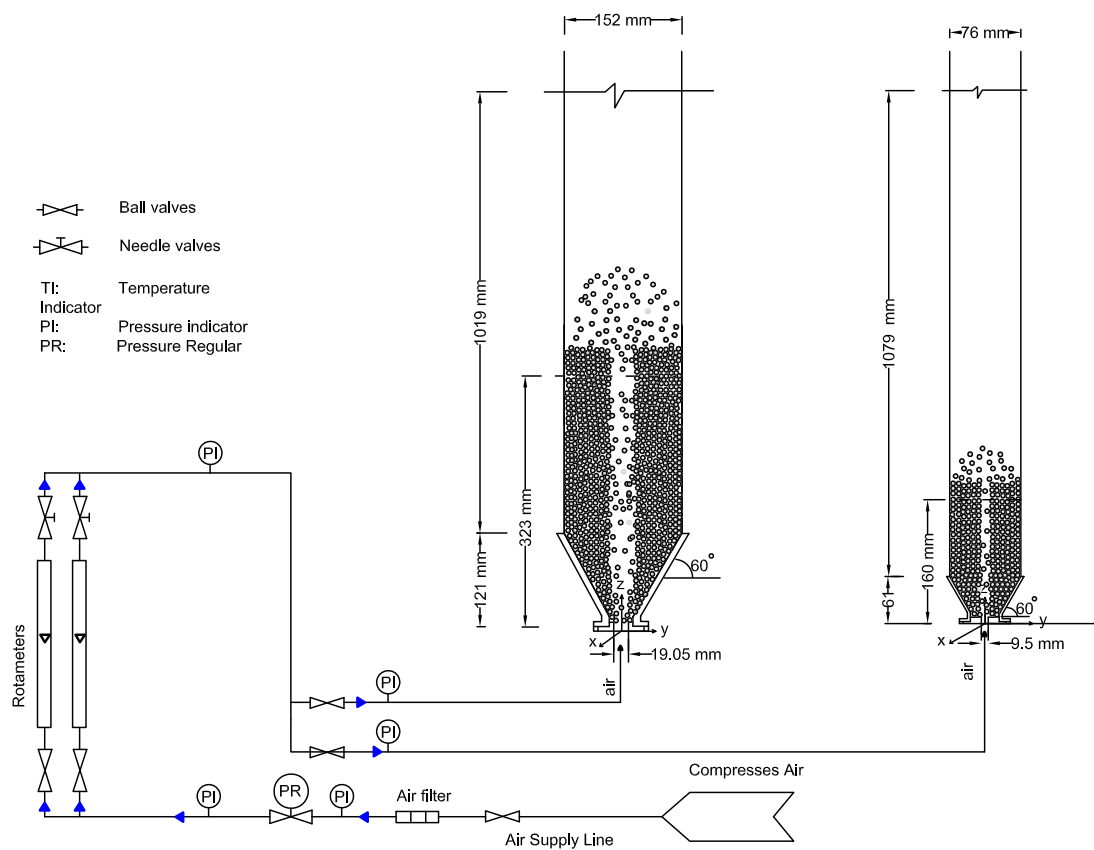


Figure 2. Schematic diagram of the 3-inch and 6-inch spouted beds.

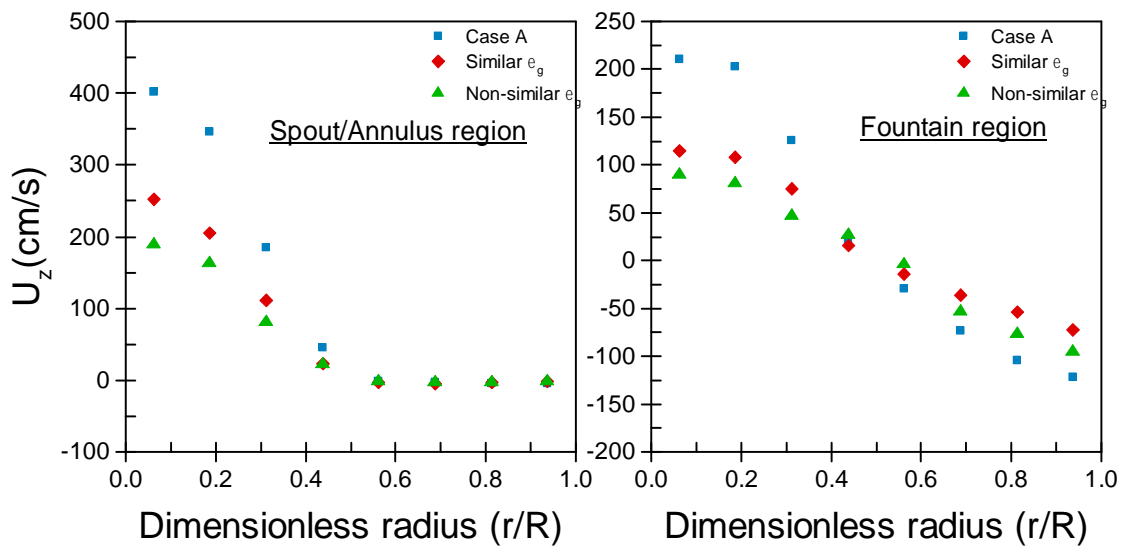


Figure 3. Azimuthally and axially averaged radial profiles of the axial particle velocity for the conditions of Case A, similar, and non-similar gas holdup profiles for 6-inch and 3-inch spouted beds in the spout/annulus and the fountain regions.

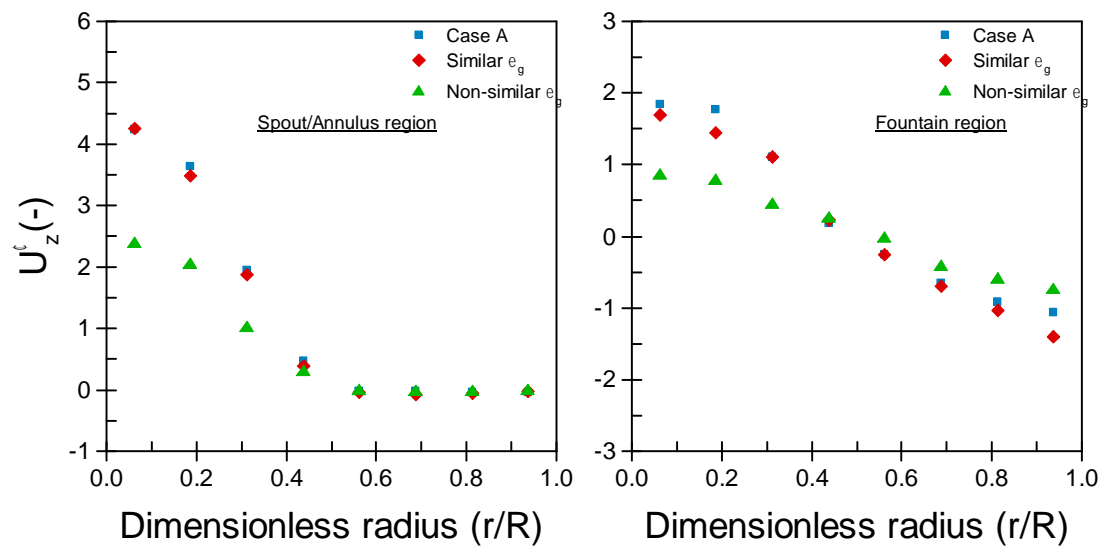


Figure 4. Azimuthally and axially averaged radial profiles of the dimensionless axial particle velocity for the conditions of Case A and similar and non-similar gas holdup profiles for 6-inch and 3-inch spouted beds in the spout/annulus and the fountain regions.

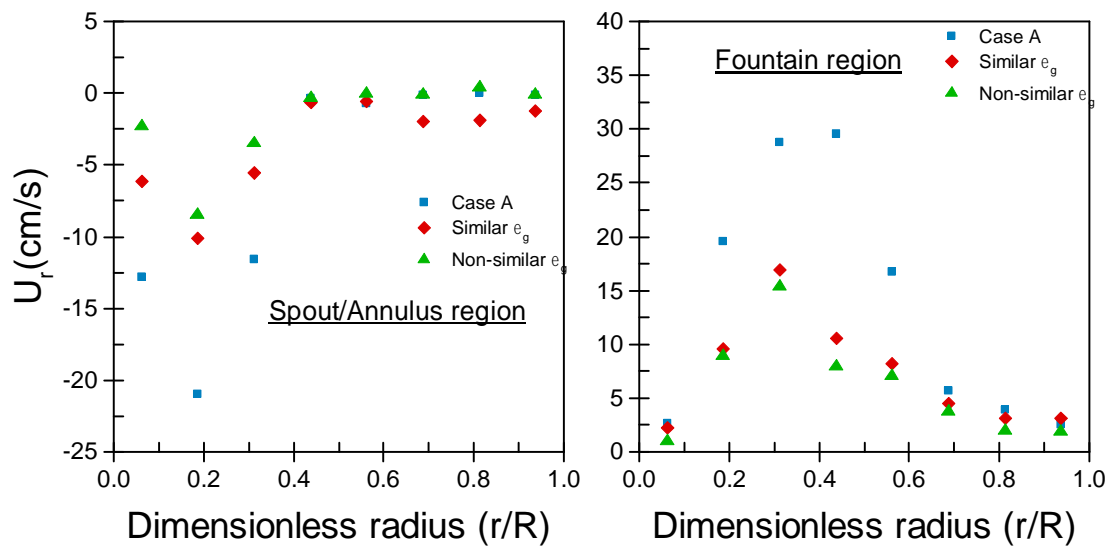


Figure 5. Azimuthally and axially averaged radial profiles of the radial particle velocity for the conditions of similar and non-similar gas-holdup profiles for 6-inch and 3-inch Spouted beds in the spout/annulus and the fountain regions.

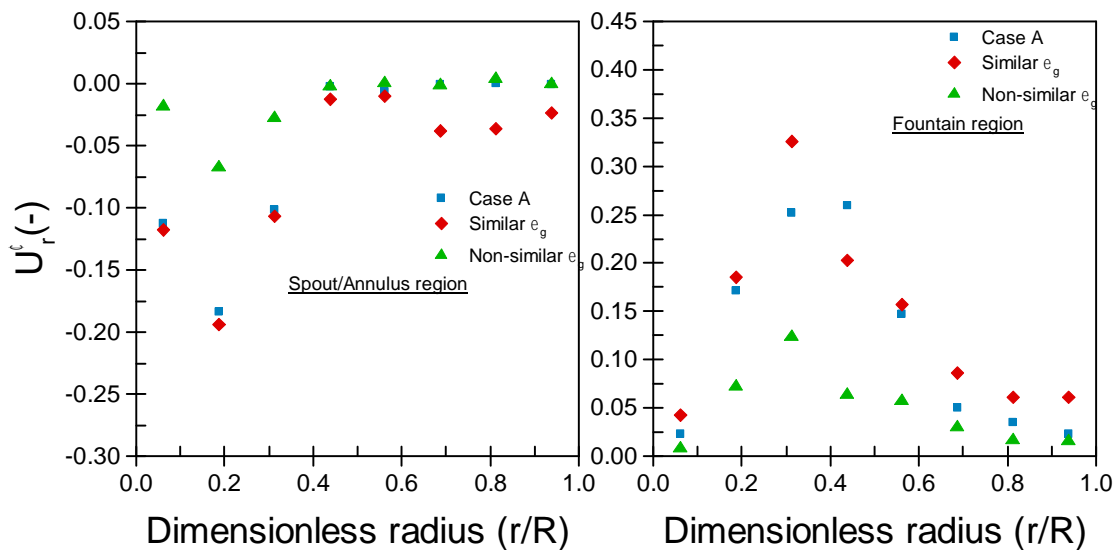


Figure 6. Azimuthally and axially averaged radial profiles of the dimensionless radial particle velocity for the conditions of similar and non-similar gas holdup profiles for the 6-inch and the 3-inch spouted beds in the spout/annulus and the fountain regions.

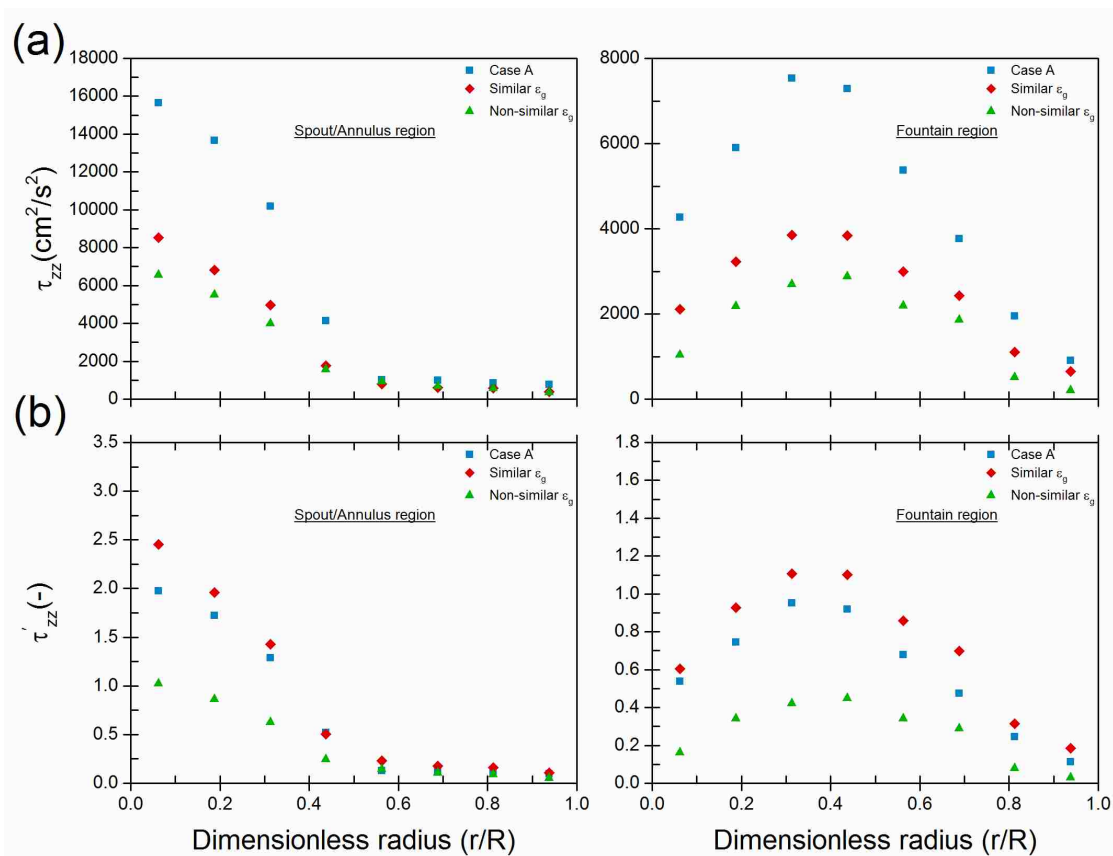


Figure 7. Azimuthally and axially averaged radial profiles of (a) the axial normal stresses and (b) the dimensionless axial normal stresses for the conditions of Case A, similar, and non-similar gas holdup profiles for 6-inch and 3-inch spouted beds in the spout/annulus and the fountain regions.

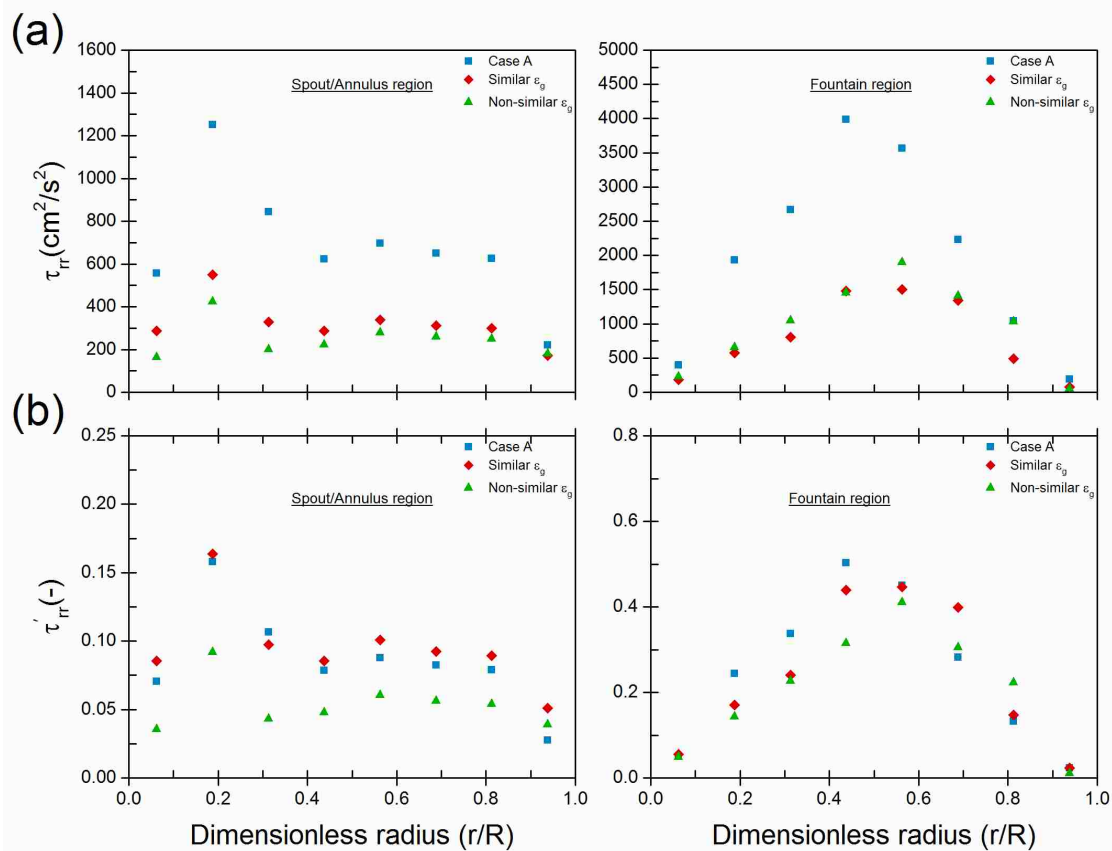


Figure 8. Azimuthally and axially averaged radial profiles of (a) the radial normal stresses and (b) the dimensionless radial normal stresses for the conditions of Case A, similar, and non-similar gas holdup profiles for 6-inch and 3-inch spouted beds in the spout/annulus and the fountain regions.

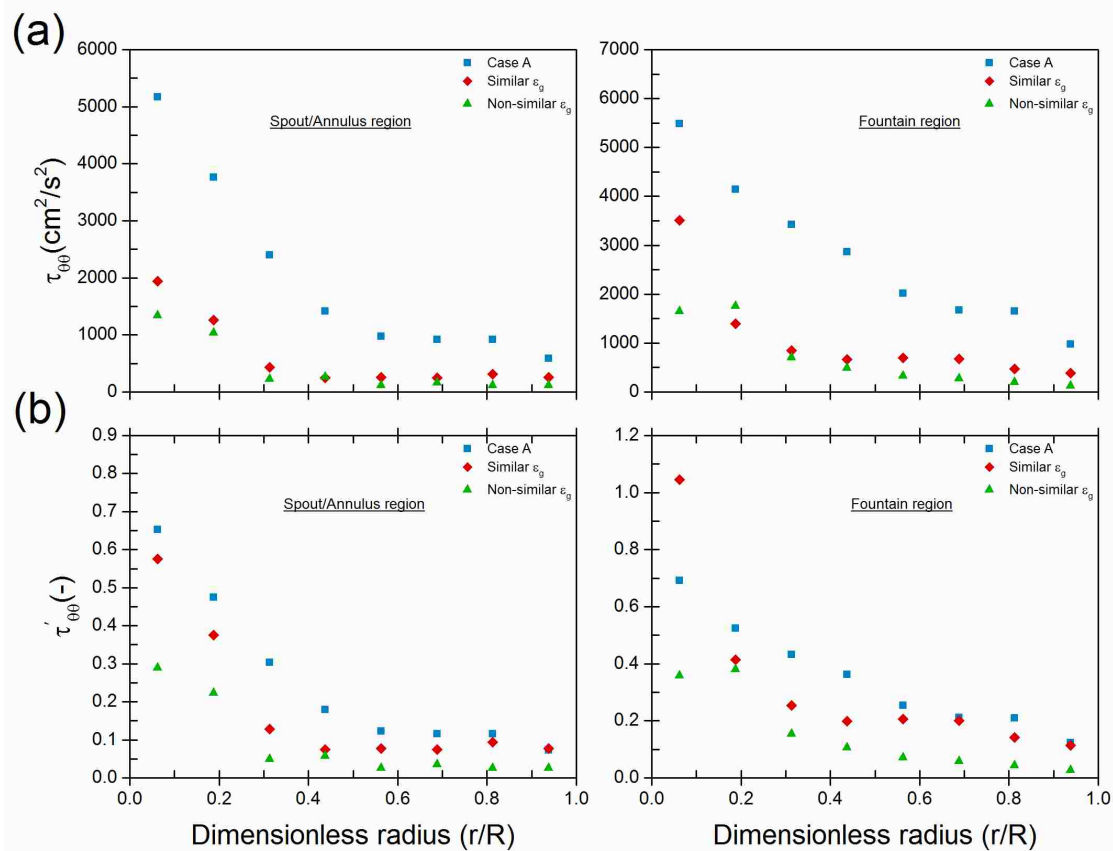


Figure 9. Azimuthally and axially averaged radial profiles of (a) the azimuthal normal stresses and (b) the dimensionless azimuthal normal stresses for the conditions of Case A, similar, and non-similar gas holdup profiles for 6-inch and 3-inch spouted beds in the spout/annulus and the fountain regions.

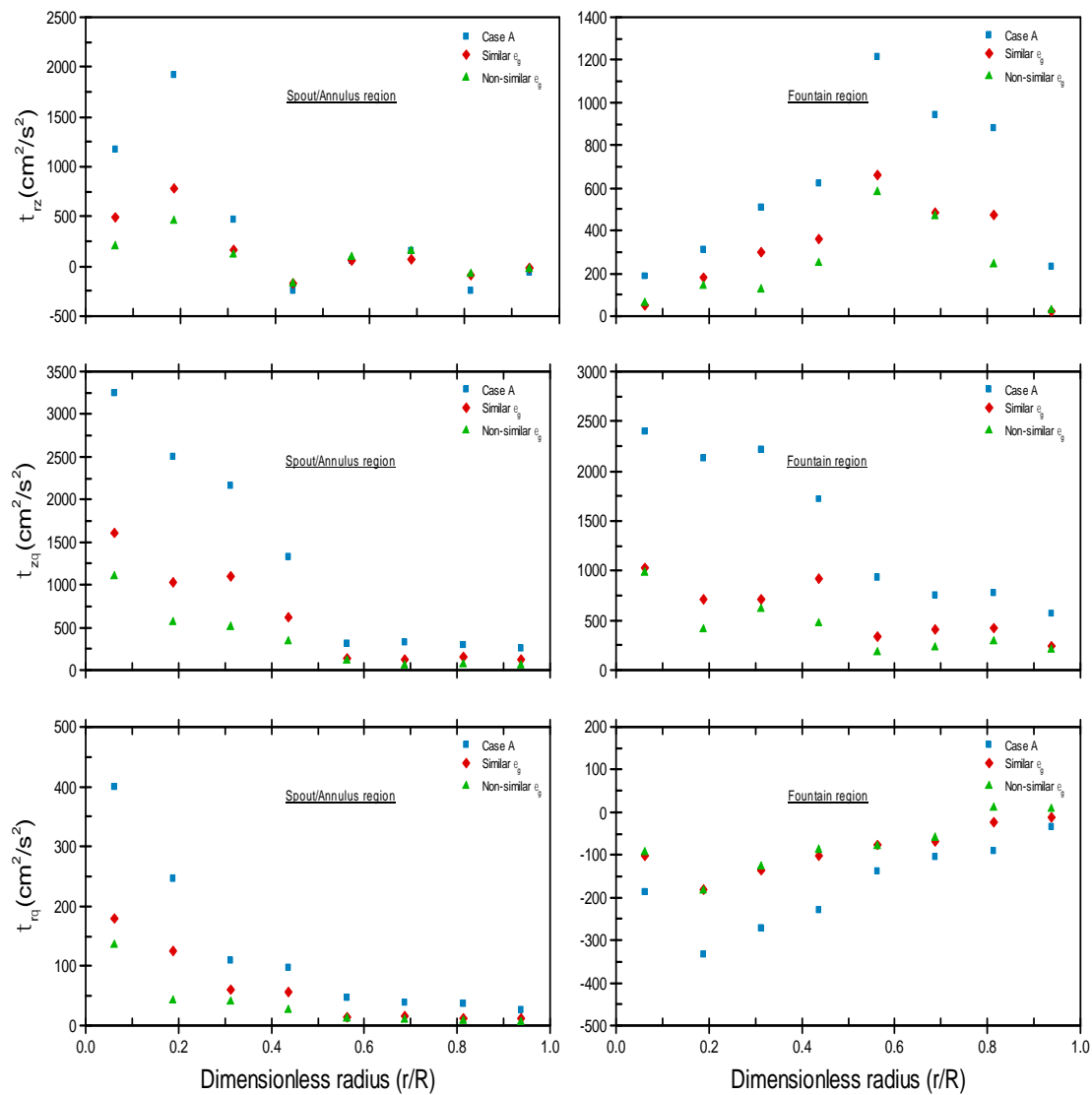


Figure 10. Comparison of the azimuthally and axially averaged radial profiles of the turbulent Reynolds shear stress components for the conditions of the reference case (case A), similar gas holdup, and non-similar gas holdup profiles.

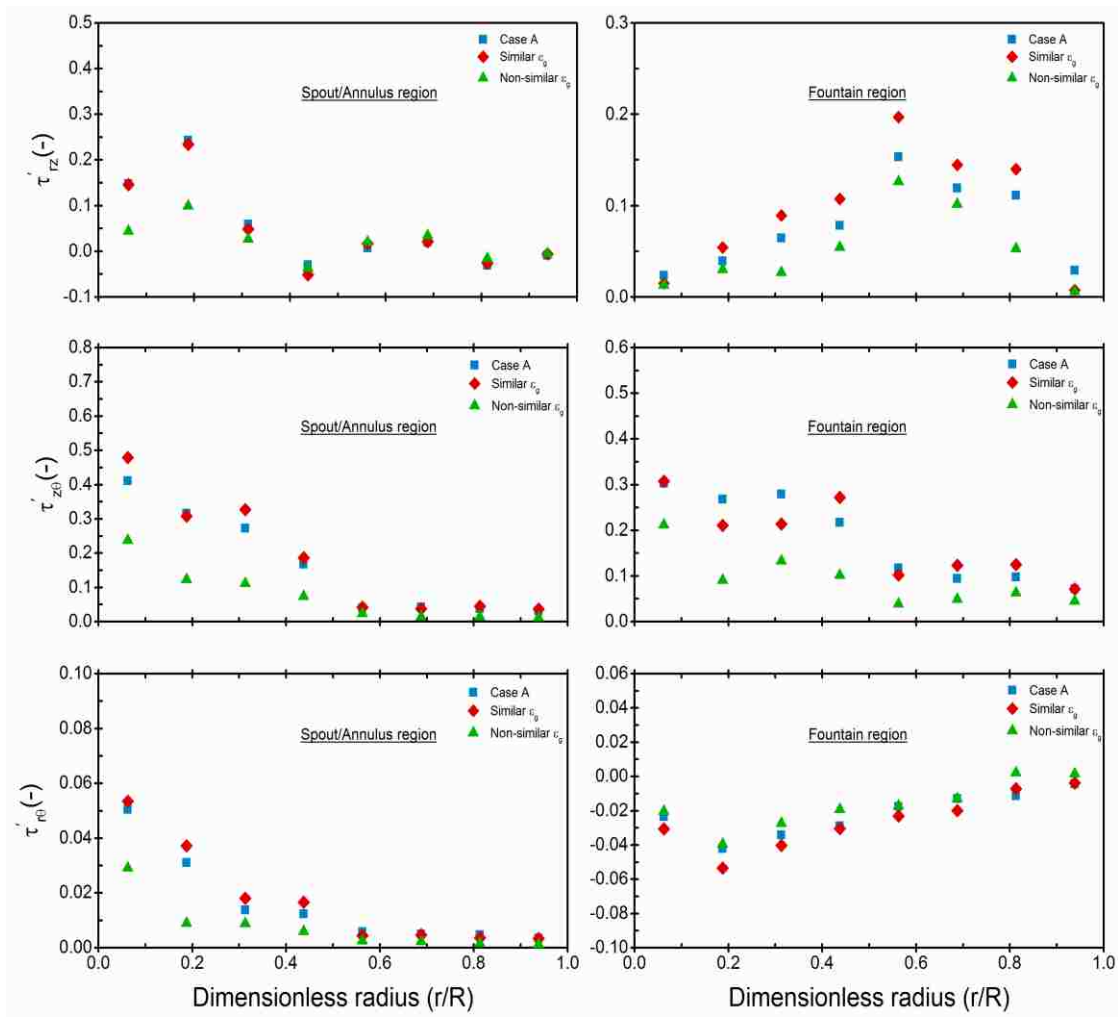


Figure 11. Comparison of the azimuthally and axially averaged radial profiles of the dimensionless shear stress components for the conditions of the reference case (case A), similar gas holdup, and non-similar gas holdup profiles.

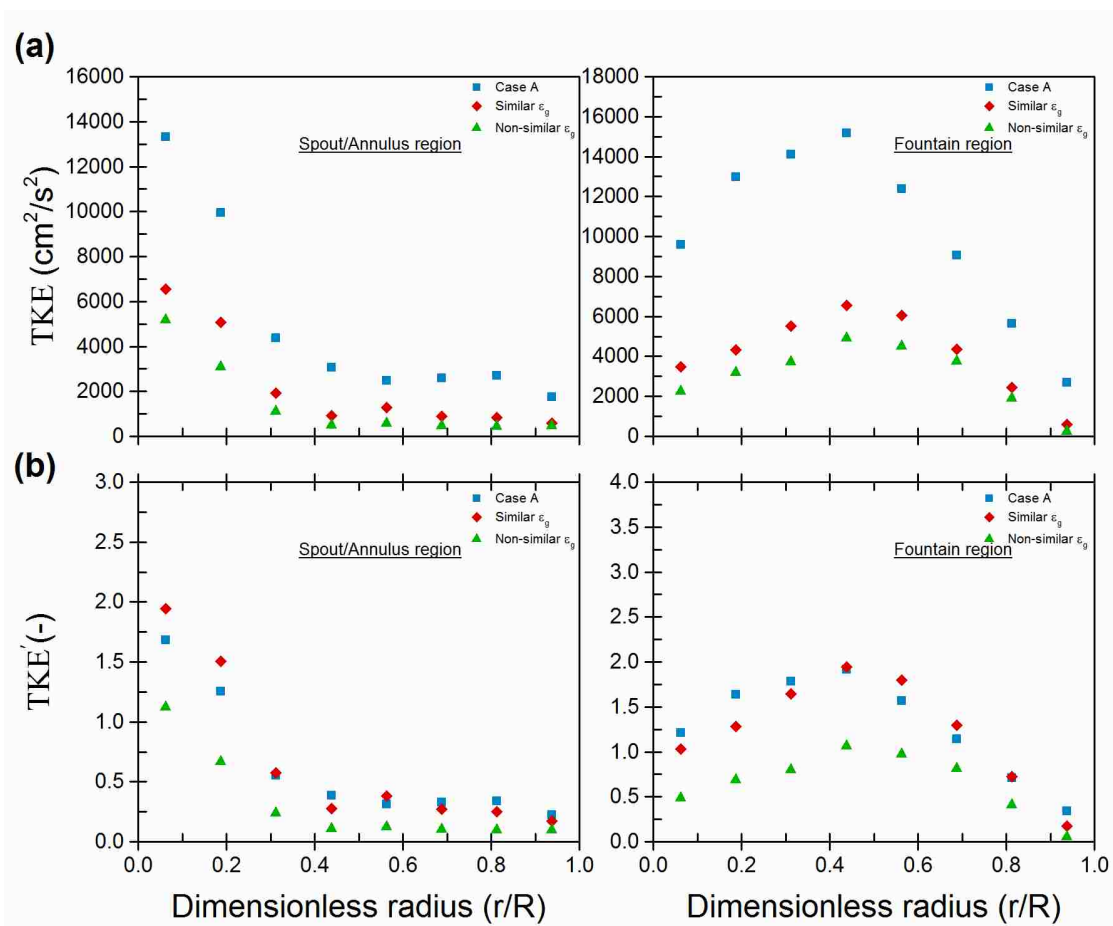


Figure 12. Comparison of the azimuthally and axially averaged radial profiles of (a) the turbulent kinetic energy (per unit bulk density) and (b) dimensionless turbulent kinetic energy for the conditions of the reference case (case A), similar gas holdup, and non-similar gas holdup profiles.

SECTION

3. CONCLUDING REMARKS AND RECOMMENDATIONS

- The following is a summary of the concluding remarks obtained from the work of this thesis:
 1. For the first time we implemented advanced non-invasive gamma ray computed tomography (CT) and radioactive particle tracking (RPT) techniques to assess based on local hydrodynamics parameters our new mechanistic scale-up methodology based on matching gas-holdup radial profile (Al-Dahhan et al., 2014, Aradhya, 2013) and the literature reported scale-up methodology based on match dimensionless groups (He et al. [6]). The local parameters that were measured are: cross sectional distributions of gas and solids holdup, radial profiles of gas and solids holdups (CT technique), solids velocity, normal stresses, shear stresses and turbulent kinetic energy (RPT technique).
 2. The new scale-up mechanistic methodology using gamma ray computed tomography (CT) technique to measure the local distributions and radial profiles of solids and gas holdups has been properly validated.
 3. Our new methodology of scale-up has been further validated using radioactive particle tracking (RPT) technique by measuring the non-dimensionalized values using the minimum spouting superficial gas velocity of the magnitude and the radial profiles of the components of the particles velocities, normal stresses, shear stresses and turbulent kinetic energy.

- The results of the CT and RPT techniques confirm that when the radial profiles of gas holdup is matched or are close to each other for two beds of different sizes and conditions, the similarity in local solids and gas holdups and local dimensionless solids velocity, Reynolds stresses and turbulent kinetic energy is attained in all three regions of the spouted bed; the spout, the annulus and the fountain.
4. However, when there were mismatching in the radial profiles of the gas holdups between set of conditions, non-similarity in these parameters were obtained and as the differences between the holdup profiles increases, the non-similarity in these parameters further enhanced. These findings further confirm the findings of Al-Dahhan et al. (2014) and Aradhya (2013). In addition, the findings confirm that the gas phase dictates the dynamics of gas-solid spouted beds and the radial profile of the gas holdup can represent the role of the gas phase on the solids dynamics of the bed.
 5. The scale-up methodology of He et al [6] based on matching dimensionless groups did not provide similarity in local solids and gas holdup distributions and their radial profiles using two sizes and different conditions of spouted beds along with gamma ray computed tomography (CT) technique.
 6. Also the methodology of He et al. [6] did not provide similarity in local solids velocity, normal stresses, shear stresses and turbulent kinetic energy measured by RPT technique. These findings (2 and 3 above) confirm the findings of (Aradhya, 2013), who made local point measurements of solids velocity and solids holdup by the use of a sophisticated optical fiber probe.

- It has been clearly demonstrated that while such methodology was validated using global parameter, it has not been validated in this work using local parameters. This is because the complex flow pattern of spouted beds due to complex interactions among the solids and between the solids and the gas phases.
7. It is noteworthy that adding more dimensionless group to match in order to capture the local hydrodynamics similarity will further complicate the scale up methodology since it will be not easy to define conditions to match large number of dimensionless groups.
 8. The CT and RPT techniques were able to distinguish the three regions of the spouted beds mentioned above.
 9. In the spout region it has been found that the cross sectional and radial profiles of solids increase with the increase of the height of the spout. This is due to the solids are being pulled by the jet of the gas phase at the interface between the spout region and the annulus region along the spout height.
 10. In the annulus region the solids move down ward as a moving bed and hence the solids holdup does not change along the bed height. The structure of the solids holdup distribution is clearly distinguished from the other regions.
 11. The knowledge and the data obtained provide valuable inside on the solids dynamics of spouted bed and presenting benchmarking data to validate computational fluid dynamics (CFD) codes and models.
 12. It is recommended that this new methodology can be enabled and applied in practice by implementing computational fluid dynamics after it is validated to search for the conditions that can provide similar gas holdup profiles measured at

the desired conditions of either lab scales or cold flow conditions. Gamma ray densitometry which is used in industry as nuclear gauge densitometry for liquid or slurry level monitoring and control can be used on site to evaluate and to refine the operating conditions for enabling the industrial implementation of our newly developed scale up methodology for gas-solid spouted beds.

13. This work confirms that validation of the scale up methods of gas-solid spouted beds for hydrodynamics similarity should reside on measuring and analyzing the local hydrodynamic parameters and not the global parameters as it has been used in the literature.

○ Recommendation for future works are the following:

1. Utilizing the results reported in this work to validate computational fluid dynamics (CFD) simulations and select proper combinations of the models and closures.
2. Demonstrating the CFD as an enabling tool to facilitate the implementation of our new scale-up methodology.
3. Implementing gamma ray densitometry (GRD) as enabling tool to assess and tune the new scale-up methodology by measuring the radial profile of the gas holdup at the scaled up gas-solid spouted bed coater and tune the conditions to ensure closer gas holdup radial profile be achieved with respect to the one measured and computed in the scaled down spouted bed.
4. Evaluating the new scale-up methodology for conditions representing the industrial applications of the spouted beds and using larger diameters such as the TRISO

nuclear fuel particles coating and other industrial processes such as coal/biomass gasification, drying, coating, etc. Augmenting this with the implementation of the validated CFD and gamma ray densitometry (GRD) as enabling tools.

5. Investigating the effect of particles density that represent the range of particles densities used in the above mentioned industrial applications on the solids and gas hydrodynamics of spouted beds at different velocities, different bed sizes, different solids loadings (the initial solids height before the gas is introduced) using CT, RPT, GRD, gas tracer technique, and pressure transducers.
6. Studying the hydrodynamics of the spouted beds when binary and multiple particles sizes and densities are used as the solids inventory (loadings) to be spouted in gas-solid spouted beds that represent the range of the mixture of solids particles presence in the bed for the industrial applications mentioned above using CT, RPT, GRD, gas tracer technique, and pressure transducers.

REFERENCES

- Energy, U.S.D.o., Office of Nuclear Energy, S.a.T., Washington, D.C., 1994. The History of Nuclear Energy.
- Gen IV, R., 2002. US DOE Nuclear Energy Research Advisory Committee and the Generation IV International Forum. A technology roadmap for generation IV nuclear energy systems. GIF002-00, December 2002. December.
- Goldberg, S.M., Rosner, R., 2011. Nuclear Reactors: Generation to Generation.
- Herzog, A.V., Lipman, T.E., Kammen, D.M., 2001. Renewable energy sources, Encyclopedia of Life Support Systems (EOLSS). Forerunner Volume-‘Perspectives and Overview of Life Support Systems and Sustainable Development.
- IAEA, 2013. energy, electricity and nuclear power estimates for the period up to 2050, 2013 ed.
- Lee, Y.-W., Park, J.-Y., Kim, Y.K., Jeong, K.C., Kim, W.K., Kim, B.G., Kim, Y.M., Cho, M.S., 2008. Development of HTGR-coated particle fuel technology in Korea. Nuclear Engineering and Design 238, 2842-2853.
- Mycle Schneider, S.T., Antony Froggatt, Doug Koplow, 2009. The World Nuclear Industry Status Report 2009
With Particular Emphasis on Economic Issues.
- NEI, 2008. Nuclear Energy Just the Facts.
- Rashad, S.M., 2008. Future of nuclear energy worldwide strategies and policies, Radio Science Conference, 2008. NRSC 2008. National, pp. 1-17.
- Verfondern, K., Nabielek, H., Kendall, J.M., 2007. Coated particle fuel for high temperature gas cooled reactors.
- Al-Dahhan, M., Aradhya, S., Zaid, F., Ali, N., Aljuwaya, T., 2014. Scale-up and On-line Monitoring of Gas-solid Systems Using Advanced and Non-invasive Measurement Techniques. Procedia Engineering 83, 469-476.

- Aradhya, S.B., 2013. Scaleup and hydrodynamics study of gas-solid spouted beds, *Chemical and Biochemical Engineering*. Missouri University of Science and Technology, pp. xxiv, 301 pages.
- Béttega, R., Corrêa, R.G., Freire, J.T., 2009. Scale-up study of spouted beds using computational fluid dynamics. *The Canadian Journal of Chemical Engineering* 87, 193-203.
- Chandnani, P.P., Epstein, N., 1986. Spoutability and spout detabilization of fine particles with a gas. Engineering Foundation, United States.
- Du, W., Bao, X., Xu, J., Wei, W., 2006a. Computational fluid dynamics (CFD) modeling of spouted bed: Assessment of drag coefficient correlations. *Chemical Engineering Science* 61, 1401-1420.
- Du, W., Bao, X., Xu, J., Wei, W., 2006b. Computational fluid dynamics (CFD) modeling of spouted bed: Influence of frictional stress, maximum packing limit and coefficient of restitution of particles. *Chemical Engineering Science* 61, 4558-4570.
- Du, W., Xu, J., Ji, Y., Wei, W., Bao, X., 2009. Scale-up relationships of spouted beds by solid stress analyses. *Powder Technology* 192, 273-278.
- Duarte, C.R., Murata, V.V., Barrozo, M.A.S., 2005. Simulation of Spouted Bed Using a Eulerian Multiphase Model. *Materials Science Forum* 498-499, 270-277.
- Duarte, C.R., Olazar, M., Murata, V.V., Barrozo, M.A.S., 2009. Numerical simulation and experimental study of fluid-particle flows in a spouted bed. *Powder Technology* 188, 195-205.
- Epstein, N., 1968. Void Fraction Variation in Spouted Bed Annulus. *Industrial & Engineering Chemistry Process Design and Development* 7, 157-158.
- Glicksman, L.R., 1984. Scaling relationships for fluidized beds. *Chemical Engineering Science* 39, 1373-1379.
- Gryczka, O., Heinrich, S., Deen, N.G., van Sint Annaland, M., Kuipers, J.A.M., Jacob, M., Mörl, L., 2009a. Characterization and CFD-modeling of the hydrodynamics of a prismatic spouted bed apparatus. *Chemical Engineering Science* 64, 3352-3375.

- Gryczka, O., Heinrich, S., Deen, N.G., van Sint Annaland, M., Kuipers, J.A.M., Mörl, L., 2009b. CFD modeling of a prismatic spouted bed with two adjustable gas inlets. *The Canadian Journal of Chemical Engineering* 87, 318-328.
- He, Y.L., Lim, C.J., Grace, J.R., 1992. Spouted bed and spout-fluid bed behaviour in a column of diameter 0.91 m. *The Canadian Journal of Chemical Engineering* 70, 848-857.
- He, Y.L., Lim, C.J., Grace, J.R., 1997. Scale-up studies of spouted beds. *Chemical Engineering Science* 52, 329-339.
- Horio, M., Nonaka, A., Sawa, Y., Muchi, I., 1986. A new similarity rule for fluidized bed scale-up. *AIChE Journal* 32, 1466-1482.
- Hosseini, S.H., Ahmadi, G., Olazar, M., 2013. CFD simulation of cylindrical spouted beds by the kinetic theory of granular flow. *Powder Technology* 246, 303-316.
- Lan, X., Xu, C., Gao, J., Al-Dahhan, M., 2012. Influence of solid-phase wall boundary condition on CFD simulation of spouted beds. *Chemical Engineering Science* 69, 419-430.
- Li, Y., Che, D., Liu, Y., 2012. CFD simulation of hydrodynamic characteristics in a multiple-spouted bed. *Chemical Engineering Science* 80, 365-379.
- Lim, C.J., Grace, J.R., 1987. Spouted bed hydrodynamics in a 0.91 m diameter vessel. *The Canadian Journal of Chemical Engineering* 65, 366-372.
- Mathur, K.B., Epstein, N., 1974a. 1 - Introduction, in: Mathur, K.B., Epstein, N. (Eds.), *Spouted Beds*. Academic Press, pp. 1-13.
- Mathur, K.B., Epstein, N., 1974b. 6 - Spouting Stability, in: Mathur, K.B., Epstein, N. (Eds.), *Spouted Beds*. Academic Press, pp. 112-124.
- Moradi, S., Yeganeh, A., Salimi, M., 2013. CFD-modeling of effects of draft tubes on operating condition in spouted beds. *Applied Mathematical Modelling* 37, 1851-1859.
- Ren, B., Zhong, W., Jin, B., Yuan, Z., Lu, Y., 2011. Computational Fluid Dynamics (CFD)–Discrete Element Method (DEM) Simulation of Gas–Solid Turbulent Flow in a Cylindrical Spouted Bed with a Conical Base. *Energy & Fuels* 25, 4095-4105.

- Rojas, L., Deytia, I., 2011. Investigation of hydrodynamic scaling relationships in shallow spouted beds.
- Rong, L.-W., Zhan, J.-M., 2010. Improved DEM-CFD model and validation: A conical-base spouted bed simulation study. *Journal of Hydrodynamics, Ser. B* 22, 351-359.
- Sanderson, J., Rhodes, M.J., Wang, X.S., Lim, K.S., 2007. An investigation of fluidized bed scaling laws by DEM simulation.
- Shaikh, A., Al-Dahhan, M., 2003. Development of an artificial neural network correlation for prediction of overall gas holdup in bubble column reactors. *Chemical Engineering and Processing: Process Intensification* 42, 599-610.
- Shaikh, A., Al-Dahhan, M., 2005. Characterization of the hydrodynamic flow regime in bubble columns via computed tomography. *Flow Measurement and Instrumentation* 16, 91-98.
- Shirvanian, P.A., Calo, J.M., 2004. Hydrodynamic scaling of a rectangular spouted vessel with a draft duct. *Chemical Engineering Journal* 103, 29-34.
- Shuyan, W., Xiang, L., Huilin, L., Long, Y., Dan, S., Yurong, H., Yonglong, D., 2009. Numerical simulations of flow behavior of gas and particles in spouted beds using frictional-kinetic stresses model. *Powder Technology* 196, 184-193.
- Sokolovskii, V., 1965. *Statistics of granular media*. Pergamon Press, Oxford.
- Wang, Q., Luo, J., Xu, C., Chen, D., Sun, B., Feng, J., 2012. Numerical Simulation of the Gas-Particle Flow Behavior in Oil Shale Semi-Coke Spouted Bed. *Energy Procedia* 17, Part A, 892-900.
- Wang, S., Zhao, L., Wang, C., Liu, Y., Gao, J., Liu, Y., Cheng, Q., 2013. Numerical simulation of gas-solid flow with two fluid model in a spouted-fluid bed. *Particuology*.
- Wang, Z.G., Bi, H.T., Lim, C.J., 2006. Numerical simulations of hydrodynamic behaviors in conical spouted beds. *China Particuology* 4, 194-203.
- Xu, J., Ji, Y., Wei, W., Bao, X., Du, W., 2007. Scale-up relationships of spouted beds.

Yang, S., Luo, K., Fang, M., Zhang, K., Fan, J., 2014. Parallel CFD–DEM modeling of the hydrodynamics in a lab-scale double slot-rectangular spouted bed with a partition plate. *Chemical Engineering Journal* 236, 158-170.

Zaid, F.M., 2013. Gas-solid fluidized bed reactors: scale-up, flow regimes identification and hydrodynamics. Missouri University of Science and Technology, Rolla, Missouri.

Zhonghua, W., Mujumdar, A.S., 2008. CFD modeling of the gas–particle flow behavior in spouted beds. *Powder Technology* 183, 260-272.

VITA

Neven joined the research group of Dr.Muthanna Al-dahhan in 2011 at Missouri University of science and technology in Rolla, MO, USA to pursue her Ph.D. degree in Nuclear Engineering. In December 2014, she received her M.S. degree in nuclear engineering from Missouri University of science and technology. During her Ph.D. studies, Neven worked on the project of evaluating of scale-up methodologies of gas-solid spouted beds for coating TRISO nuclear fuel particles using advanced measurement technique. This work has been supported by U.S. Department of Energy (DOE) – Nuclear Energy University Program (NEUP) and GAANN (Department of Education). She also worked as research assistant on the project of heat transfer study in a pebble bed nuclear reactor as one of the promising 4th generation nuclear reactors. The work was sponsored by US department of energy-Nuclear energy university program (NEUP).

Her doctoral work led to 2 peer-reviewed journal papers (published) and three more submitted, four proceedings papers, and four oral presentations at national and international conferences. She also was awarded in her Ph.D. studies by the Missouri S&T Chancellor's Fellowship – Fellow, and the Missouri S&T – GAANN fellow related to alternative energy given by US department of Education (Graduate Assistance in Area of National Need). She also was sponsored to present her work in Netherlands, Noordwijkerthour, International conference on Fluidization XIV: From Fundamentals to Products. Neven received her Ph.D. degree in May 2016.